AFAPL-TR-78-9

LEVEL II

THE BALANCE OF ROLLERS FOR HIGH DN BEARINGS

MARTIN EUSEPI
PRADEEP GUPTA

MECHANICAL TECHNOLOGY INCORPORATED
968 ALBANY-SHAKER ROAD
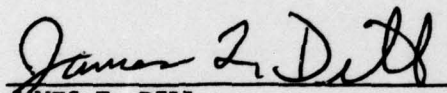*LATHAM, NEW YORK 12110*
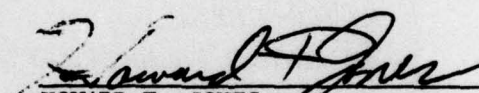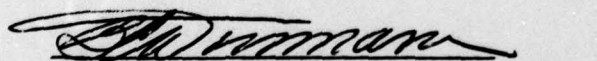
MARCH 28, 1978

79 03 13 036

NOTICE

When Government drawings, specifications, or other data are used for any
purpose other than in connection with a definitely related Government
procurement operation, the United States Government thereby incurs no
responsibility nor any obligation whatsoever; and the fact that the
Government may have formulated, furnished or in any way supplied the said
drawings, specifications, or other data, is not to be regarded by impli-
cation or otherwise as in any manner licensing the holder or any other
person or corporation, or conveying any rights or permission to manufacture,
use or sell any patented invention that may in any way be related thereto.

This report has been reviewed by the Information Office (ASD/OIP) and is
releasable to the National Technical Information Service (NTIS). At
NTIS, it will be available to the general public, including foreign
nations.

This technical report has been reviewed and is approved for publication.

JAMES F. DILL
Project Engineer

HOWARD F. JONES
Chief, Lubrication Branch

BLACKWELL C. DUNNAM
Chief, Fuels and Lubrication Division

Copies of this report should not be returned unless return is required by
security consideration, contractual obligation, or notice on a specific
document.

AIR FORCE/56780/17 August 1978 — 250

REPORT DOCUMENTATION PAGE	READ INSTRUCTIONS BEFORE COMPLETING FORM

1. REPORT NUMBER	2. GOVT ACCESSION NO.	3. RECIPIENT'S CATALOG NUMBER
AFAPL-TR-78-9		

4. TITLE (and Subtitle)	5. TYPE OF REPORT & PERIOD COVERED
THE BALANCE OF ROLLERS FOR HIGH DN BEARINGS.	FINAL REPORT. 1 May 1977 to 15 Nov 1977
	6. PERFORMING ORG. REPORT NUMBER
	MTI-78TR27

7. AUTHOR(s)	8. CONTRACT OR GRANT NUMBER(s)
M. Eusepi P. Gupta	F33615-77-C-3100

9. PERFORMING ORGANIZATION NAME AND ADDRESS	10. PROGRAM ELEMENT, PROJECT, TASK AREA & WORK UNIT NUMBERS
Mechanical Technology Incorporated 968 Albany-Shaker Road Latham, New York 12110	Project No. 3048 Task No. 304806 Work Unit No. 30480609

11. CONTROLLING OFFICE NAME AND ADDRESS	12. REPORT DATE
Air Force Aero Propulsion Laboratory Air Force Systems Command Wright-Patterson Air Force Base, Ohio 45433	28 March 1978
	13. NUMBER OF PAGES
	93

14. MONITORING AGENCY NAME & ADDRESS(if different from Controlling Office)	15. SECURITY CLASS. (of this report)
	UNCLASSIFIED
	15a. DECLASSIFICATION/DOWNGRADING SCHEDULE

16. DISTRIBUTION STATEMENT (of this Report)

APPROVED FOR PUBLIC RELEASE; DISTRIBUTION UNLIMITED.

17. DISTRIBUTION STATEMENT (of the abstract entered in Block 20, if different from Report)

18. SUPPLEMENTARY NOTES

19. KEY WORDS (Continue on reverse side if necessary and identify by block number)

Roller Bearings
Bearing Inspection
Roller Dynamics

20. ABSTRACT (Continue on reverse side if necessary and identify by block number)

A gas bearing spin-up device has been built for determining the residual
unbalance remaining in rollers for high speed bearing applications after
the rollers have successfully completed the manufacturing and final in-
spection process. The device has successfully determined the mean unbalance
in a group of 30 rollers to be in the range of 5.0 to 5.6 x 10^{-6} in.-oz. per
end with a standard deviation in the range of 2.7 to 3.3 x 10^{-6} in.-oz. The
spin-up device uses capacitance type non-contacting sensors to measure the

DD FORM 1473 1 JAN 73	EDITION OF 1 NOV 65 IS OBSOLETE

62203F

roller's response. The measurement resolution has been determined to be .000002 x 10⁻⁶ inch and its sensitivity approximately 250 volt/inch. For the roller investigated, the minimum measurable unbalance is approximately 0.5 x 10⁻⁶ in.-oz. .000005 in.-oz.

In a second phase of this study, a complement of 32 rollers, screened for minimum unbalance in the balancing fixture, was assembled into a zero radial clearance bearing which was then tested to 2.5 million DN under a 500-lb. radial load. At the conclusion of 40 test hours, four of the rollers in the above bearing were replaced with four new rollers which were deliberately unbalanced. An additional 40 test hours at 2.5 million DN and 500-lb. radial load were logged with no visible effects caused by the roller unbalance.

FOREWORD

79 03 13 036

TABLE OF CONTENTS

TABLE OF CONTENTS (Cont'd.)

LIST OF FIGURES

LIST OF FIGURES (cont'd)

LIST OF TABLES

I. INTRODUCTION

As the speeds of roller bearings have increased into the $2.0-3.0 \times 10^6$ DN range, cage failures caused by roller skewing have become an increasing problem. The usual sequence of events in such failures is for one or two rollers out of a bearing's full complement to experience eccentric end wear (wear on opposite ends of the roller 180° apart circumferentially). As the wear progresses, the roller will skew farther and farther causing high cyclic stresses on the cage cross rails which eventually fail in high cycle fatigue.

Roller skewing is generally considered to be unstable motion of the roller due to a small unbalance rotating at a roller's high rotational speed (on the order of 10^5 rpm in some applications). A typical cylindrical roller is subject to a number of tolerances on the various geometrical parameters, such as roller diameter, crown radius, flat length, corner radii, etc. Most efforts to control roller skewing have been directed toward tightening these geometric tolerances in roller manufacture to insure roller balance through dimensional control. There is also the possibility, however, that material inhomogeneities such as inclusions or voids could cause unbalance even in a geometrically "perfect" roller. In terms of the roller dynamics all of these imperfections will influence the roller motion in so far as they contribute to the deviations between the roller geometric center and the mass centers and also those between the polar inertial axis and the geometric axis. Thus, the effect of all the manufacturing tolerances can be pooled in terms of these two types of deviations.

The purpose of the program reported herein is to evaluate the extent of roller unbalance and its effect on bearing performance. This work was organized into several subtasks which are described as follows:

1. **Analytical Evaluation of Roller Motion**

   For this task a 6-degree of freedom dynamic analysis of roller motion in a typical turbine engine roller bearing was made at speeds up to DN values of 2.5×10^6. The analysis included elastohydrodynamic effects, as well as conventional line contact theories, and accounted for roller inertial and gyroscopic forces by including the effects of deviations between geometric and mass centers and differences between polar inertial and geometric axes.

-1-

2. Spin-Up Device to Measure Extent of Roller Unbalance

To evaluate the extent of roller unbalance, 21 out of a lot of
30 new rollers were examined in a roller spin-up device. The
spin-up device had the capability of spinning individual rollers
and to permit a two-plane measurement of the response each roller
had when operating at the selected balance speed of 13,500 rpm.
Calibration of the spin-up device by means of trial weights per-
mitted the evaluation of the actual residual unbalance of each
roller.

In conjunction with the design of the spin-up device, a study
to determine the feasibility of employing laser techniques to
correct roller unbalance was made. Included in this study was
the examination of surface effects where metal removal had taken
place and the relationship between pulse energy and metal removal
rate. For this study rotation of the impacted rollers was not
attempted.

3. Roller Bearing Test Evaluation

From a group of 150 rollers the spin-up balancing device was used
to select 32 rollers exhibiting the smallest amount of residual
unbalance. These finely balanced rollers were assembled into a
bearing which was then tested at a DN value of 2.5 million. At
the conclusion of a 40 hour test the bearing was disassembled and
examined to determine if roller skewing had occurred.

After a thorough examination, four deliberately unbalanced rollers
were used to replace four of the original rollers and the bearing
was reassembled and retested. At the conclusion of the second 40
hour test at 2.5 million DN, the bearing was disassembled and ex-
amined to determine if the unbalanced rollers exhibited excessive
endwear.

The following report sections describe the approach which was taken to arrive
at the evaluation of each task along with the final conclusions resulting from
each evaluation.

II. GEOMETRIC TOLERANCES AND RESULTING DYNAMICS OF ROLLER MOTION IN HIGH SPEED ROLLER BEARINGS

1. Introduction

The angular rotation of the roller, or roller skew, can only be simulated by formulating and integrating the classical differential equations for roller motion in real time. The generalized motion of the roller mass center has to be located in a space fixed, or inertial, coordinate frame while the angular motion about the mass center is best treated in a roller fixed frame. Such a generalized formulation has been recently made available by Gupta [1] for cylindrical roller bearings.

Once an analytical model for the bearing performance simulation is available, investigations leading to the relationships between roller skew and the operational and geometric parameters have a substantial design significance. Amongst the operational parameters bearing misalignment is one of the primary factors which results in roller skew, as it has been demonstrated elsewhere [2]. The geometric factors are related to the manufacturing imperfections or tolerances on rollers, races, and the cage. The objective of the present investigation is to examine roller skew as a function of the expected deviations in the roller geometry.

The present investigation considers both of the above types of geometrical deviations in simulating the general motion of the roller. Although a rigorous analysis of the general roller motion has been presented elsewhere [1], and overview of the equations of motion and the computations of the applied forces on the roller is presented in the next section. A bearing model consisting of a typical high speed roller bearing is then discussed. Finally, some roller motion simulations are presented and the factors influencing roller skew are discussed.

2. Generalized Equations of Roller Motion

The motion of a roller in a generalized simulation of the dynamic per-
formance of a roller bearing can be considered in two parts:

(1) Motion of the roller mass center in an inertial reference frame.

(2) Rotational motion of the roller about its mass center.

Motion of Ball Mass Center

As shown in Figure 1, the translational motion of the roller center is best
considered in a cylindrical coordinate frame, which is fixed in space and it,
therefore, represents the inertial frame of reference. The classical dif-
ferential equations of motion are written as

$$\ddot{x} = F_x/m$$
$$\ddot{r} - r\dot{\theta}^2 = F_r/m \qquad (1)$$
$$r\ddot{\theta} + 2\dot{r}\dot{\theta} = F_\theta/m$$

where (F_x, F_r, F_θ) are components of the net applied forces on the roller and
m is the mass of the roller.

For a given position of the roller mass center and all translational and
angular velocities, the applied forces are calculated from the various
interactions in the bearing, such as:

- Roller-race interaction

- Roller end – race flange interaction

- Roller-cage interaction

- Lubricant drag, churning or other interactions

As will be discussed in the next section, the present investigation will
emphasize the motion of one roller between the two races whose mass
centers are fixed in space. Hence only roller-race interaction will be
relevant in determining the applied forces and moments on the rollers.

-4-

ROLLER FRAME

$\hat{z}$

$\hat{y}$

O

$\hat{x}$

r

Z

θ

x

INERTIAL
FRAME

Y

X
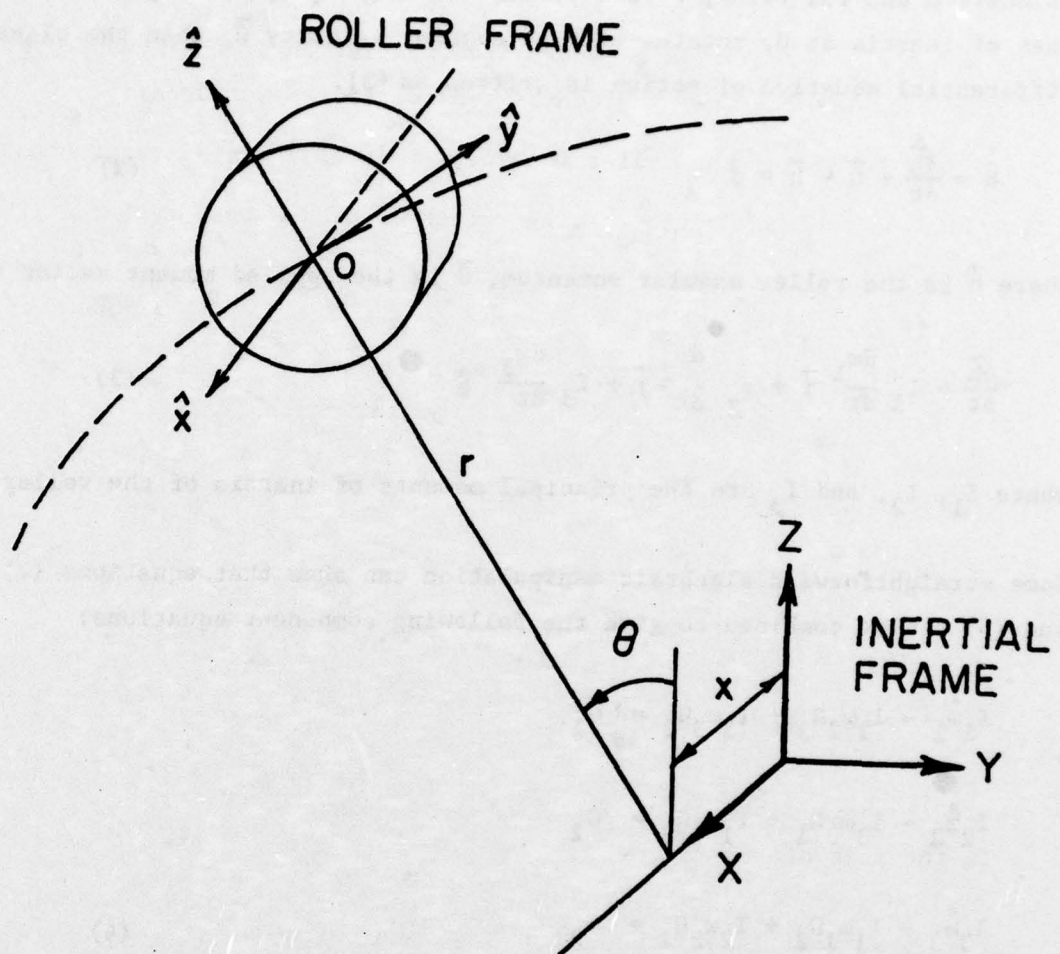
Figure 1. Coordinate Frames for Roller Motion

Rotational Motion of the Roller

If the roller is considered to rotate about a fixed point, 0, with angular velocity $\vec{\omega}$ and the triad, formed by unit vectors $\vec{i}, \vec{j}, \vec{k}$ along the principal axes of inertia at 0, rotates with an angular velocity $\vec{\Omega}$, then the classical differential equation of motion is written as [3].

$$\dot{\vec{h}} = \frac{\delta \vec{h}}{\delta t} + \vec{\Omega} \times \vec{h} = \vec{G} \tag{2}$$

where $\vec{h}$ is the roller angular momentum, $\vec{G}$ is the applied moment vector and

$$\frac{\delta \vec{h}}{\delta t} = I_1 \frac{d\omega_1}{dt} \vec{i} + I_2 \frac{d\omega_2}{dt} \vec{j} + I_3 \frac{d\omega_3}{dt} \vec{k} \tag{3}$$

where I_1, I_2, and I_3 are the principal moments of inertia of the roller.

Some straightforward algebraic manipulation can show that equations (2) and (3) can be combined to give the following component equations:

$$I_1 \dot{\omega}_1 - I_2 \omega_2 \Omega_3 + I_3 \omega_3 \Omega_2 = G_1$$

$$I_2 \dot{\omega}_2 - I_3 \omega_3 \Omega_1 + I_1 \omega_1 \Omega_3 = G_2$$

$$I_3 \dot{\omega}_3 - I_1 \omega_1 \Omega_2 + I_2 \omega_2 \Omega_1 = G_3 \tag{4}$$

In case of a "perfectly" cylindrical roller, the transverse moment of inertia I_2 and I_3 will be equal. However, this symmetry does not simplify the situation to any great extent since the polar axis has to be fixed in the roller. Also since the geometric and mass centers will be different, it will be convenient to consider the roller angular motion in a roller fixed frame and preserve all generalities. A roller fixed frame will essentially mean that the triad of unit vectors $\vec{i}, \vec{j}, \vec{k}$, of equation (3) is fixed in the roller.

Thus, $\vec{\Omega} = \vec{\omega}$ and equations (4) reduce to the classical Euler equations of motion

$$I_1\dot{\omega}_1 - (I_2 - I_3)\omega_2\,\omega_3 = G_1$$

$$I_2\dot{\omega}_2 - (I_3 - I_1)\omega_3\omega_1 = G_2 \qquad\qquad (5)$$

$$I_3\dot{\omega}_3 - (I_1 - I_2)\omega_1\omega_2 = G_3$$

Clearly, the components of the moment vector $\vec{G}$ will now be in the body fixed reference frame.

The applied moment vector $\vec{G}$ is once again determined from the various interactions mentioned in the case of roller mass center motion. It is easy to understand that while the normal contact forces at each interaction dominate the mass center motion, the angular motion is dependent on the moments which result from the tractive forces at the various interactions. Hence, the definition of a roller-race traction model will be important.

Since the applied moments are conveniently expressed in the inertial coordinate frame, it will be necessary to define a law of transformations between the inertial and body fixed frames. Such details have been presented elsewhere [1] and they will be skipped here for brevity.

Roller-Race Interactions

As will be discussed in the next section, the applied force and moment vectors will be determined by the roller-race interaction model. Basically the interaction results in normal and tractive forces which constitute the generalized force and moment vectors.

(1) Normal Contact Force: In order to compute the normal contact load, the mass center of the roller is located with respect to the race geometric center at any instant in time. Knowing the difference between the mass and geometric centers of the roller, this leads to the definition of roller geometric center with respect to the race geometric center. The geometry of the roller and race is now used to compute the geometric interference or the elastic deflection

-7-

in the case of roller-race contact. A conventional Palmgren type
of load-deflection relation [4] is then used to compute the normal
load. All the mathematical details of such a procedure have been
described elsewhere by the author [1].

(2) <u>Tractive Forces</u>: In terms of the applied moments resulting in
angular motion of the roller, the traction characteristics at the
roller-race interaction are very important. In most rolling
bearings, the concentrated race contacts are generally found to be
in the elastohydrodynamic regime and the computation of traction
for a prescribed lubricant is not an easy task. The effective
tractive coefficient not only varies with the sliding and rolling
speeds, but other variables such as contact stress and lubricant
behavior in the range of operating temperatures are also greatly
important. For a given lubricant, a traction model is derived by
actual laboratory experiments performed to measure traction as
a function of slip under a range of operating conditions. Such
a model for a MIL-L-7808 type lubricant has been presented by
Walowit and Smith [5]. Some typical traction curves for the
model are shown in Figure 2. This model is used in the present
investigation to compute traction as a function of slip, which,
in turn, is readily computed from the roller and race angular
velocities at any instant in time.

Since the geometry of the roller surface generally varies along its length,
it is convenient to treat the roller-race interaction in terms of several
elementary discs along the roller length. A proper summation will give the
total normal and tractive forces.

-8-
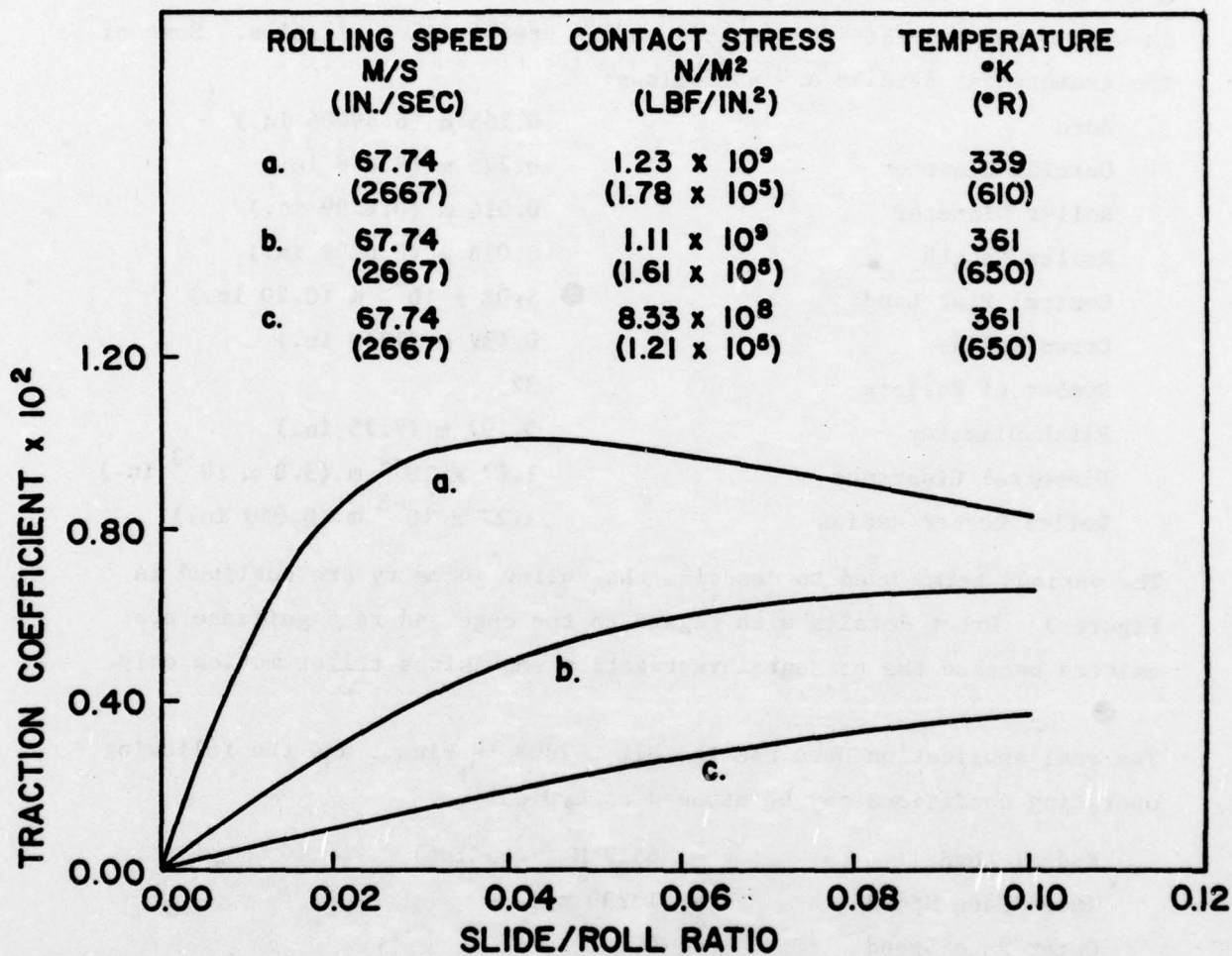
Figure 2. Typical Traction Curves for the MIL-L-7808 Lubricant for the Range of Operating Conditions

3. A Model Roller Bearing

A 165 mm bore cylindrical roller bearing typical of the design employed
in high speed applications is used in the present investigation. Some of
the geometrical details are as follows:

Bore	0.165 m (6.49606 in.)
Outside Diameter	0.225 m (8.858 in.)
Roller Diameter	0.016 m (0.6299 in.)
Roller Length	0.016 m (0.6299 in.)
Central Flat Land	5.08×10^{-3} m (0.20 in.)
Crown Radius	0.432 m (17.0 in.)
Number of Rollers	32
Pitch Diameter	0.197 m (7.75 in.)
Diametral Clearance	1.47×10^{-4} m (5.8×10^{-3} in.)
Roller Corner Radius	1.27×10^{-3} m (0.050 in.)

The various terms used to describe the roller geometry are outlined in
Figure 3. Other details with regard to the cage and race guidance are
omitted because the present investigation emphasizes roller motion only.

The real application does use the MIL-L-7808 lubricant and the following
operating conditions may be assumed as typical

Radial Load	=	6517 N (1465 lbf)
Inner Race Speed	=	13230 rpm
Outer Race Speed	=	0,
Inner Race Temperature	=	361°K (650°R)
Outer Race Temperature	=	339°K (610°R)

For the purpose of the present investigation, a simple quasi-static
computation under the above operating condition is first performed in
order to determine the relative position of the races and the size of the
load zone. As shown in Figure 4, the races are then held in this eccentric
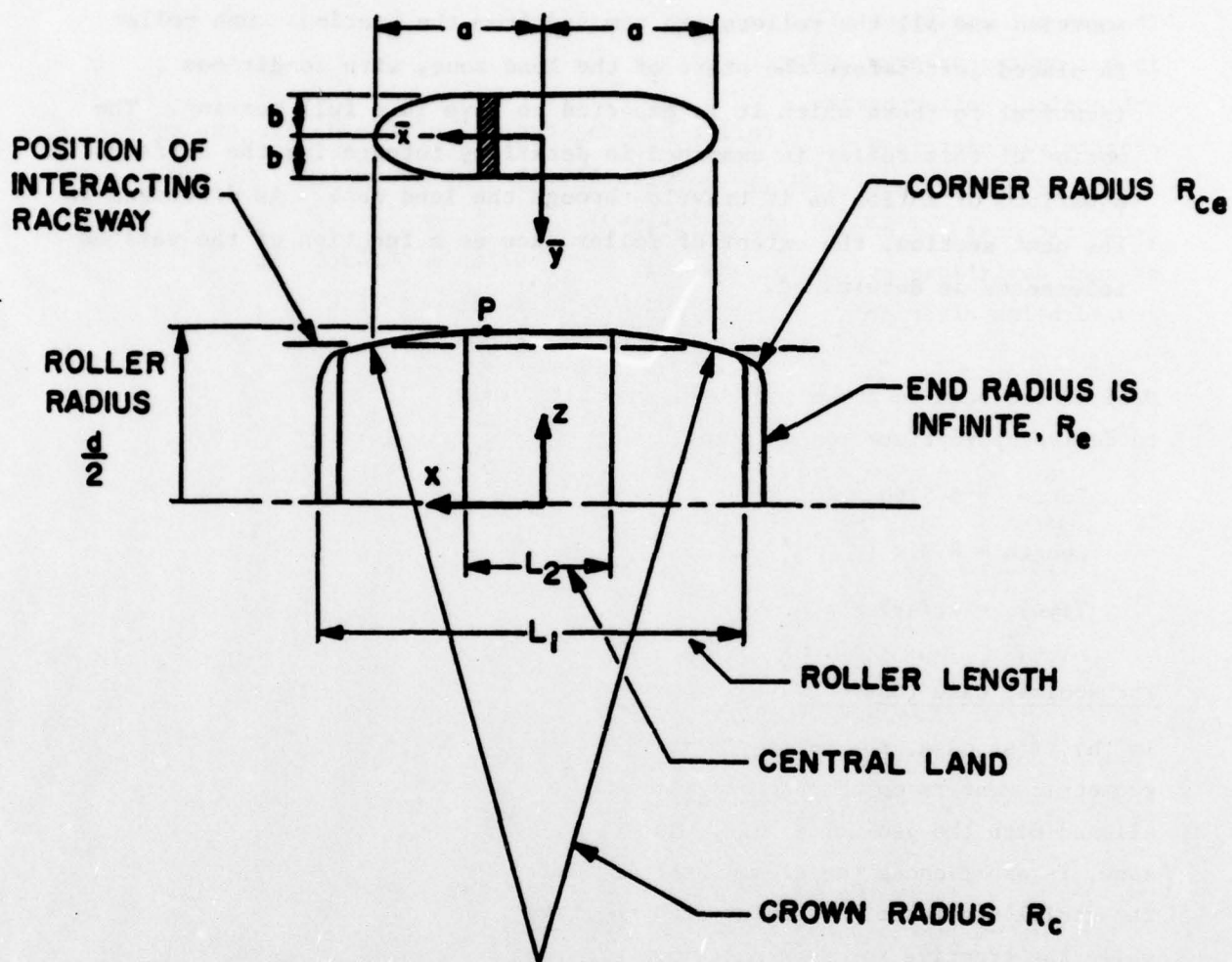
Figure 3. Roller-Race Contact Geometry

position and all the rollers are removed from the bearing. One roller
is placed just before the start of the load zone, with conditions
identical to those which it is expected to have in a full bearing. The
motion of this roller is examined in detail by integrating the differential
equations of motion as it travels through the load zone. As discussed in
the next section, the extent of roller skew as a function of the various
tolerances is determined.
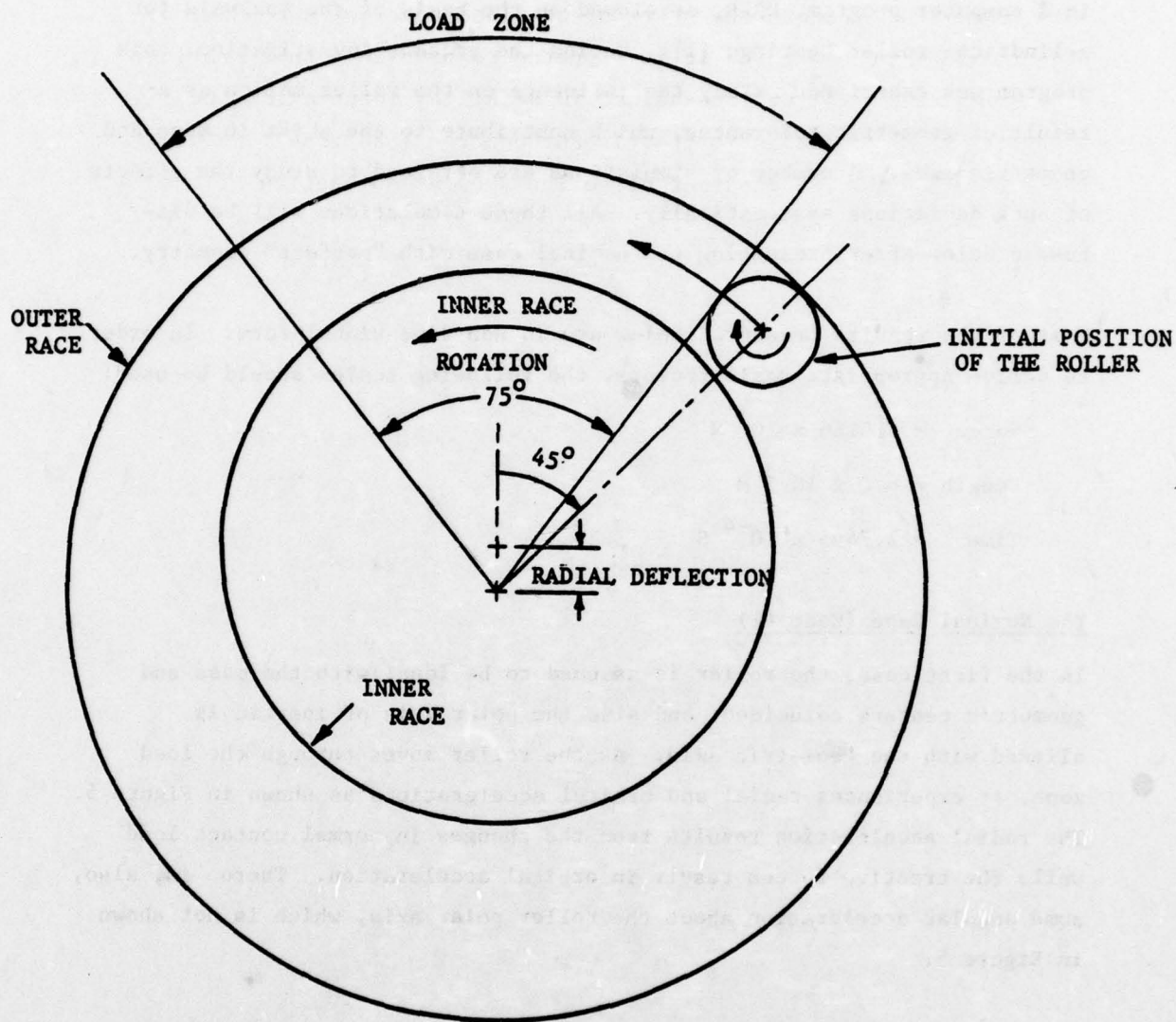
Figure 4.   Exaggerated View of the Bearing Model Used to Study
            the Roller Motion

-13-

4. Roller Motion Simulations

The general equations of motion, outlined earlier, are numerically integrated in a computer program, DREB, developed on the basis of the analysis for cylindrical roller bearings [1]. During the present investigation, this program was exercised to study the influence on the roller motion as a result of geometric tolerances, which contribute to the shift in mass and geometric axes. A number of simulations are obtained to study the effects of such deviations systematically. All these simulations will be discussed below after presenting the nominal case with "perfect" geometry.

Most of the results presented below are in non-dimensional form. In order to derive appropriate scale factors, the following scales should be used:

Force = 6.5166×10^3 N

Length = 8.0×10^{-3} M

Time = 1.7495×10^{-4} S

The Nominal Case (Case #1)

In the first case, the roller is assumed to be ideal with the mass and geometric centers coincident, and also the polar axis of inertia is aligned with the geometric axis. As the roller moves through the load zone, it experiences radial and orbital accelerations as shown in Figure 5. The radial acceleration results from the changes in normal contact load while the tractive forces result in orbital acceleration. There is, also, some angular acceleration about the roller polar axis, which is not shown in Figure 5.

If Figure 5 is examined closely, it will be seen that there is a definite high frequency in the acceleration profiles. In fact, the observed frequency is somewhat higher in the load zone when compared with the unloaded region. This high frequency corresponds to the roller-race contact resonance, and the mechanics of the motion is very similar to that identified by Gupta, et al. [6] for the case of ball bearings. In the loaded zone, there will be two springs in parallel, corresponding to the

-14-
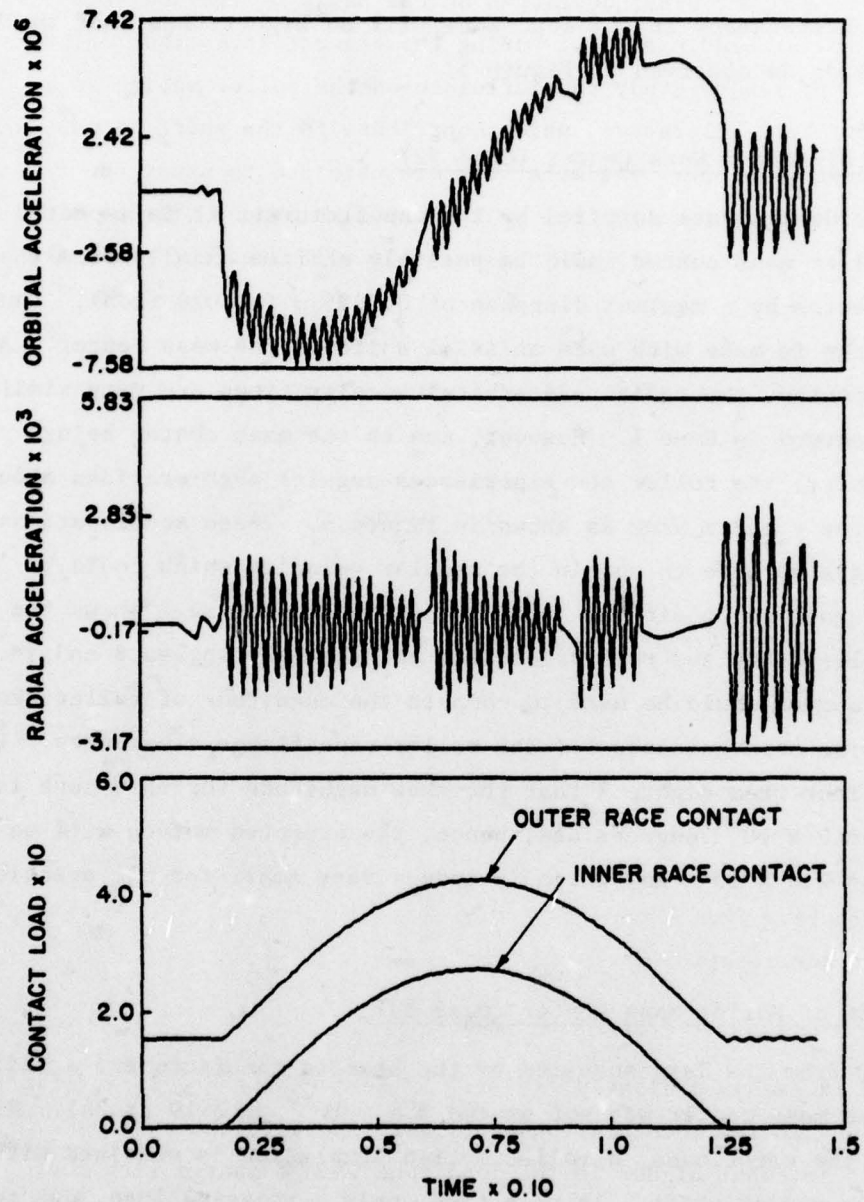
Figure 5. Radial and Orbital Accelerations for the Nominal
Case with No Geometrical Deviations

outer and inner race contacts, while in the unloaded zone, the roller will
only contact the outer race due to the centrifugal loading. Thus,
the vibration frequency in the load zone will be higher than that in the
no load region as observed in Figure 5.

Axial Shift of Roller Mass Center (Case #2)

Based on the design data supplied by the manufacturer, it is expected
that the roller mass center could be possibly shifted axially from the
geometric center by a maximum distance of 0.0005 m ($\sim$0.020 inch). Thus,
the second run is made with such an axial shift of the mass center. As
might be expected, the radial and orbital accelerations are very similar
to those observed in Case 1. However, due to the mass center being
shifted axially, the roller now experiences angular accelerations about
the transverse y and z axes as shown in Figure 6. These accelerations
may be integrated once to obtain the angular velocity which could be
integrated again to obtain the angular positions. Figure 7 shows the
ratio of roller skew and roll velocities and the skew angles β and γ*.
These skew angles could be used to compute the magnitude of roller skew and,
hence, provide some guidance for the roller-race flange clearances. It
is fairly clear from Figure 7 that the skew magnitude for this case is
no more than 2×10^{-4} degrees and, hence, the expected motion will be
no more than 2.8×10^{-5} mm, which is indeed very small for all practical
matters.

Radial Shift of Roller Mass Center (Case #3)

Once again, from the data supplied by the bearing manufacturer, a radial
shift of the mass center may not exceed 2.5×10^{-6} mm ($\sim$10 μinch). Simply
to examine the worst case, a roller motion simulation is obtained with
this maximum radial shift. In this case, only a rotating load, due to radial

---

* These angles represent rotations about the transverse y and z axes,
  respectively, [1], and they are very similar to the classical Euler
  angles.
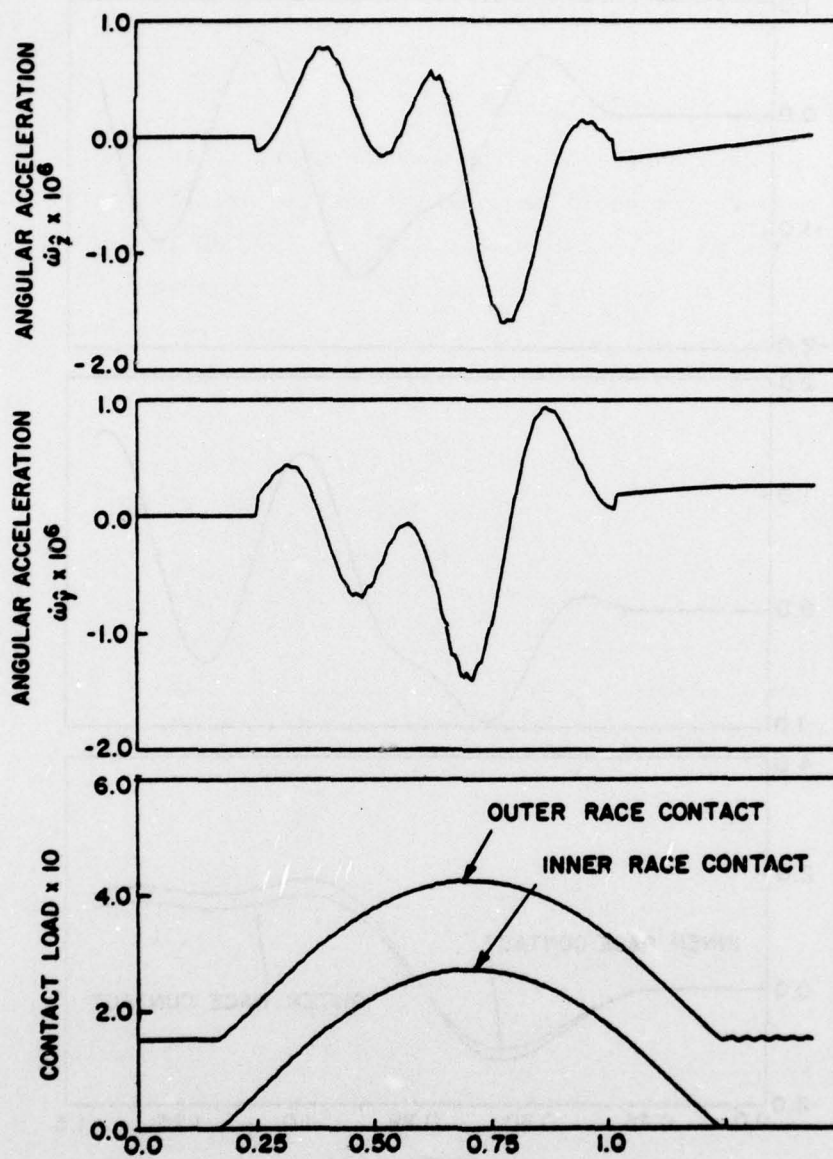
Figure 6.   Angular Accelerations Resulting from the Axial
Shift in Roller Mass Center
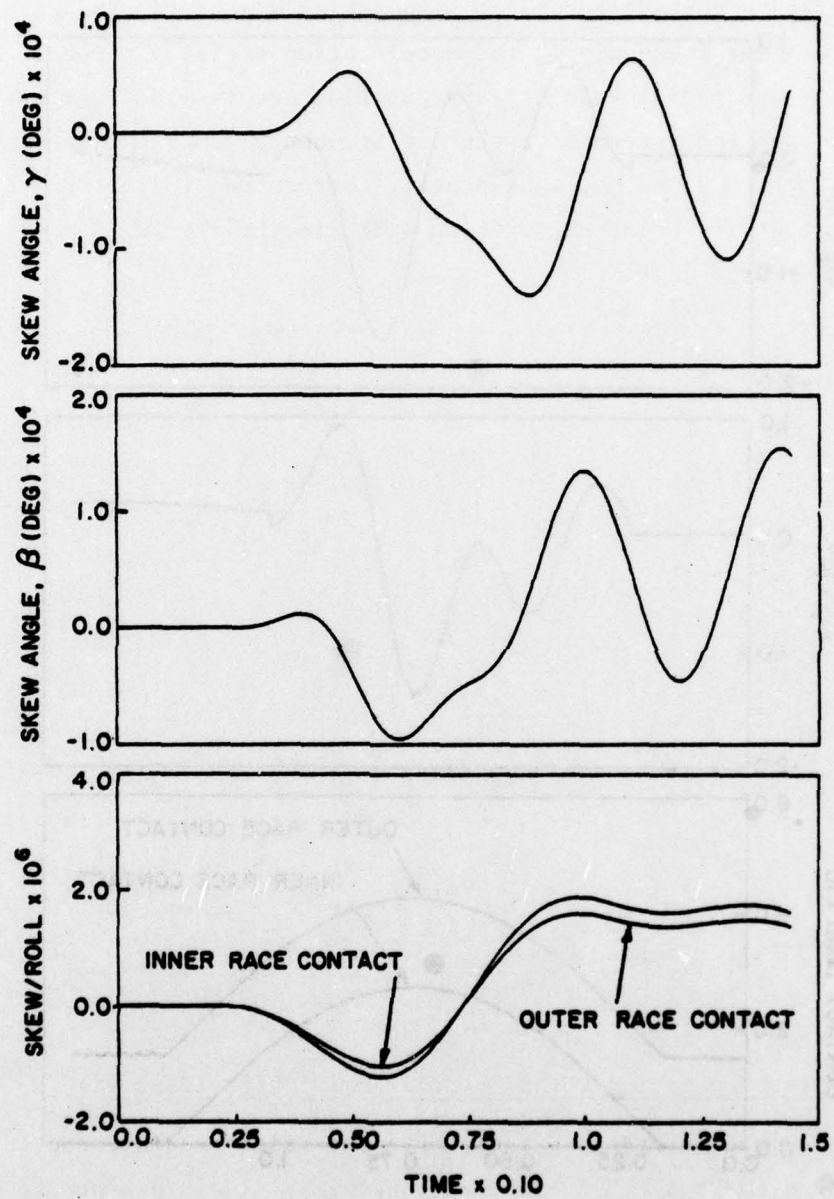
Figure 7. Roller Skew as a Result of Axial Shift of the Mass Center

unbalance, is experienced by the roller, and there is no reason for the
roller to skew. The radial and orbital accelerations, with respect to the
load zone, are shown in Figure 8. It should be noted that, in addition to
the roller-race contact resonance frequencies discussed earlier, there is
a definite lower frequency in the acceleration profiles shown in Figure 8.
In fact, if the radial velocity and position are examined, as shown in
Figure 9, then the presence of the low frequency component is very clear.
This low frequency, as may be expected, corresponds to the roller angular
velocity about its polar axis, which will also be the angular velocity of
the rotating unbalance.

Angular Shift of Polar Inertial Axis (Case #4)

From the available geometric data, it is difficult to estimate the expected
shift in the polar inertial axis. However, primarily from the run-out data
on the roller ends, it is estimated that a reasonable upper bound on the
angular shift may be assumed as 0.3 degrees. Such an angular shift by
itself may not mean very much in terms of roller skew since the roller is
constrained by the races, and the resulting skew motions may be quite small
when compared with this shift. However, it is interesting to investigate
the dynamics for the purpose of determining the oscillating roller skew
velocities. These velocities are plotted in terms of skew-to-roll ratios
in Figure 10 with reference to the load cycle. It is interesting to see
a definite oscillation in the resulting angular motion. The fact that
there is no skew velocity at time equals zero is merely due to the fact
that the initial conditions are set in such a manner while integrating the
equations of motion.

Combined Mass Center and Polar Inertial Axis Shift (Case #5)

This is the most interesting case where the axial, radial, and angular shifts
of the above cases are all combined together. Also, in order to cover a
relatively larger range of the no load regions, these simulations are
obtained for a much greater length of time than any of the above. Figure 11
shows the load cycle and the observed skew-to-roll ratios. For the purpose
of examining the roller motion in more detail, it will be necessary to note
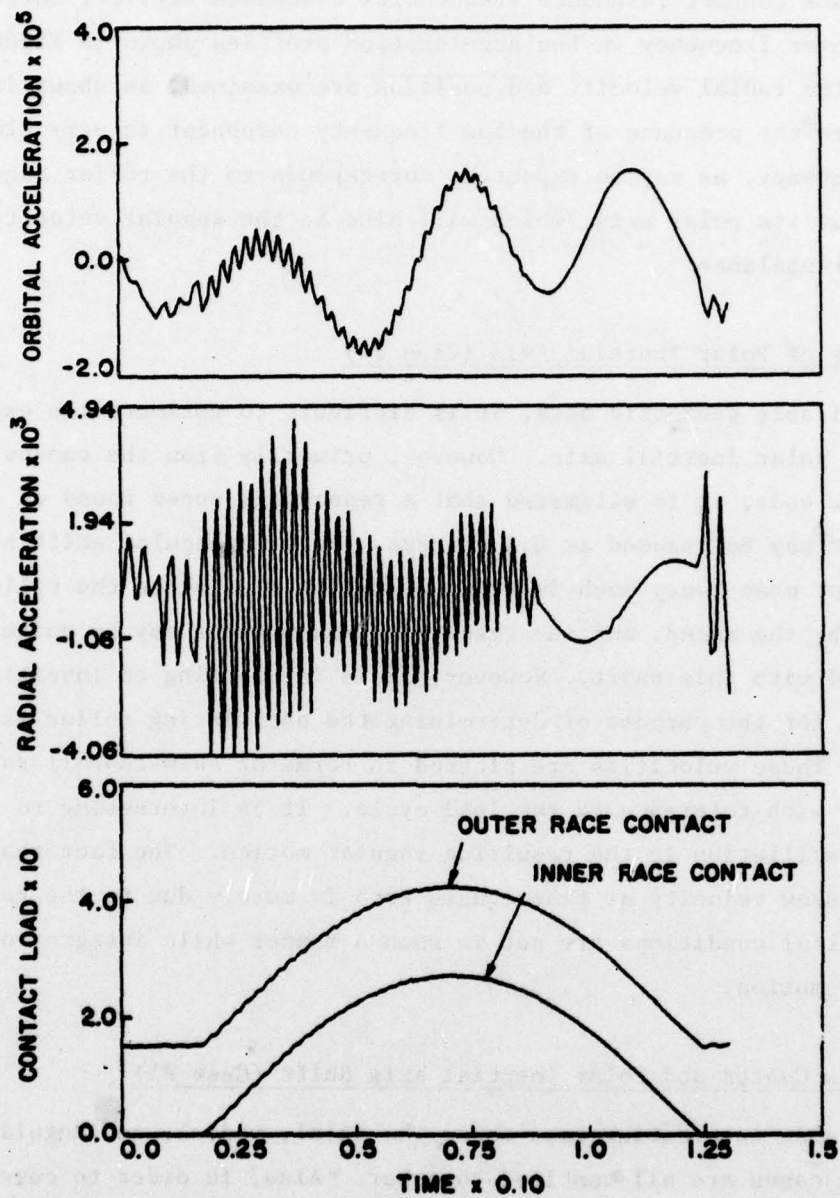
Figure 8. Acceleration of the Roller Resulting from a Radial Unbalance
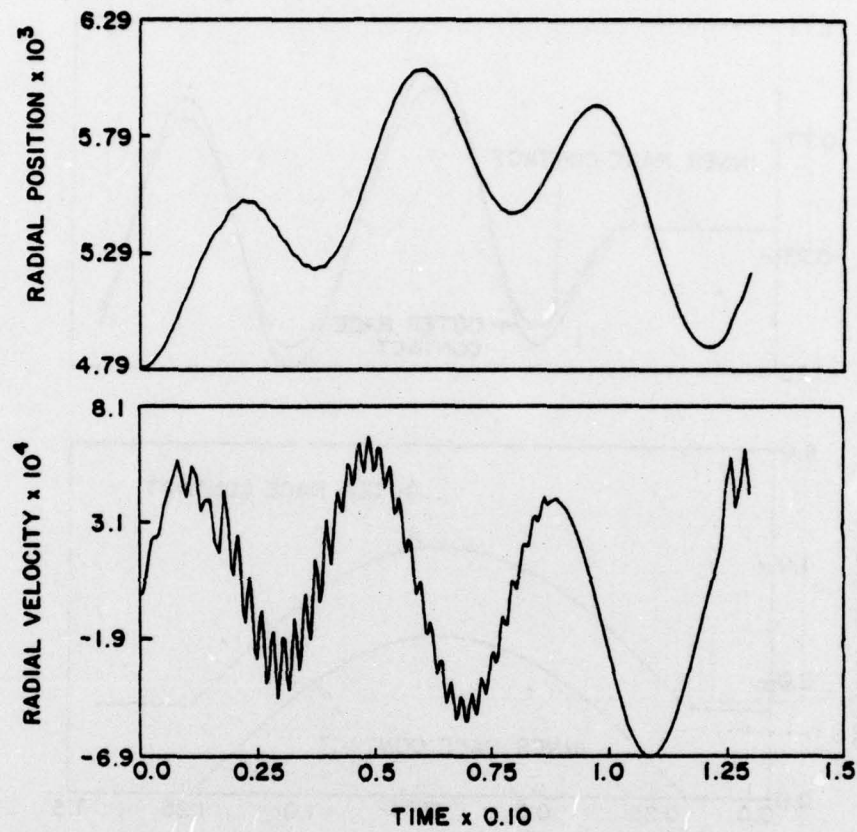
Figure 9. Radial Velocity and Position of Roller Mass
Center Resulting from Radial Unbalance
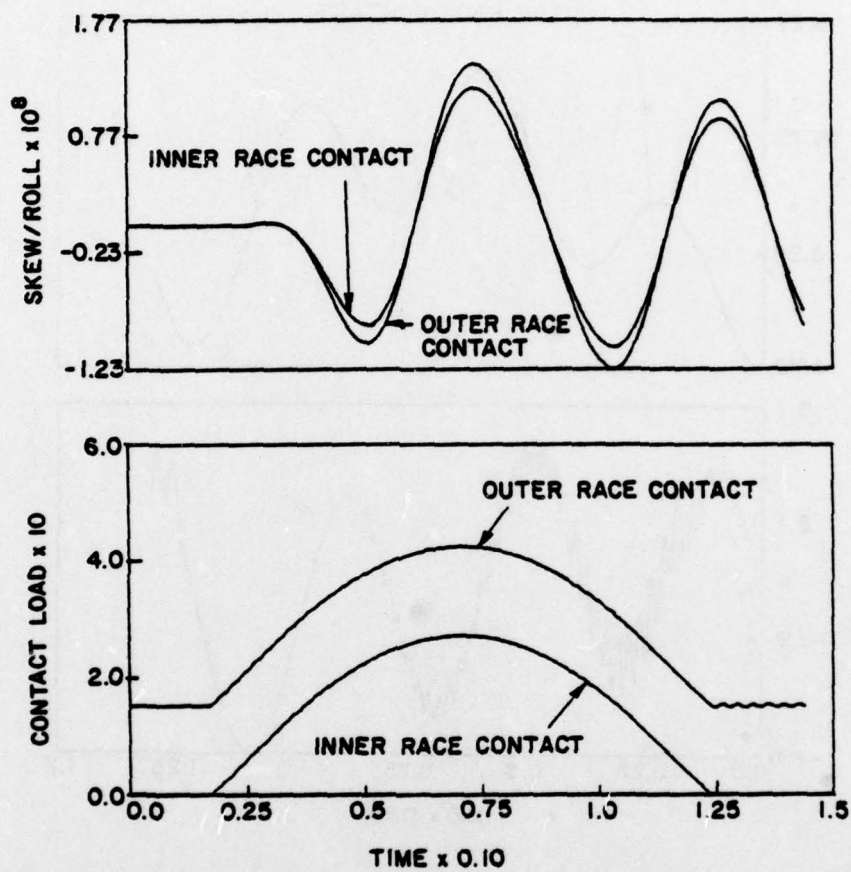
Figure 10. Roller Skew Resulting from an Angular Shift in the Polar Inertial Axis of the Roller
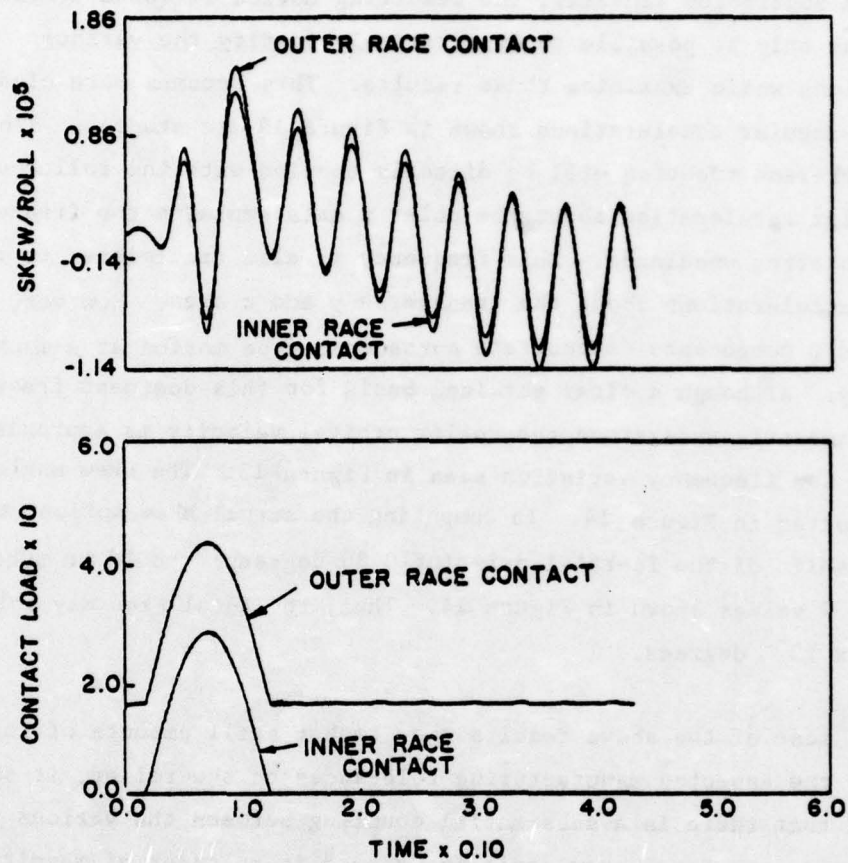
Figure 11.   Roller Skew Resulting from a Combined Mass
Center and Polar Inertial Axis Shifts

the mass center accelerations in Figure 12 and the angular acceleration
in Figure 13. The mass center accelerations demonstrate the two
frequencies corresponding to roller-race resonance and the roller angular
velocity as seen earlier in Case #3. Since all the various deviations
cannot be superposed linearly, the resulting motion is quite complicated
and it may only be possible to qualitatively justify the various
oscillations while examining these results. This becomes more clear
when the angular accelerations shown in Figure 13 are studied. Since
the roller-race traction will be directly coupled with the roller unbalance,
the angular acceleration about the polar x axis contains the frequency
of the rotating unbalance. This frequency is also transmitted to the
angular accelerations about the transverse y and z axes. However,
the y and z components demonstrate gyroscopic type motion at a much lower
frequency. Although a clear physical basis for this dominant frequency
is not presently understood, the roller orbital velocity is approximately
half the low frequency variation seen in Figure 13. The skew angle β and
γ are plotted in Figure 14. In computing the actual skew motion, the
initial shift of the inertial axis (of 0.30 degrees) should be subtracted
from the β values shown in Figure 14. Thus, the total skew may only be
about 3×10^{-3} degrees.

Although most of the above results show rather small amounts of total
skew for the expected manufacturing tolerances on the roller, it should
be noted that there is a substantial coupling between the various shifts.
For example, the total skew angle in Case #5 is an order of magnitude
larger than that in Case #2. Hence, for a given design, it will be neces-
sary to run a few roller motion simulations to determine the extent of
roller skew; or given an extent of skew the desired tolerances may be
estimated. When a number of such simulations become available for varied
applications, it may be possible to formulate some design guides. Until
then, it will be necessary to use a computer program, such as DREB, for
such design purposes.
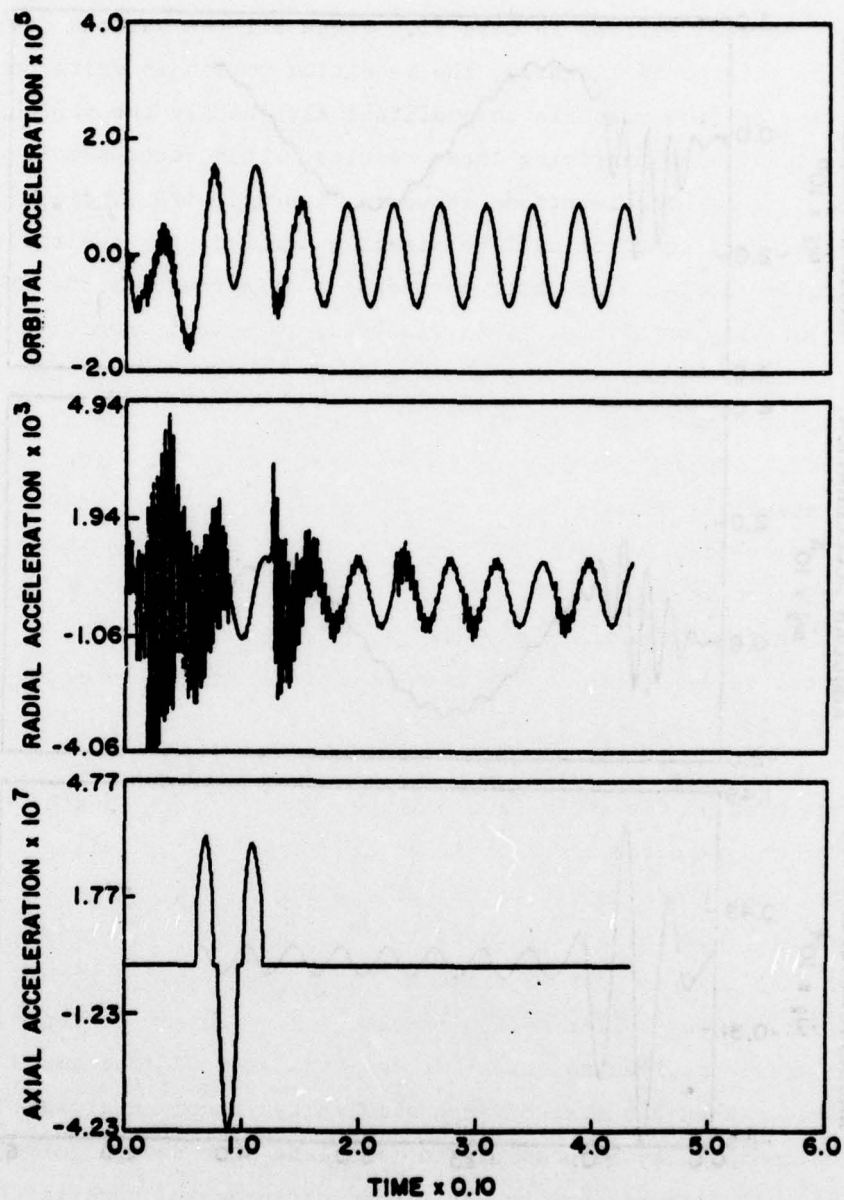
Figure 12. Roller Mass Center Accelerations Resulting from a Combined Mass Center and Polar Inertial Axis Shifts
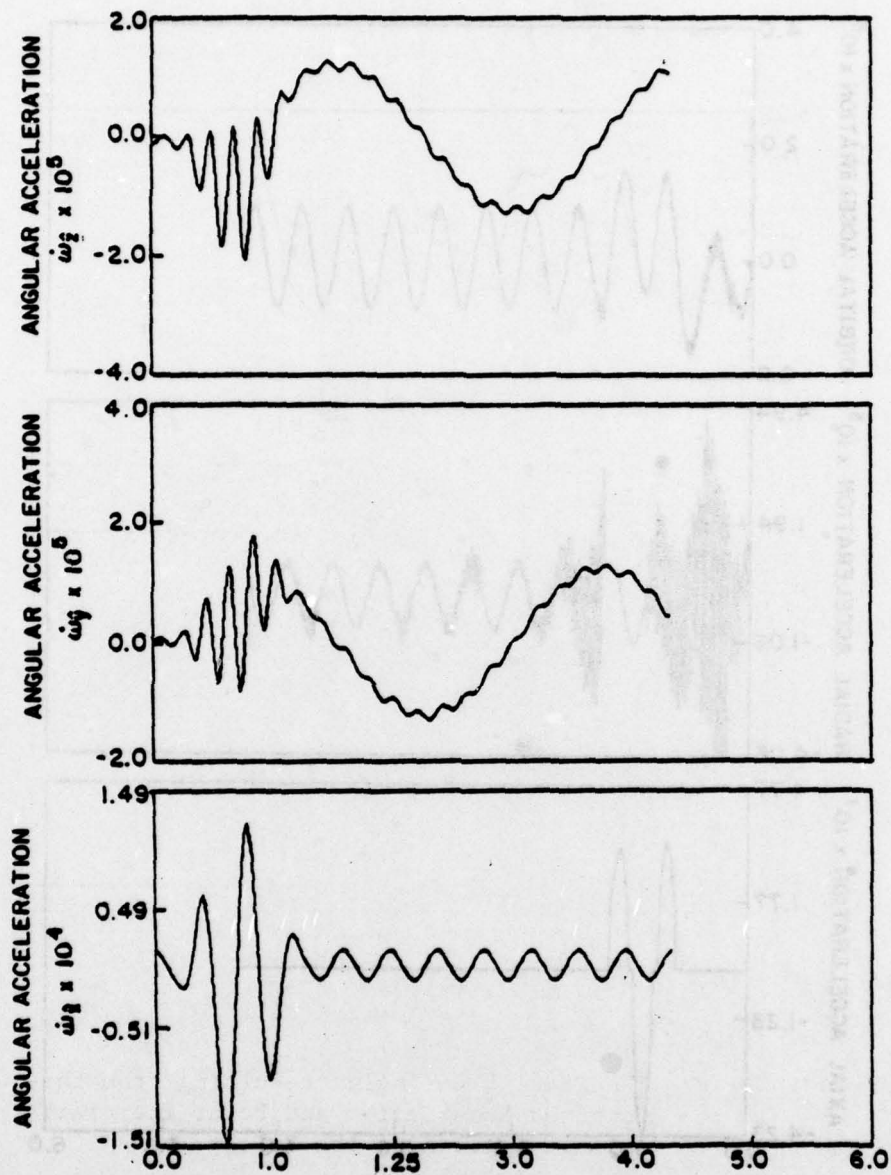
Figure 13. Angular Accelerations of the Roller Resulting from the Combined Mass Center and Polar Inertial Axis Deviations
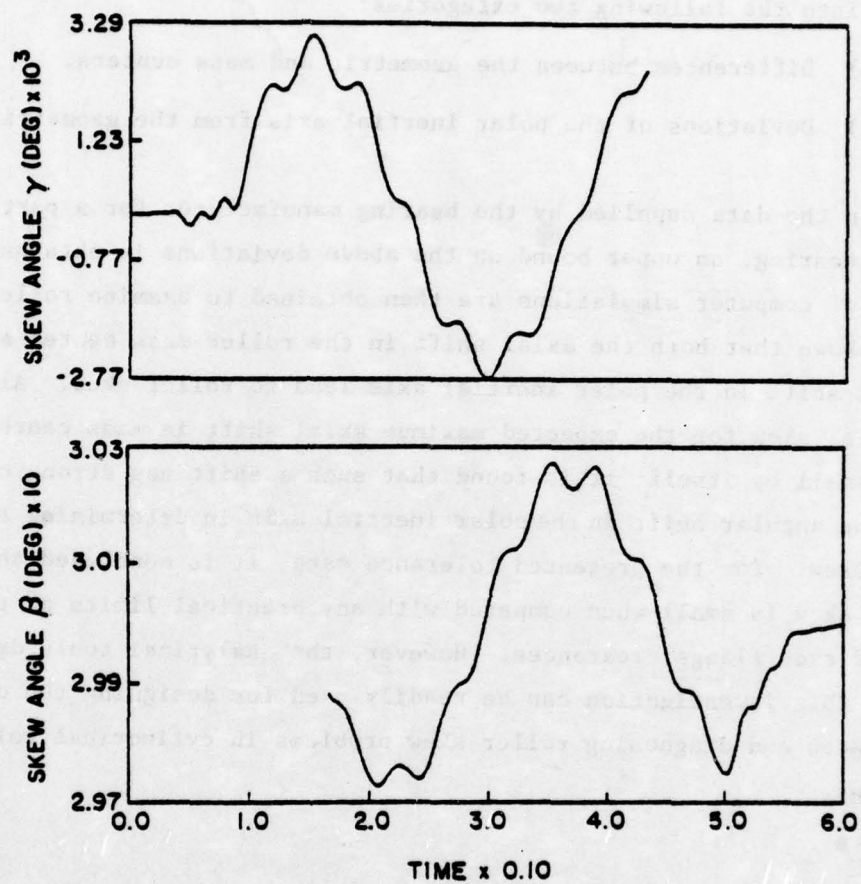
Figure 14. The Total Skew Angles Resulting from the Combined Mass Center and Polar Inertial Axis Deviations of the Roller

5. Conclusions

The dynamics of roller motion as influenced by manufacturing tolerances have been investigated. Since, from a dynamic stand point, the changes in inertial parameters will alter the general motion, all the geometrical tolerances are pooled into the following two categories:

(1) Differences between the geometric and mass centers.

(2) Deviations of the polar inertial axis from the geometric axis.

Based on the data supplied by the bearing manufacturer for a particular roller bearing, an upper bound on the above deviations is obtained. A number of computer simulations are then obtained to examine roller skew. It is shown that both the axial shift in the roller mass center and an angular shift in the polar inertial axis lead to roller skew. Although the total skew for the expected maximum axial shift in mass center seems to be small by itself, it is found that such a shift has strong coupling with the angular shift in the polar inertial axis in determining the total skew. For the presented tolerance data, it is concluded that the roller skew is small when compared with any practical limits on the roller end and race flange clearances. However, the analytical tools developed during this investigation can be readily used for designing the different tolerances and diagnosing roller skew problems in cylindrical roller bearings.

III. SPIN-UP ROLLER BALANCER RIG

The contribution of roller unbalance to the problem of roller skewing
has not been established at the present time. The possibility exists,
however, that roller unbalance, caused either by roller manufacturing
tolerances or by nonhomogeneous roller material, can lead to the
development of significant skewing forces which may accelerate bearing
failure.

In order to establish the level of unbalance generally found in typical
rollers of high speed roller bearings, it was necessary to construct a
balancing spin-up rig. This rig was constructed to test the 16 x 16 mm
rollers from the bearing described on P. 10. The resulting spin-up
rig design and subsequent evaluation of a group of 30 rollers supplied
by the Air Force are presented in this report section.

1. Spin-Up Rig Design

The spin-up rig design consists of a two-plane externally pressurized
gas bearing for the support of the subject roller, a pair of air jets
axially oriented to provide a means for positioning the roller central to
the support bearing, two tangentially oriented jets for applying the spin
torque, and a pair of noncontacting position sensors to measure the dynamic
response of spinning rollers.

Spin-Up Bearing Design

The first step in the spin-up rig design was the selection of the roller
support bearing. An air-hydrostatic (externally pressurized) bearing was
selected because of its low friction torque and clean operation. Several
bearing types were evaluated including those shown in Figure 15. The single
row central feed bearing was discarded as an impractical bearing type
because, when acting alone, this bearing provides a negligible angular
stiffness. Both the double row single bearing and single row double bearing
were analyzed for performance so that a logical selection could be made.

Each bearing was analyzed according to design equations and procedures
found in "Design of Gas Bearing," Volumes I and II, Mechanical Technology
Incorporated, 1971. The analysis considers, as common parameters, those shown
on the following page,
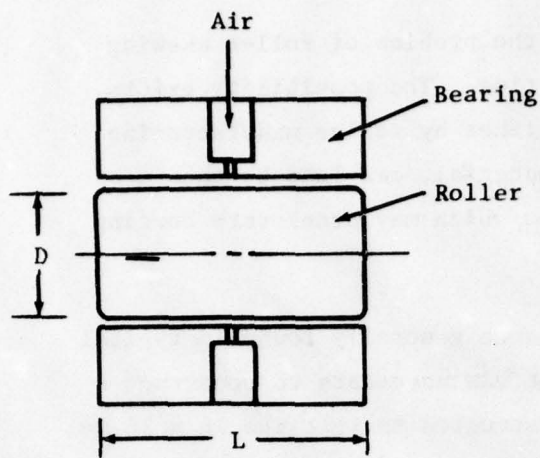
Air

Bearing

Roller

Single Row - Central Feed

D

L

Air   Air

Bearing

Roller

Double Row Single Bearing

D

L_1

L

Air   Air

Bearing

Roller

Single Row Double Bearing

D

Vent
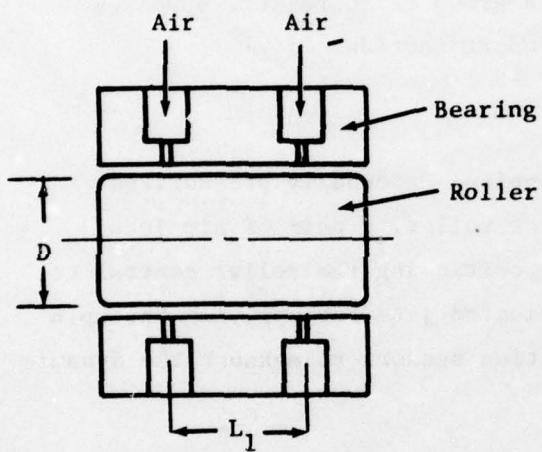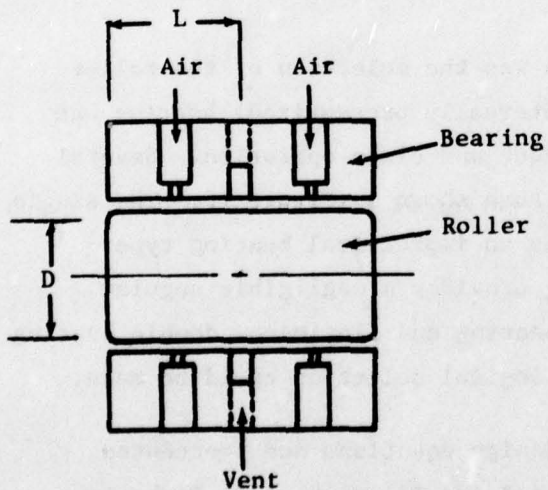
Figure 15. Spin-Up Support Bearing Type

- For Room Temperature Air

    Gas Constant: $R = 2.47 \times 10^5 \dfrac{\text{in.}^2}{\text{sec}^2 \, {}^\circ R}$

    Viscosity: $\mu = 2.7 \times 10^{-9} \dfrac{\text{lb sec}}{\text{in.}^2}$

    Density: $\rho = 1.12 \times 10^{-7} \dfrac{\text{lb sec}^2}{\text{in.}^4}$

- For the Roller

    Weight: $W_r = 0.055$ lb

    Density: $\rho = 1.42 \times 10^{-4} \dfrac{\text{lb sec}^2}{\text{in.}^4}$

    Polar Moment of Inertia: $I_p = 1.41 \times 10^{-5}$ in.-lb-sec^2

    Transverse Moment of Inertia: $I_T = 8.25 \times 10^{-6}$ in.-lb-sec^2

Each bearing type was sized so that its overall length was equal to the roller length between the corner break-out locations on the crown. This length selection resulted in the following fixed nominal bearing geometric parameters.

	Single Row Double Bearing	Double Row Single Bearing
Length	L = 0.21	0.42
Diameter	D = 0.63	0.63
L/D	= 0.333	0.667

A parametric study for each bearing type was performed for the following dependent variables:

Number of Air Feed Holes Per Row: N

Diameter of Feed Holes: d_o

Radial Clearance: C

Supply Pressure: P_s

Calculated performance for the two bearing types based on the fixed parameters already listed is shown in Table 1.

TABLE 1

CALCULATED PERFORMANCE FOR TWO BEARING TYPES

		Single Row Double Bearing	Double Row Single Bearing	Final Design Single Row Double Bearing
Diameter (nominal)	$D =$	16 mm	16 mm	16 mm
Length	$L =$	0.42 inch	0.42 inch	0.42 inch
Clearance (radial)	$C =$	7×10^{-4} inch	7×10^{-4} inch	7×10^{-4} inch
Number of feed orifices per row	$N =$	22	20	20
Orifice diameter	$d_o =$	0.050 inch	0.025 inch	0.042 inch
Operating eccentricity ratio	$E =$	0.5	0.5	0.5
Nominal supply pressure	$P_s =$	8 psig	13 psig	13 psig
Nominal flow rate	$Q =$	0.14 SCFM	0.08 SCFM	0.10 SCFM
Radial stiffness	$K_R^* =$	172 lb/in.	128 lb/in.	
Angular stiffness	$K_\theta^* =$	calculated from K_R	$0.76 \frac{\text{in.-lb}}{\text{RAD}}$	
Radial damping	$B_r =$	$1.25 \times 10^{-2} \frac{\text{lb-sec*}}{\text{in.}}$	$1.82 \times 10^{-2} \frac{\text{lb-sec}}{\text{in.}}$	
Angular damping	$B_\theta =$	calculated from B_r	$1.08 \times 10^{-4} \frac{\text{lb-sec}}{\text{in.-RAD}}$	
Radial critical speed	$f_r =$	10,300 rpm	9,200 rpm	
Angular critical speed	$f_A =$	6,050 rpm	3,800 rpm	

The final bearing design which was used in the spin-up rig was a compromise between the two tabulated designs. The fewer number of orifices from the double row design were maintained with the larger orifice size of the double bearing design. The final double bearing design was established by providing a vented mid-plane groove separating the bearing into two halves. This design compromise permitted a bearing design more easily fabricated to assure somewhat higher critical speed levels and better amplification of the unbalance response.

$K_\theta = K_R L^2/2$ in.-lb/RAD

$B_\theta = B_r L^2/2$ lb-sec/in.-RAD

Spin-Up Rig Construction

The general configuration of the spin-up balancing rig is shown in Figure 16. Identified in this side elevation view is the test roller (1) supported by the hydrostatic air bearing (2). The bearing obtains air supply through the inlet air fitting (3), in the drilled passages (4) leading to an internal manifold. Spin-up torque for the roller is provided by two drive nozzles (5), one secured to each side of the main support housing (6). Internal manifolding within the rig base (7) and the housing (6) provide the air passages for the spin-up nozzles.

Two axial positioning jets are also included in the spin-up design but are not shown in Figure 16. The axial jets are used to accurately position the rollers so that they are located symmetrically in the spin-up bearing.

Measurement of the response of a spinning unbalanced roller is obtained by determining the output voltage of two capacitance position sensors (8) which are secured to both sides of the housing and view each end of a roller just inboard of the corner breakout location on the crown.

A photographs of the fully assembled spin-up balancer is shown in Figure 17. Identified on the photograph are all the significant rig components and, in addition, a balancing phase angle marker attached to the hydrostatic bearing.

Spin-Up Balancer Instrumentation

Successful application of the spin-up balancing rig depends on the ability to accurately measure the roller response during a balance evaluation. A successful and very accurate measurement instrument applied to this program is a capacitive probe distance measuring system built by Wayne Kerr, Ltd., incorporating specially designed probes provided by MTI's Boice Instrument Division.

The probe amplifier combination is matched to provide a 1.0 volt output voltage for full range of the particular probe employed. For these tests, two special probes having a full scale range between 0.001 and 0.002 inch were constructed. Figure 18 presents a photograph of one of the special probes. Both probes were supplied with precision calibrations which are shown in Figure 19; this figure shows that the probe sensitivities actually attained were 1.235 and 1.291×10^{-3} inches/volt.
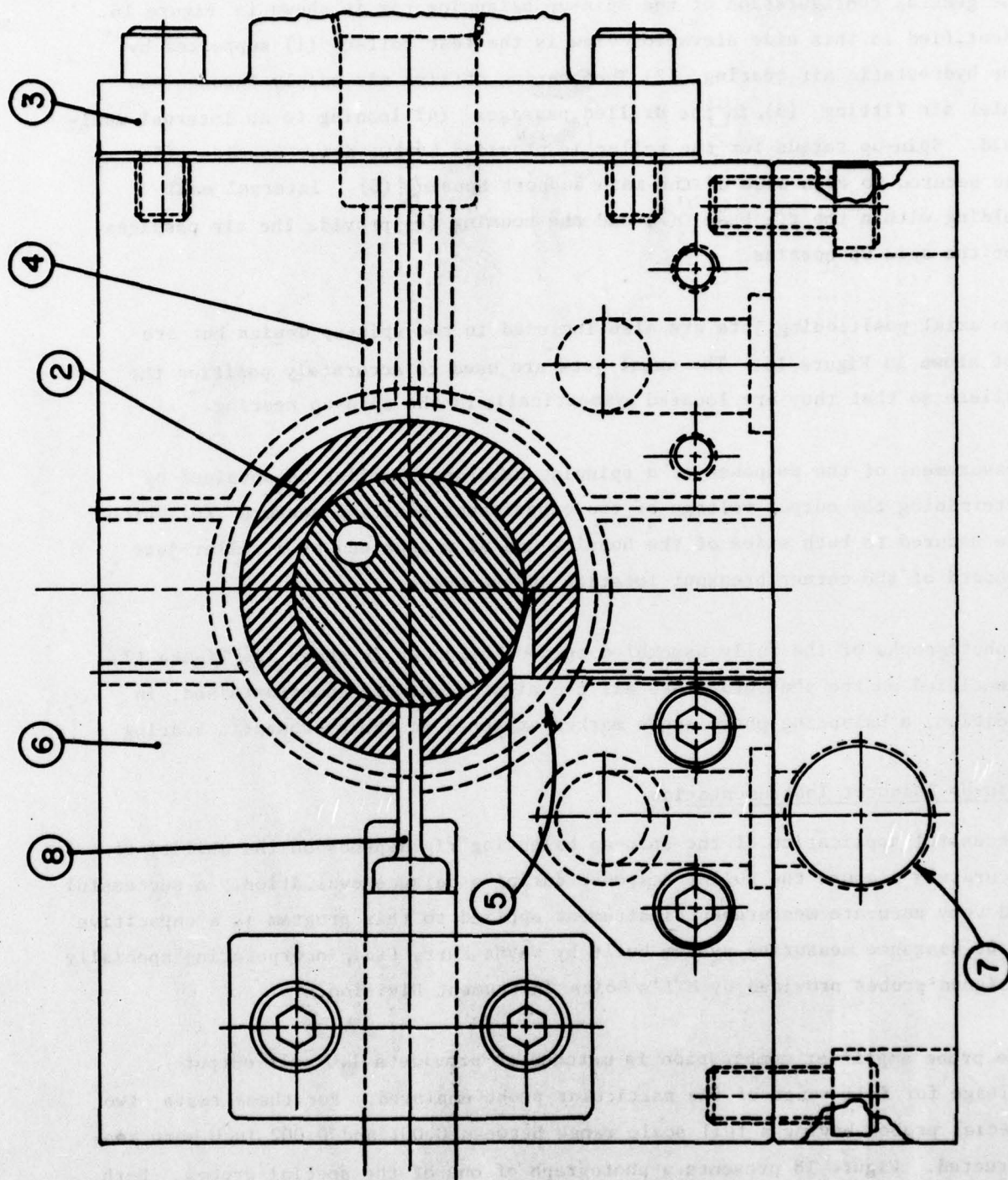
Figure 16. Spin-Up Balancing Rig Elevation View
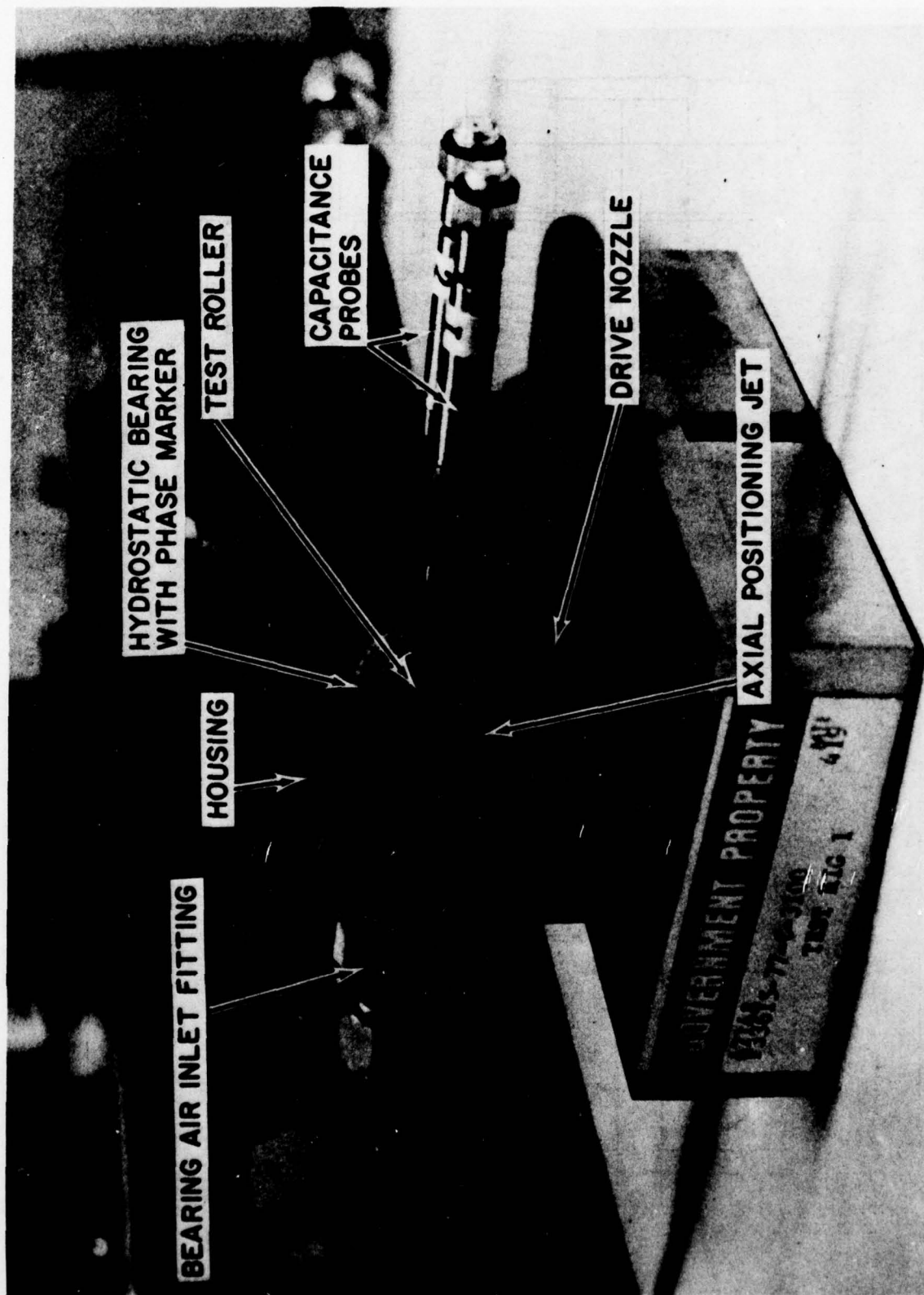
Figure 17. Spin-Up Balancing Rig Photograph View
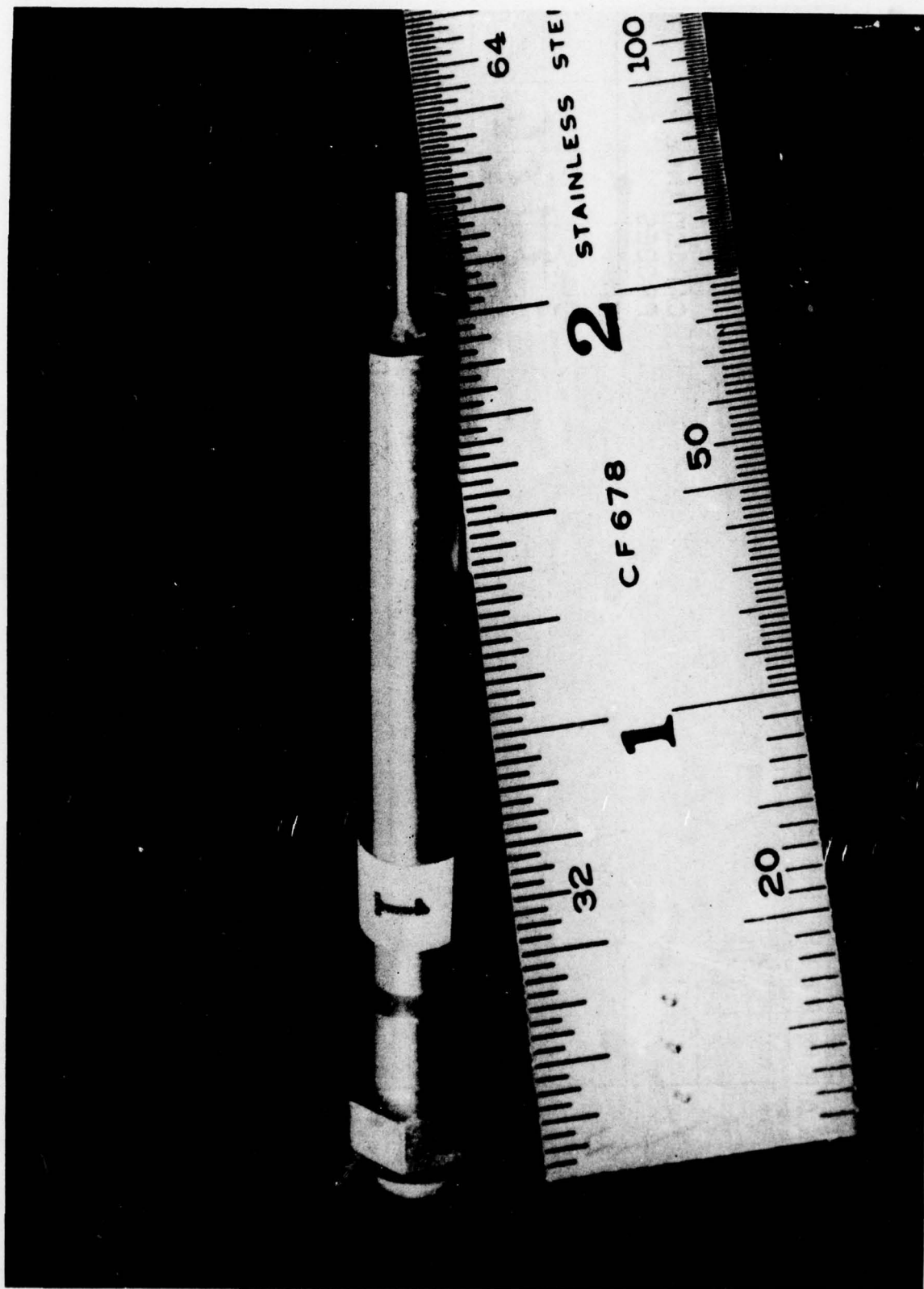
Figure 18. Capacitance Probe
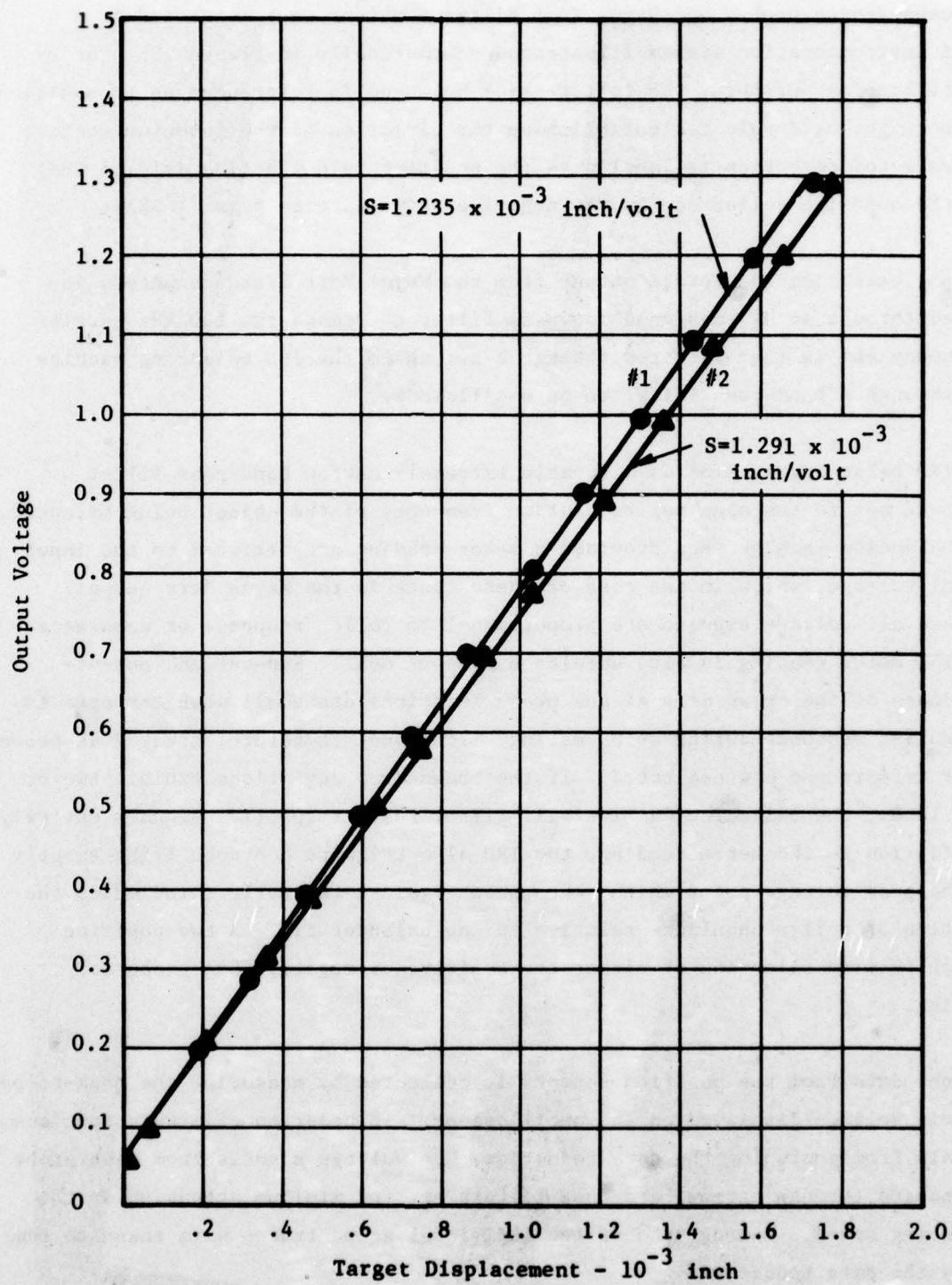
Figure 19. Capacitance Probe Calibration

The capacitance probes and Wayne Kerr distance meters were connected into a total instrumentation system illustrated schematically in Figure 20. For identification purposes, the roller being balanced is referenced as to position by the right-hand rule for establishing the direction of the momentum vector; the selected direction is labeled as the positive spin reaction axis (+ SRA) and the opposite roller end as the negative spin reaction axis (- SRA).

For any balancing run, probe output from the Wayne Kerr distance meters is passed through an MTI-designed low-pass filter to remove the 100 kHz carrier frequency and is then directed through a switch to the IRD balancing machine and through a band-pass filter to an oscilloscope.

The IRD balancing machine is a tunable, extremely narrow band-pass filter which is set to the once per revolution frequency of the object being balanced. The balancing machine then provides a meter reading proportional to the input signal voltage, which in the case of these tests is the Wayne Kerr output. Because all voltage signals are proportional to roller response or unbalance, the IRD meter reading is also unbalance proportional. Run-out and out-of-roundness of the crown drop at the probe locations are small when compared to the roller response during spin testing. They are, therefore, treated as second order effects and are neglected. If the crown drop deviations exhibit two or more lobes, the balancing machine will filter their respective signals entirely. In addition to the meter reading, the IRD also triggers a strobe light exactly at the peak voltage point which, when shown against the roller, indicates the location of roller unbalance relative to the balancer rig. A two-position switch permits selection of either the positive or negative SRA probe for reading.

Further data from the position sensors is collected by measuring the peak-to-peak dynamic voltage displayed on the oscilloscope. In order to eliminate spurious signals from confusing the data reduction, the voltage signals from each probe are passed through narrow band-pass filters set for minimum attention at the balancing speed. Photographs of the individual scope traces were taken to simplify the data reduction.

The entire instrumentation system through to the oscilloscope was calibrated to account for system attenuation. Each filter inserted in the signal line produces

-38-

Roller

+SRA

#1   #2

SN 487   Wayne Kerr
          DM-100   Wayne Kerr   SN 458
                                    DM-100

          A_1 A_2

SN 51   MTI Filter
          FBO-LC-15   MTI Filter   SN 61
                                    FBO-LC-15

B_1 B_2

                    IRD Balancer
                    MOD 600

SN 440   SKL Filter
          308A   SKL Filter   SN 604
                                    308A

C_1 Tektronix C_2
                     502A
                     Oscilloscope
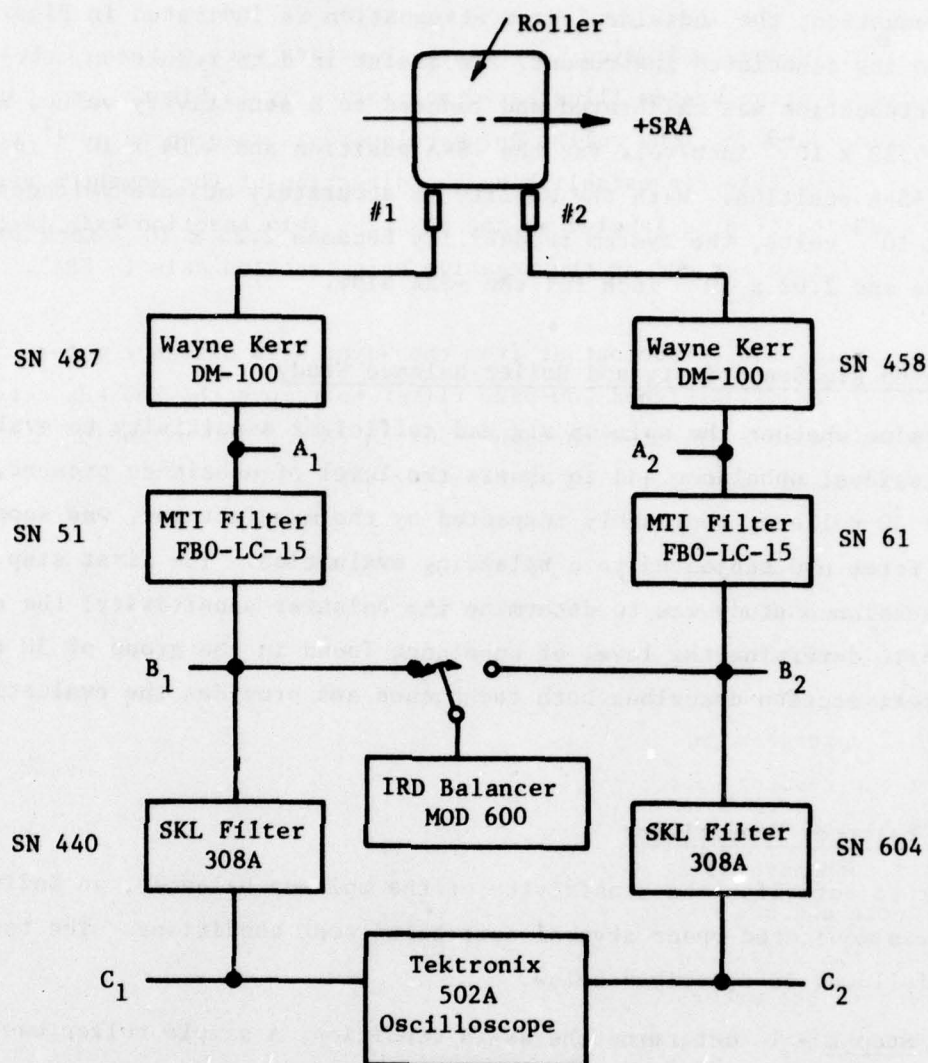
Voltage Levels

$A_1 = 1.000$ $A_2 = 1.000$
$B_1 = 0.934$ $B_2 = 0.945$
$C_1 = 0.275$ $C_2 = 0.319$

Overall Sensitivity; Probe #1 - 4.50×10^{-3} inch/volt;
                     Probe #2 - 4.04×10^{-3} inch/volt

Figure 20. Instrumentation Schematic: Spin-Up Rig Evaluation

some attenuation; the individual item attenuation is indicated in Figure 20 adjacent to its associated instrument. To assist in data reduction, the total system attenuation was calibrated and reduced to a sensitivity value, which becomes 4.50×10^{-3} inch/volt for the -SRA position and 4.04×10^{-3} inch/volt for the +SRA position. With the ability to accurately measure voltages as low as 0.5×10^{-3} volts, the system readability becomes 2.25×10^{-6} inch for the -SRA side and 2.02×10^{-6} inch for the +SRA side.

2. Spin-Up Rig Sensitivity and Roller Balance Study

To determine whether the spin-up rig had sufficient sensitivity to evaluate roller residual unbalance and to assess the level of unbalance present, a group of 30 rollers, thoroughly inspected by the manufacturer, was supplied by the Air Force and subjected to a balancing evaluation. The first step in the roller unbalance study was to determine the balancer sensitivity; the second step was to determine the level of unbalance found in the group of 30 rollers. This report section describes both techniques and provides the evaluation results.

Spin-Up Balancer Sensitivity

In order to establish the sensitivity of the spin-up balancer, an individual roller was monitored under several controlled test conditions. The test procedure followed is described below.

- Step 1 - To determine the as-is condition, a sample roller was installed in the spin-up rig and the axial positioner jets located so they held the roller central to the spin-up bearing with 0.005 inch clearance per side. The pressure to the jets was adjusted to 30 psig, the bearing pressure to 20 psig, and drive nozzle pressure versus roller speed data taken. The results of this test indicated a tester critical speed of 9100 rpm and produced the speed versus pressure curve shown in Figure 21.

- Step 2 - A roller of known weight was index marked with a felt-tip pen on one end and then rotated at 13,500 rpm in the spin-up rig. After taking the balance machine readings of amplitude and phase angle, the scope display amplitudes for both the positive and negative SRA
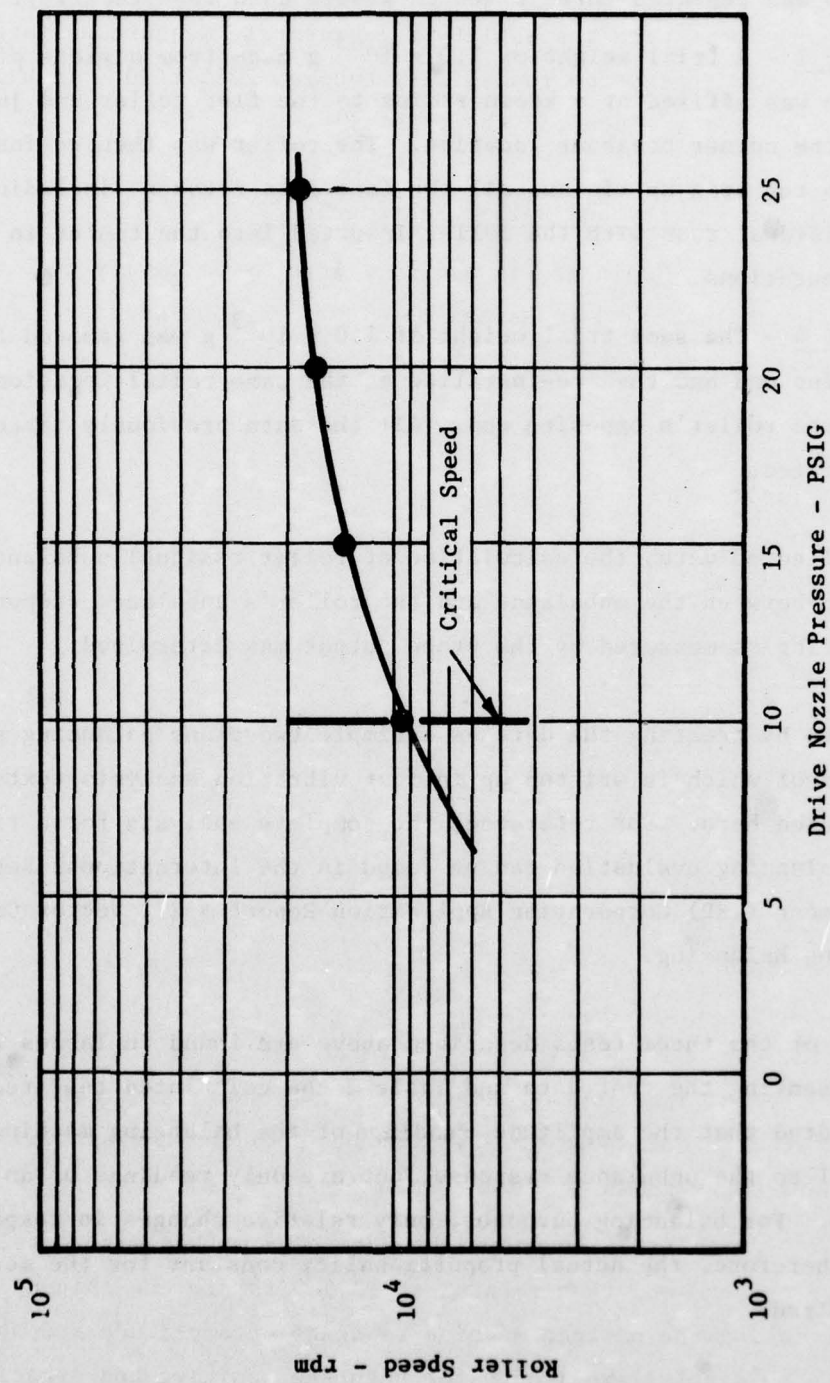
Figure 21. Spin-Up Rig Drive Nozzle Calibration

probes were photographed. After taking the test data, the roller was reversed in the spin-up rig and the test data retaken. This step was repeated three times to assure data repeatability.

- Step 3 - A trial weight of 1.0×10^{-3} g made from a piece of plastic tape was affixed at a known radius to the flat roller end just inboard of the corner breakout location. The roller was then re-installed into the spin-up rig and all the test data retaken, including three individual runs with the roller inserted into the tester in both orientations.

- Step 4 - The same trial weight of 1.0×10^{-3} g was removed from the roller end and then re-installed at the same radial location but on the roller's opposite end. All the data previously taken were repeated.

From the collected data, the calculation of roller residual unbalance and the relationship between the unbalance and the roller's unbalance response in the spin-up bearing as measured by the probe output was determined.

This was done by treating the data as a simple two-plane balancing problem, the solution of which is written up in most vibration analysis texts and will not be repeated here. For reference, the complete analysis for a rigid body two-plane balancing evaluation can be found in the International Research and Development (IRD) Corporation Application Report #327, Vector Calculations for Two-Plane Balancing.

The results of the three tests described above are found in Tables 2 and 3, Table 2 presenting the test data and Table 3 the calculated test results. It should be noted that the amplitude readings of the balancing machine are proportional to the unbalance response, but are only readings of an arbitrary meter scale. For balancing purposes, only relative changes in response are required; therefore, the actual proportionality constant for the meter reading is not required.

TABLE 2

SPIN-UP BALANCER SENSITIVITY TEST DATA

ORIGINAL ROLLER

Forward*
Double Amplitude

#1 Probe	#2 Probe	Scope Sensitivity
1.9 cm	2.4 cm	5 mv/cm

Reverse*
Double Amplitude

#1 Probe	#2 Probe	Scope Sensitivity
2.2 cm	2.4 cm	5 mv/cm

Trial Weight		Balance Machine Readings			
		+SRA		-SRA	
Size	Location	Relative Amplitude	Phase Angle	Relative Amplitude	Phase Angle
	None	.095	255°	.085	185°
		.095	255°	.085	185°
		.090	250°	.085	185°
1×10^{-3} g	+SRA	.225	230°	.045	140°
		.230	230°	.045	140°
		.230	225°	.035	130°
1×10^{-3} g	-SRA	.165	235°	.030	55°
		.165	230°	.035	55°
		.170	235°	.030	60°
	None	.095	65°	.090	345°
		.100	65°	.095	345°
		.100	65°	.095	345°
1×10^{-3} g	+SRA	.070	170°	.135	5°
		.065	170°	.135	10°
		.065	170°	.135	10°
1×10^{-3} g	-SRA	.045	100°	.190	10°
		.045	100°	.185	10°
		.045	100°	.190	10°

Forward = Identified end of roller at -SRA side of balancer

Reverse = Identified end of roller at +SRA side of balancer

TABLE 3

SPIN-UP BALANCER SENSITIVITY

CALCULATED RESULTS

Forward Data

Run	Trial Weight 10^{-3} g	+SRA		-SRA	
		Relative Amplitude	Phase Angle	Relative Amplitude	Phase Angle
1	0.000	.093	253°	.085	185°
2	1.000	.228	228°	.042	137°
3	1.000	.167	233°	.032	57°

Correction Weight on Near End = 1.434
at Phase Angle = -155.6°
Correction Weight on Far End = 1.49
at Phase Angle = 14.3°

Reversed Data

Run	Trial Weight 10^{-3} g	+SRA		-SRA	
		Relative Amplitude	Phase Angle	Relative Amplitude	Phase Angle
1	0.000	.098	65°	.093	345°
2	1.000	.067	170°	.135	8°
3	1.000	.045	100°	.188	10°

Correction Weight on Near End = 1.310
at Phase Angle = 12.9°
Correction Weight on Far End = 1.264
at Phase Angle = 167.3°

Location	Unbalance* 10^{-6}in.-oz.		Response Double Amplitude 10^{-6} inch		Sensitivity Unbalance/Response		Angular Displacement of Unbalance	
	FWD	REV	FWD	REV	FWD	REV	FWD	REV
+SRA	11.8	10.1	42.7	48.5	0.28	0.21	169°	155°
-SRA	12.2	10.4	49.5	48.5	0.25	0.21		

*Based on roller weight W_R = 24.7356g (0.0545 lb).

The results indicated that the tested roller had a residual unbalance of approximately 10-12 x 10^{-6} in.-oz. per end and that the unbalance was displaced about 162° end-for-end.

The overall accuracy of all the calculated results and the differences between the forward and reverse roller position data hinges on four important parameters. These are:

1. The exact weight of the trial weight
2. The exact radial placement of the trial weight
3. The exact angular placement of the trial weight
4. Instrumentation accuracy

As an example, a balancing run taken on a second roller within the thirty roller group produced the balance results shown in Table 4.

TABLE 4
BALANCE RESULTS - SECOND ROLLER WITHIN 30 ROLLER GROUP

Run	Trial Weight 10^{-3} g	+SRA Relative Amplitude	+SRA Phase Angle	-SRA Relative Amplitude	-SRA Phase Angle
1	0.000	.159	224°	.169	90°
2	1.000	.040	80°	.150	113°
3	1.000	.230	223°	.232	75°

Correction Weight on Near End = 0.813
at Phase Angle = -79.4°
Correction Weight on Far End = 2.624
at Phase Angle = 123.5°

A second zero trial weight run with the same roller resulted in slightly different +SRA data, the new data being at a relative amplitude of 0.158 and as phase angle of 227°. The calculations for the new zero weight condition produced the results shown in Table 5.

-45-

TABLE 5

CALCULATIONS FOR NEW ZERO WEIGHT CONDITION

Run	Trial Weight 10^{-3} g	+SRA Relative Amplitude	+SRA Phase Angle	-SRA Relative Amplitude	-SRA Phase Angle
1	0.000	.158	227°	.169	90°
2	1.000	.040	80°	.150	113°
3	1.000	.230	223°	.232	75°

Correction Weight on Near End = 0.631
at Phase Angle =-88.5°
Correction Weight on Far End = 2.534
at Phase Angle =-126.8°

From these two runs, it can be seen that for the roller response in this spin-up rig only a 0.001 amplitude and a 3° difference for the zero condition at the +SRA end amounted to an approximate 28 percent change in correction weight at the + end with phase angle shift of 9°, and a 3-1/2 percent correction weight change at a phase angle change of 3.3°.

It is evident from the above that the accuracy in the measurement of the roller response has a serious effect on the final results. To further identify the area of test error, a third roller was evaluated, but in this case the trial weights were discarded after each data run and were replaced with new weights.

The results of these data runs are used in Tables 6 and 7 for the test data and calculated results, respectively.

TABLE 6

SPIN-UP BALANCER TEST DATA

Forward*

Double Amplitude

#1 Probe	#2 Probe	Scope Sensitivity in volt/cm
2.5 cm	4.2 cm	5

Reverse*

Double Amplitude

#1 Probe	#2 Probe	Scope Sensitivity in volt/cm
3.2 cm	3.4 cm	5

Trial Weight		Balance Machine Readings				
Size	Location	+SRA		−SRA		
		Relative Amplitude	Phase Angle	Relative Amplitude	Phase Angle	
	None	.185	150	.130	20	Forward
		.185	150	.130	20	
		.185	150	.130	20	
$1.0 \times 10^{-3} g$	+SRA	.160	115	.080	15	
		.160	110	.070	10	
		.160	110	.080	10	
$1.0 \times 10^{-3} g$	−SRA	.240	.165	.240	25	
		.245	165	.240	20	
		.245	165	.240	20	
	None	.160	225	.165	90	
		.155	225	.170	90	
		.160	225	.170	90	Reverse
$1.0 \times 10^{-3} g$	+SRA	.040	80	.150	115	
		.040	80	.150	115	
		.040	80	.150	110	
$1.0 \times 10^{-3} g$	−SRA	.230	225	.230	75	
		.230	220	.230	75	
		.230	225	.235	75	

Forward: Identified end of roller at −SRA side of balancer.
Reverse: Identified end of roller at +SRA side of balancer.

TABLE 7
SPIN-UP BALANCER SENSITIVITY CALCULATED RESULTS

Forward Data

Run	Trial Weight 10^{-3} g	+SRA Relative Amplitude	+SRA Phase Angle	-SRA Relative Amplitude	-SRA Phase Angle
1	0.000	.185	150°	.130	20°
2	1.000	.160	112°	.077	12°
3	1.000	.247	165°	.240	21°

Correction Weight on Near End = 1.905
at Phase Angle = -90.7°
Correction Weight on Far End = 1.372
at Phase Angle = -139.4°

Reverse Data

Run	Trial Weight 10^{-3} g	+SRA Relative Amplitude	+SRA Phase Angle	-SRA Relative Amplitude	-SRA Phase Angle
1	0.000	.159	224°	.169	90°
2	1.000	.040	80°	.150	113°
3	1.000	.230	223°	.232	75°

Correction Weight on Near End = 0.812
at Phase Angle = -79.4°
Correction Weight on Far End = 2.624
at Phase Angle = -123.5°

Location	Unbalance* 10^{-6} in.-oz. FWD	REV	Response Double Amplitude 10^{-6} inch FWD	REV	Sensitivity Unbalance Response in.-oz./inch FWD	REV	Angular Displacment of Imbalance FWD	REV
+SRA	15.8	6.7	56.2	84.8	.28	.08		
-SRA	11.3	21.7	72.0	68.7	.16	.32	49	44

*Based on roller weight W_R = 24.6914g

The sensitivity data for the third roller tested, although it essentially reflects the data collected for the first roller, is significantly more scattered indicating the effects of the trial weight placement and size error effect.

Roller Residual Unbalance

At the conclusion of the spin-up rig sensitivity evaluation, all except 9 of the 30 rollers supplied by the Air Force for the balancing evaluation were checked for residual unbalance. The procedure followed for evaluating each roller was:

- The roller was weighed.

- The roller was identified and spun to 13,500 rpm in the balancing rig and all data for balance taken.

- A trial weight of approximately 0.5×10^{-3}g was added to the +SRA roller end at a radius of approximately 0.235 inch and all the balance data retaken.

- The trial weight at the +SRA side was replaced with a trial weight at the -SRA, along the same longitudinal roller axis and at the same radius and all the balance data retaken.

- The results of the two-plane balancing calculation determined the necessary weight correction multiplier to achieve perfect balance. The weight correction multiplier, when used in the following relationship, determined the residual unbalance of the roller.

  Residual Unbalance = Trial Weight x Trial Weight Correction x Conversion Factor (grams to ounces) x The Trial Weight Radius

Table 8 shows the balance data as recorded during the testing; Table 9 shows the calculated residual unbalance in both inch-ounces and inches along with the angular displacement between the unbalance vectors at the roller ends. The mean value of residual unbalance along with the standard deviation among the rollers studied is shown in Table 10.

TABLE 8
ROLLER RESIDUAL UNBALANCE TEST DATA

Balancing of Trial Rollers

Roller #	Photo#	CRO Sens	Sweep	Amplitude	IRD Readings Angle	Amplitude	Angle	Trial Weight (g) wt	Angle side	Roller Weight (g)
10	3	5 mv/cm	10 msec/cm	30	0°	25	100°	0		24.7045
-				57	350°	31	140°	$.5 \times 10^{-3}$	270 +side	
-				15	15°	20	50°	$.5 \times 10^{-3}$	270 -side	
11	4	"	"	32	320°	33	60°	0		24.7131
-				62	320°	32	80°	$.5 \times 10^{-3}$	270 +side	
-				24	310°	42	35°	$.5 \times 10^{-3}$	270 -side	
12	5	"	"	35	220°	35	145°	0		24.7356
-				45	295°	45	170°	$.5 \times 10^{-1}$	270 +side	
-				9	190°	38	230°	$.5 \times 10^{-1}$	270 -side	
13	6	"	"	43	30°	46	230°	0		24.6936
-				49	280°	35	50°	$.5 \times 10^{-1}$	270 +side	
-				52	190°	60	350°	$.5 \times 10^{-1}$	270 -side	
14	7	"	"	24	110°	24	255°	0		24.6940
-				26	40°	18	240°	$.5 \times 10^{-3}$	270 +side	
-				30	120°	34	300°	$.5 \times 10^{-2}$	270 -side	
15	8	"	"	44	80°	29	220°	0		24.7584
-				46	45°	36	210°	$.5 \times 10^{-3}$	270 +side	
-				46	90°	29	260°	$.5 \times 10^{-3}$	270 -side	
16	9	"	"	38	160°	27	290°	0		24.7161
-				13	130°	25	260°	$.5 \times 10^{-3}$	270°+side	
-				59	160°	50	300°	$.5 \times 10^{-3}$	270°-side	
17	10	10 mv/cm	10 msec	47	90°	53	320°	0		24.6907
-				49	60°	45	320°	$.6 \times 10^{-3}$	270°+side	
-				80	325°	52	105°	$.6 \times 10^{-3}$	270°-side	
18	11	5 mv/cm	10 msec	30	215°	25	300°	0		24.7230
-				24	280°	31	275°	$.5 \times 10^{-3}$	270°+side	
-				40	190°	58	310°	$.5 \times 10^{-3}$	270°-side	
19	12	5 mv/cm 10 msec		52	110°	29	10°	0		24.7435
-				35	230°	19	25°	$.5 \times 10^{-3}$	270°+side	
-				66	200°	47	0°	$.5 \times 10^{-3}$	270°-side	
20	13	"	"	32	235°	28	0°	0		24.7399
-				39	290°	15	18°	$.6 \times 10^{-3}$	270°+side	
-				40	220°	51	350°	$.6 \times 10^{-3}$	270°-side	

TABLE 8 (Cont'd.)

ROLLER RESIDUAL UNBALANCE TEST DATA

Balancing of Trial Rollers

Roller #	Photo#	CRO Sens	Sweep	Amplitude	IRD Readings Angle	Amplitude	Angle	Trial Weight wt	Angle	side	Roller Weight
21	14			20	30°	24	230°	0			24.7191
-				47	5°	32	210°	$.5 \times 10^3$	270°	+side	
-				13	60°	22	270°	$.5 \times 10^3$	270°	-side	
22	15			41	355°	35	130°	0			24.7355
-				74	350°	44	150°	$.5 \times 10^3$	270°	+side	
-				24	10°	15	120°	$.5 \times 10^3$	270°	-side	
23	16			30	5°	21	290°	0			24.7072
-				56	355°	16	280°	$.5 \times 10^3$	270°	+side	
-				16	25°	42	220°	$.5 \times 10^3$	270°	-side	
24	17	10 mv/cm	10 msec	57	210°	46	30°	0			24.7565
-				44	240°	39	45°	$.5 \times 10^3$	270°	+side	
-				68	200°	60	15°	$.5 \times 10^3$	270°	+side	
25	18	5 mv/cm	10 msec	32	160°	30	30°	0			24.7504
-				8	150°	22	50°	$.5 \times 10^3$	270°	+side	
-				46	165°	44	15°	$.5 \times 10^3$	270°	-side	
26	19	5 mv/cm	10 msec	34	55°	20	70°	0			24.7172
-				34	28°	20	90°	$.5 \times 10^3$	270°	+side	
-				28	65°	26	35°	$.5 \times 10^3$	270°	-side	
27	20			55	180°	65	195°	0	0		24.7199
-				9	320°	30	190°	$.5 \times 10^3$	270°	+side	
-				30	175°	18	270°	$.5 \times 10^3$	270°	-side	
28	21			28	330°	7.5	0°	0	0		24.7453
-				57	340°	3.5	140°	$.5 \times 10^3$	270°	+side	
-				13	280°	28	310°	$.5 \times 10^3$	270°	-side	
29	22			15	190°	19	80°	0	0		24.7439
-				14	330°	24	110°	$.5 \times 10^3$	270°	+side	
-				30	170°	26	20°	$.5 \times 10^3$	270°	-side	
30	23	5 mv/cm	10 msec	26	165°	27	150°	0	0		24.7414
-				65	310°	35	160°	$.5 \times 10^3$	270°	+side	
-				37	160°	3	120°	$.5 \times 10^3$	270°	-side	

TABLE 9

ROLLER RESIDUAL UNBALANCE EVALUATION RESULTS

Radius of Unbalance Trial Weights = 0.235 inch Unbalance Wc(g)(0.03527)(.235) ii inch unbalance = in.-oz. unbalance / Roller Weight

Roller Number	+SRA Trial Weight g	+SRA Correct	+SRA Unbalance Weight	+SRA Unbalance 10-6	+SRA uinch unbalance	-SRA Trial Weight (g)	-SRA Correct	-SRA Unbalance Weight (g)	-SRA Unbalance in.-oz.x10^6	-SRA u inch unbalance	+SRA Angle	+SRA Correct Angle	+SRA Act. Angle	-SRA Angle	-SRA Correct Angle	-SRA Act. Angle	+SRA-SRA Angle
10	.5x10^-3	1.35	675.	5.6	12.8	.5x10^-3	2.65	1325	11.0	25.2	270	-82.9	187.1	270	-46.0	224	-3?
11	.5x10^-3	1.33	665	5.5	12.6	.5x10^-3	2.47	1235	10.2	23.4	270	-144.7	125.3	270	-118.1	151.9	-27
12	.5x10^-3	0.73	365	3.0	6.9	.5x10^-3	0.07	35	0.3	.07	270	59	329	270	112	22	-53
13	.5x10^-3	0.90	450	3.7	8.6	.5x10^-3	1.18	590	4.9	11.2	270	130.1	40.1	270	3.7	273.7	126.
14	.5x10^-3	0.70	350	2.9	6.6	.5x10^-3	0.77	385	3.2	7.3	270	-46.8	223.2	270	93.6	3.6	-140
15	.5x10^-3	1.42	710	5.9	13.5	.5x10^-3	1.42	710	5.9	13.4	270	-62.4	207.6	270	44.2	314.2	-107
16	.5x10^-3	0.98	490	4.1	9.3	.5x10^-3	1.36	680	5.6	12.9	270	34.8	304.8	270	135.	45	-100
17	.6x10^-3	3.39	2034	16.8	38.7	.5x10^-3	0.90	540	4.5	10.3	270	-170.9	99.1	270	20.0	290	-191
18	.5x10^-3	1.19	595	4.9	11.3	.6x10^-3	1.22	610	5.0	11.6	270	85.9	355.9	270	166.2	76.2	-80
19	.5x10^-3	1.42	710	5.9	13.5	.5x10^-3	0.67	335	2.8	6.4	270	15.8	25.8	270	-143.	127	159
20	.6x10^-3	0.98	588	4.9	11.2	.5x10^-3	1.47	882	7.3	16.8	270	101.4	11.4	270	178.7	88.7	-77
21.	.5x10^-3	0.42	210	1.7	3.99	.6x10^-3	1.44	720	6.0	13.7	270	169.4	79.4	270	75.8	345.8	-226
22	.5x10^-3	0.70	350	2.9	6.6	.5x10^-3	2.24	1112	9.3	21.1	270	-92.3	117.7	27.	13.5	256.5	-78
23	.5x10^-3	1.14	570	4.7	10.8	.5x10^-3	0.61	305	2.5	5.8	270	-140.5	129.5	270	-65.6	204.4	-74.9
24	.5x10^-3	1.11	555	4.6	10.6	.5x10^-3	1.61	580	4.8	11.0	270	45.6	315.6	270	-125.4	144.6	171
25	.5x10^-3	1.96	980	8.1	18.6	.5x10^-3	2.06	1030	8.5	19.6	270	-41.4	228.6	270	96.1	173.9	54.7
26	.5x10^-3	1.68	840	7.0	16.0	.5x10^-3	2.11	1055	8.7	20.0	270	-104.9	165.1	270	-96.8	173.2	-8.1
27	.5x10^-3	0.63	315	2.6	6.0	.5x10^-3	0.68	340	2.8	6.5	270	-2.7	267.3	270	12.5	282.5	-15.2
28	.5x10^-3	0.67	335	2.8	6.4	.5x10^-3	0.52	260	2.2	4.9	270	-103.2	166.8	270	-85.0	185.	-18.2
29	.5x10^-3	0.84	420	3.5	8.0	.5x10^-3	1.17	585	4.8	11.1	270	-38.6	231.4	270	-60.4	209.6	21.8
30	.5x10^-3	1.38	690	5.7	13.1	.5x10^-3	1.54	770	6.4	14.6	270	4.4	274.4	270	10.5	280.5	-6.1

TABLE 10
ROLLER BALANCE EVALUATED—MEAN AND STANDARD DEVIATION VALUES

Location	Mean Value 10^{-6} in.-oz.	Standard Deviation 10^{-6} in.-oz.
+SRA	5.08	3.29
-SRA	5.56	2.76

Summary of Spin-Up Balance Tests

The evaluation of the spin-up balancer has shown it to be a viable device for evaluating the residual unbalance in bearing rollers of the size found in typical main shaft turbine engine applications. The spin-up rig's method of bearing support and of spinning the rollers shows excellent capability. The only suggested alteration in the basic design would be to increase the number of drive nozzles to four so they could be installed as diametrically opposed pairs rather than as single jets. This new arrangement would eliminate the effect of roller side loading which became evident at high jet pressures.

The instrumentation system incorporated into the spin-up rig had an overall calibrated sensitivity slightly in excess of $200 \frac{\text{volts}}{\text{inch}}$ (222 volts/inch for Channel 1 and 248 volts/inch for Channel 2) which permitted readings of unbalance as low as 0.5×10^{-6} in.-oz., well below the mean unbalance found in production rollers.

The measurement of residual unbalance in the group of 30 rollers using the spin-up rig proceeded without difficulty and indicated that determination of the qualitative unbalance was a relatively simple procedure.

The results of the qualitative measurement of unbalance showed that a somewhat uniform level of unbalance existed among the rollers with only one roller indicating a high unbalance level.

There was some difficulty experienced, however, in determining the quantitative level of unbalance in each of the rollers. The largest drawback was found to be in obtaining measurement accuracy. It became necessary to use large trial weights in order to have confidence in measuring weight. In addition, the

accuracy in positioning the trial weight and in reading phase angles all con-
tributed to the measurement difficulty.

As an example, the magnitude of the trial weights which could be satisfactorily
used varied between 500 to 1000 x 10^{-6} g; however, the accuracy of the beam bal-
ance used in determining trial weights was within 200 x 10^{-6} g, which resulted
in a significant weight measurement error. The mean unbalance level found in
the group of thirty rollers was approximately 5.4 x 10^{-6} in.-oz. per plane, so
that unbalance would require correction weight removal of only 600 x 10^{-6} g which
approaches the weight measurement limit of accuracy.

IV. LASER TECHNIQUES FOR BALANCING ROLLERS

A practical method of metal removal to correct roller unbalance requires that the removal technique be precisely controlled both from a quantitative and qualitative standpoint. A convenient method of weight removal is to employ a laser beam. If properly selected, a laser could remove metal from a desired location on a roller without the necessity of removing the roller from the balancing fixtures.

As a first level study to establish the suitability of using a laser beam as the means for removing roller material for balancing purposes, the following experiments on non-rotating rollers were conducted.

    A. With a laser gun having a 1.0×10^{-3} sec width pulse and employing a 10 diopter lens, a single roller was subjected to pulses of successive energy levels. This test established the general level of cratering which might be expected and also indicated whether the metal removal could be confined to the corner radius of the roller.

    B. With the same laser gun and lens used in the first experiment, successive rollers were bombarded with ten individual pulses of constant power. Each of six rollers was subjected to a different power level. The results of this test determined the amount of metal removal as a function of beam energy.

    C. A third test, conducted at a constant beam energy level, evaluated the lens diopter effect. Ten pulses of constant energy were impinged on a roller at each of three values of lens diopter. The effect of lens power on the amount of metal removal was determined from this experiment.

The energy levels of the laser pulses were preselected at the laser control console.

1. Test Set-Up

A chemical stand clamp was used to fix the location of the sample roller relative to the laser gun apparatus. The roller was positioned so that the corner radius was exposed to the direct line of the laser ray. A schematic of the test set-up is shown in Figure 22a.

The laser gun provided a coherent light beam with a pulse width of 0.001 second over a power range of 0 through 2.99 kv. The reflecting and beam positioning mirrors permit the laser targeting beam and subsequent power
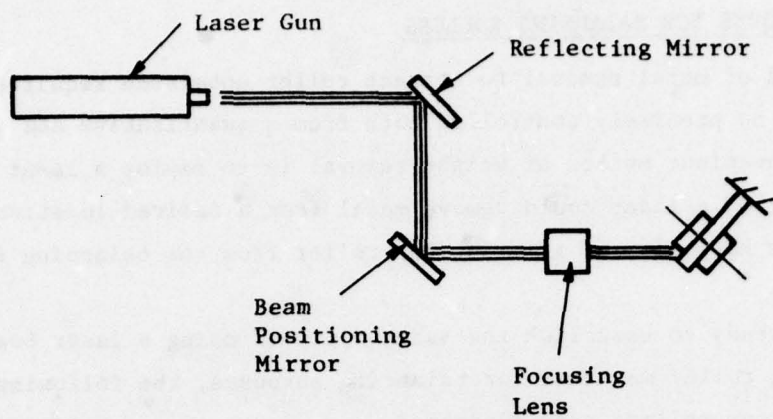
Figure 22a. Laser Metal Removal Test Set-Up
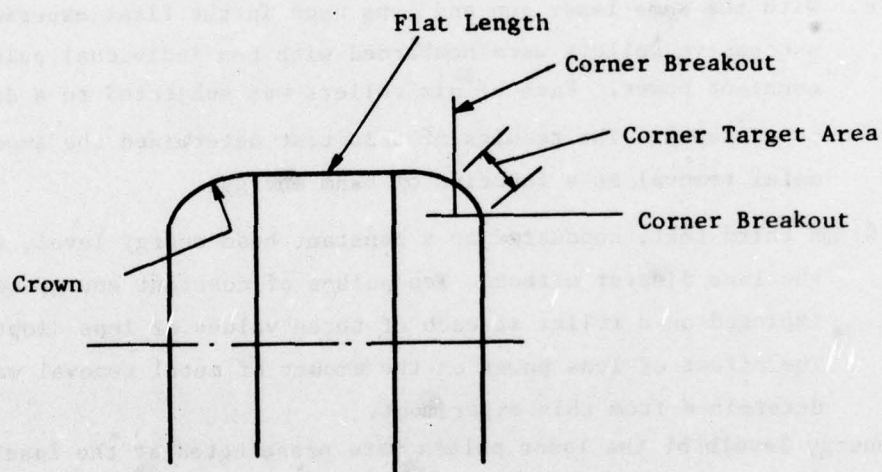
Figure 22b. Laser Beam Target Location Definition

beam burst to be selectively positioned on the proper target location. The focusing lens provides the beam focusing capability that provides the small target area required for metal removal.

The target area for removing metal was limited to the roller corners as shown in Figure 22b. Any extension of the removed material area past the corner breakout dimensions will seriously effect the behavior of the roller within the bearing and could even lead to premature bearing failure.

2. Test Results

Test No. 1 - Cratering and Target Positioning Test

A roller, arbitrarily selected from a group of 30 high speed bearing rollers supplied by the Air Force for balancing and laser metal removal studies, was subjected to individual bursts from a laser at successively increasing levels of beam power. A 10 diopter focusing lens was used for these tests and provided a 0.020 diameter beam at the focusing point on the roller.

Photographs of all six laser burst results are shown in Figure 23. Table 11 provides the listing of the burst power levels and the magnification for each photograph.

TABLE 11
LASER POWER LEVELS USED FOR FIRST TEST SEQUENCE

Photograph Number	Power	Magnification
23a	1.4 Kvolts	22.5X
23b	1.6 "	30.0X
23c	1.8 "	22.5X
23d	2.0 "	22.5X
23e	2.5 "	30.0X
23f	2.99 "	22.5X

In each of the six photographs, it is evident that even at the low levels of beam power a significant crater was produced by the action of the laser beam. Although the beam impact area was on the order of 0.020 in. which is significantly

Figure 23c

Figure 23f
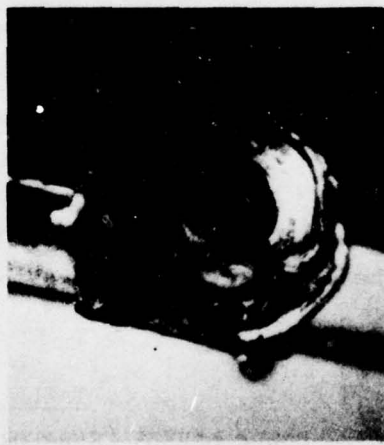
Figure 23b

Figure 23e

Figure 23a

Figure 23d

Figure 23. Effect of Laser Burst on Roller Corner Radii

less than the width of the roller corner, the cratering extends beyond the corner breakout location which could interfere with proper roller behavior. In addition, at higher beam power levels, there appear to be spatterings of resolidified molted metal which had spilled over the outer edge of the impact crater. Good examples of this effect are illustrated in Figures 23d and 23e. These particles of metal may not adhere sufficiently to the parent material to remain attached at the high rotational speeds to which the rollers are subjected.

Test No. 2 - Metal Removal

At the conclusion of test sequence, one each of six unused rollers, arbitrarily selected from the original complement of 30, was subjected to 10 laser bursts of constant power level. The weight of each roller was recorded both prior to and subsequent to the laser impingements. Table 12 lists the test results.

TABLE 12

METAL REMOVAL TEST LASER BEAM STUDY

Roller Identification	Initial Weight (g)	Final Weight (g)	Laser Beam Power (Kv)	Weight Removed Per Burst (g)
2	24.7144	24.6994	2.5	1.5×10^{-3}
3	24.7549	24.7516	2.0	3.3×10^{-4}
4	24.7561	24.7557	1.8	4.0×10^{-5}
5	24.7314	24.7310	1.6	4.0×10^{-5}
6	24.7187	24.7184	1.4	3.0×10^{-5}
7	24.7293	24.6977	2.99	3.2×10^{-3}

Graphically, the results of the weight removal tests are shown in Figure 24.

At the lower level of laser beam power, the accuracy of the roller weight becomes critical in evaluating material removal capability. The data spread shown for the low beam power levels represents the maximum spread from a possible error of 2×10^{-4} g in both the initial and final roller weights, an error based on the resolution of the precision balance used for the measurements.
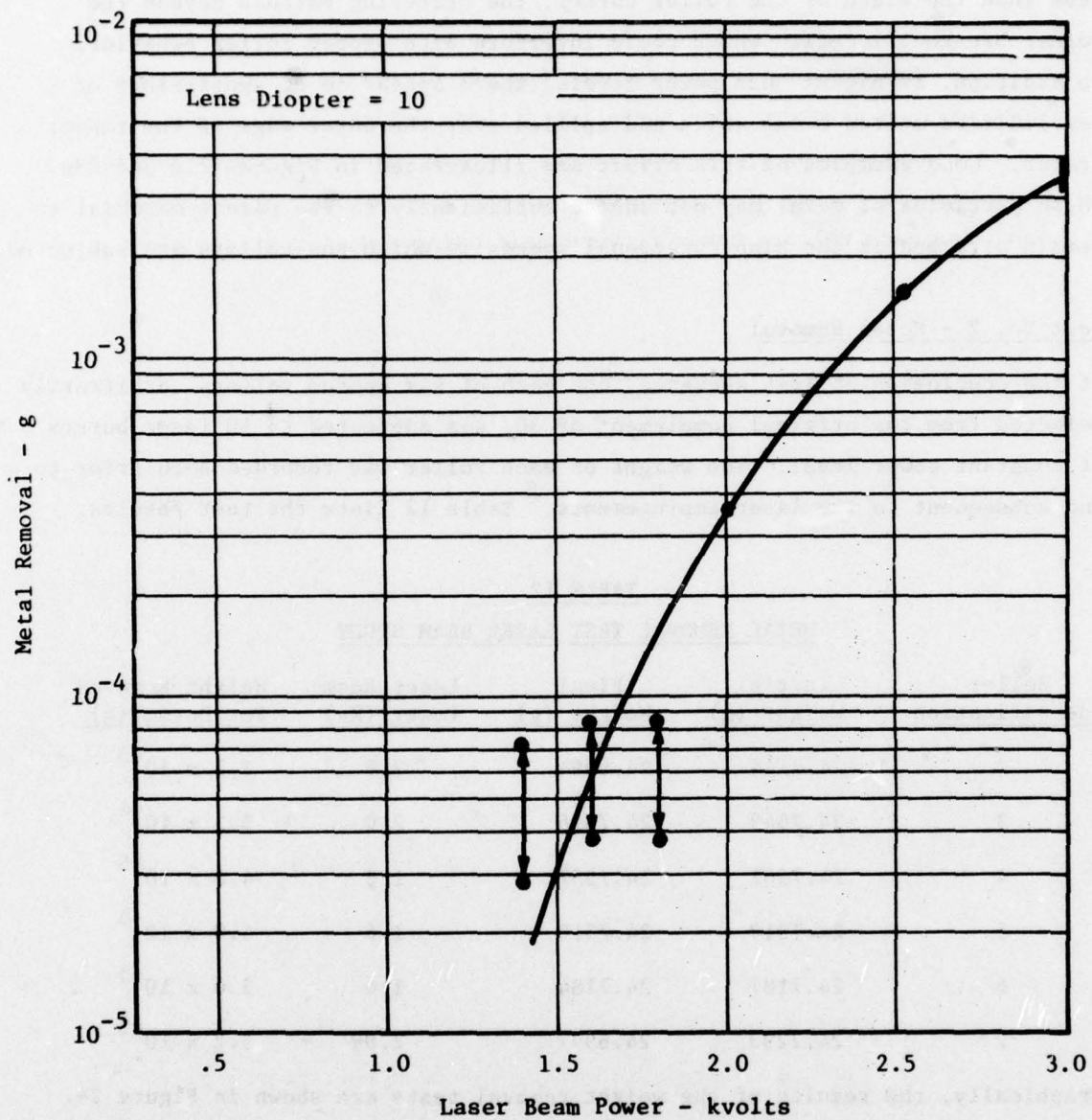
Figure 24. Metal Removal as a Function of Laser Beam Power

Laser Focusing Lens Diopter Test

The third test for determining the effectiveness of removing roller material by laser beam impingement was to evaluate the effect of laser beam focusing as defined by lens diopter. For these tests three rollers, again selected from the initial grouping of 30 supplied by the Air Force, were each subjected to ten individuals bursts of a laser beam with a 2.99 kvolt energy level. The ten bursts for each roller, however, were made using a different diopter focusing lens.

TABLE 13

LASER FOCUSING LENS DIOPTER EFFECT

Lens Diopter	Total Metal Removed	Single Bursts Metal Removed
8	50.5×10^{-3}g	5.05×10^{-3}g
10	42.0×10^{-3}g	4.20×10^{-3}g
12	41.5×10^{-3}g	4.15×10^{-3}g

The test results are also shown graphically in Figure 25. A slight increase in the amount of metal removed as the lens diopter decreases is indicated by the data; however, the limit to which this data can be extrapolated is not established by the limited amount of data available.

Summary of Laser Techniques for Metal Removal

Laser light beams have been successfully employed in the removal of corrective balance weights for several years. They have not, however, been used for removing material from precision parts such as the rollers used in high DN bearing designs.

The requirements which must be met if laser techniques are to be successfully applied to the correction of precision roller unbalance include:

- Amount of material removed must be precise.

- Position and focus of impinging beam must be accurate.

- Cratering and spatter at the beam impingement location must be minimal.
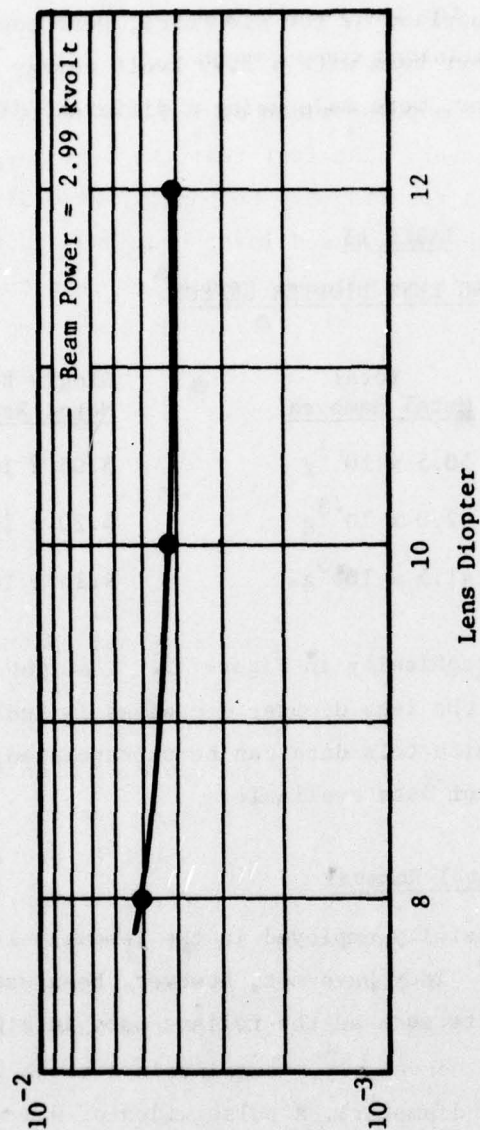
Figure 25. Laser Focusing Lens Diopter Effect

• Burst duration must be short compared to passage time of roller unbalance location during a balancing.

The tests conducted for this program have been addressed to only the static requirements of laser balancing and, for the results present in the preceding report section, the following conclusions can be made.

1. High beam energy levels at a pulse width of 1×10^{-3} sec produce serious cratering and spatter. The fact that the beam target was stationary rather than rotating may be partly responsible for this result. Although the focused laser beam had a diameter of only 0.020 inch, which is significantly smaller than the permissible target area on the test rollers, the cratering from the higher energy beams extended beyond the target area and past the corner breakout locations. Spatter of solidified molten metal was also found in the target area at the higher beam energy levels. This material, which may not have a secure bond to the parent roller material, could come loose during bearing operation to produce contamination problems.

The anticipated difficulty produced by cratering and spatter may be reduced if the laser beam impinges on a rotating roller. Centrifugal forces developed at the roller surface when it is rotating at balancing speeds in excess of 10,000 rpm could be significant in throwing off the debris generated by the laser burst. The laser beam pulse width, however, must be kept short to prevent the removal of metal over too broad an area. As an example, the 1.0×10^{-3} sec beam pulse width used for this study would produce a track 11.3 mm long or 22 percent of the circumference along the roller corner at the balancing speed of 13,500 rpm used during the balancer evaluation. Conversely, to maintain a track length of 1.0 mm (twice the beam diameter), a pulse width of 0.1×10^{-3} sec would be required.

2. Accuracy of Metal Removal Rate - The use of low energy laser beams produces a small enough amount of removed material that sufficient balancing accuracy can be achieved. The results of the balancing evaluation covered in the first part of this report indicated that

-63-

an average amount of metal removal required to perfectly balance
a majority of the rollers investigated would be approximately 0.6 x
10^{-3}g. This amount of material would be removed by a single 1.0 x
10^{-3} sec pulse width burst of about 2-1/4 kvolts or 5 bursts at 1.6
kvolts.

3. Effect of Lens Diopter - Some effect of lens diopter was noted at
the high beam energy level tested. This effect would be reduced
at lower beam energy levels leading to the conclusion that the lens
diopter value over the range covered by this report is not significant.

V. ROLLER BEARING TEST EVALUATION

After the successful conclusion of the spin-up rig evaluation, a test of a
165-mm bore roller bearing fitted with rollers selected from a group of 150
supplied by the Air Force was performed. The purpose of this test was to
attempt to relate roller skew or uneven end wear with roller unbalance. The
test proceeded as follows:

- Step 1 was the screening of the 150 rollers in the spin-up rig to
  select 32 rollers with the least amount of residual unbalance. These
  rollers were for assembly into a 165-mm bore baseline test bearing.

- Step 2 was the assembly and test of the 32 selected rollers in the
  baseline bearing at the following conditions.

  1. DN = 2.5×10^6 (N=15,000 rpm)

  2. Lube oil: MIL-L-7808G

  3. Lube oil inlet conditions: 2 gpm @ 250°F

  4. Radial Load = 500 lb (min load + margin to prevent
     skidding)

The data to be collected included:

- Speed

- Load

- Inlet oil conditions (flow rate, temperature)

- Outlet oil conditions (temperature)

- Outer race temperature (5 places)

- Cage speed

The test was to last for 40 hours after which the bearing was to be disassembled
and inspected.

- Step 3. Four (4) rollers, selected from the remainder of the 150
  supplied rollers, were to be further unbalanced on one end only
  for a total weight reduction of 2, 4, 6, and 8×10^{-3}g, respectively;
  the unbalance weight removal was to be in line with the residual
  unbalance determined from the screening tests. These unbalanced
  rollers were to replace four rollers judged as being most affected
  by the baseline test.

-65-

● Step 4. The original baseline bearing with four new rollers and
23 original rollers was to be tested for 40 hours under the identi-
cal conditions tested for Step 2, concluding with a visual inspection
of the bearing.

The baseline and unbalanced roller tests were to be conducted on
the test stand described in the following report section.

1. Roller Bearing Tester

The bearing tester was reconstructed from an existing test facility by replacing
the bearing inner race seat on a high-speed spindle and by providing a new
housing and outer race seat. The tester is described as follows.

Figure 26 shows the installation of the basic test facility and indicates
the 100-HP, DC, variable speed drive motor coupled through a 7.04/1 step-up
gear box to the high-speed spindle. The high-speed spindle is shown with
an earlier test bearing installed.

The new test head including both the inner and outer race seats is illustrated
in Figure 27. Identified on this figure is the high-speed spindle (1) onto
which the test bearing inner race seat (2) is installed. The seat is provided
with an interference fit sufficient to maintain contact with the spindle shaft
at 15,000 rpm and is also secured in position with a locknut (3). An axial
inner race seat, insert (4), is provided as a replaceable item to permit
rework without the necessity of replacing the entire inner race seat.

The test bearing (5) is installed on the inner race seat with an appropriate
interface and is held in place with a combination locking nut and oil scoop
(6). A free outer race seat (7), machined with an interference fit to the
roller bearing's outer race, provides the necessary race alignment guidance.
Both the inner and outer race seats are machined from M50 tool steel to match
them to the bearing properties.

The outer race seat (7) includes a clevis arrangement for the attachment of
the radial load cable assembly (8). Radial load is applied to the bearing by
a pneumatic cylinder; the cylinder's calibration is shown in Appendix A.

-66-

100 HP DC DYNAMOMETER

GEARBOX

SPINDLE

PREVIOUS FLUID FILM BEARING
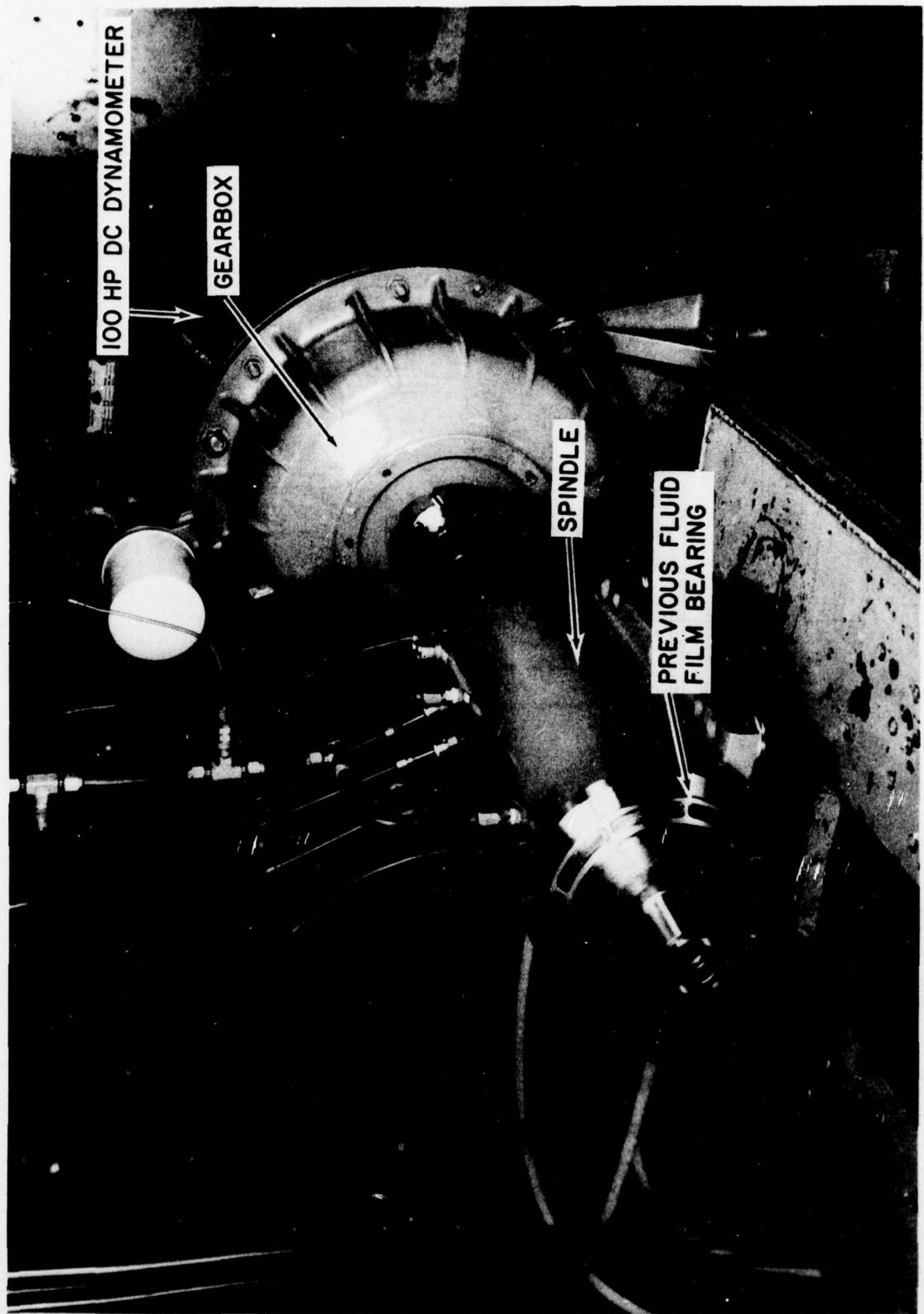
Figure 26. Roller Bearing Test Facility
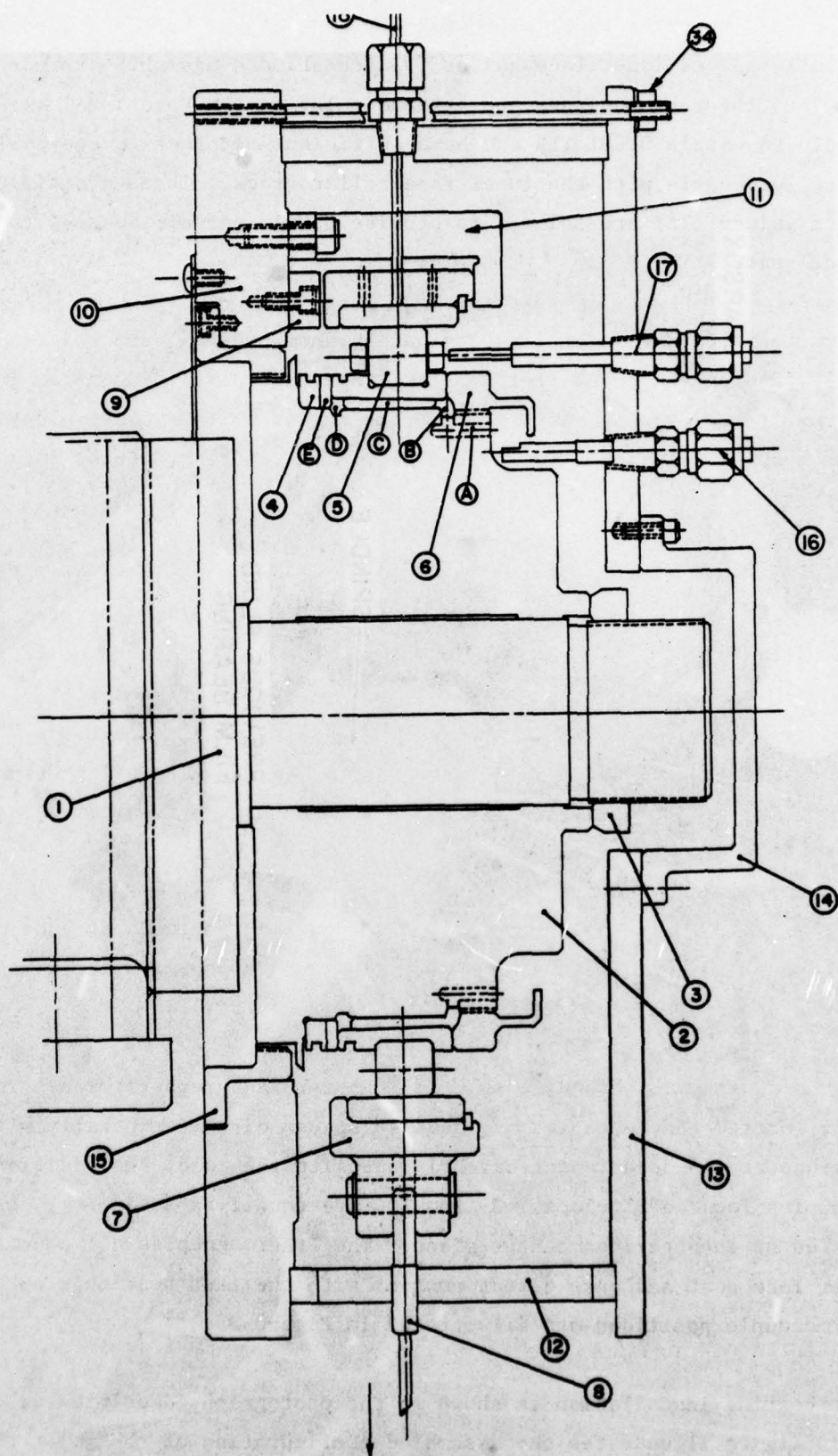
Figure 27. Test Head Construction
-68-

Containment of the outer race is provided by two sets of Teflon coated guides. Three equally spaced inner face guides (9) are shimmed against the rear support plate (10) so they are coplanar and perpendicular to the rotational axis of the spindle to within 0.001 TIR and have sufficient set back to centrally locate the load cable with the inner race roller track. Three additional outer face guides (11) are shimmed to provide 0.001 inch clearance with the outer race seat.

The entire test bearing is enclosed by an aluminum housing tube (12), a front cover (13), and an end cover (14). A large drainage port is provided in the housing tube to allow easy exit of the lubrication oil. A close clearance labyrinth seal (15) is installed on the back plate to restrict the loss of test lubricant from the rear of the housing.

Lubricating oil is injected into the oil scoop by four jets (16) attached to the front cover. Lubricating oil pumped by centrifugally generated pressure passes through a row of 72 drilled holes "A" into a forward collecting manifold "B" then under the bearing race through the inner race slots "C" into a second collecting manifold "D" and out of the bearing through slots "E" machined into the axial inner race seat insert. Lubricating oil passing under the bearing race was pumped by centrifugal action through feed holes in the inner race to lubricate the bearing.

Bearing test instrumentation connected to the housing includes an eddy current probe (17) for measuring cage speed (shaft speed is measured using a magnetic pick-up located at the opposite end of the spindle shaft).

Five thermocouples (18) are used to measure outer race temperatures. Three centrally located thermocouples are equally spaced circumferentially with one of the group at top dead center directly opposite the load; two additional thermocouples located 8° clockwise from TDC are equally spaced 3/8 inch on either side of the bearings center plane. The thermocouples all penetrate the outer race seat and make direct contact with the test bearing's outer race. The thermocouple positions are illustrated in Figure 28.

The test bearing installation is shown in the photograph identified as Figure 29. This figure illustrates the assembled configuration of the major test
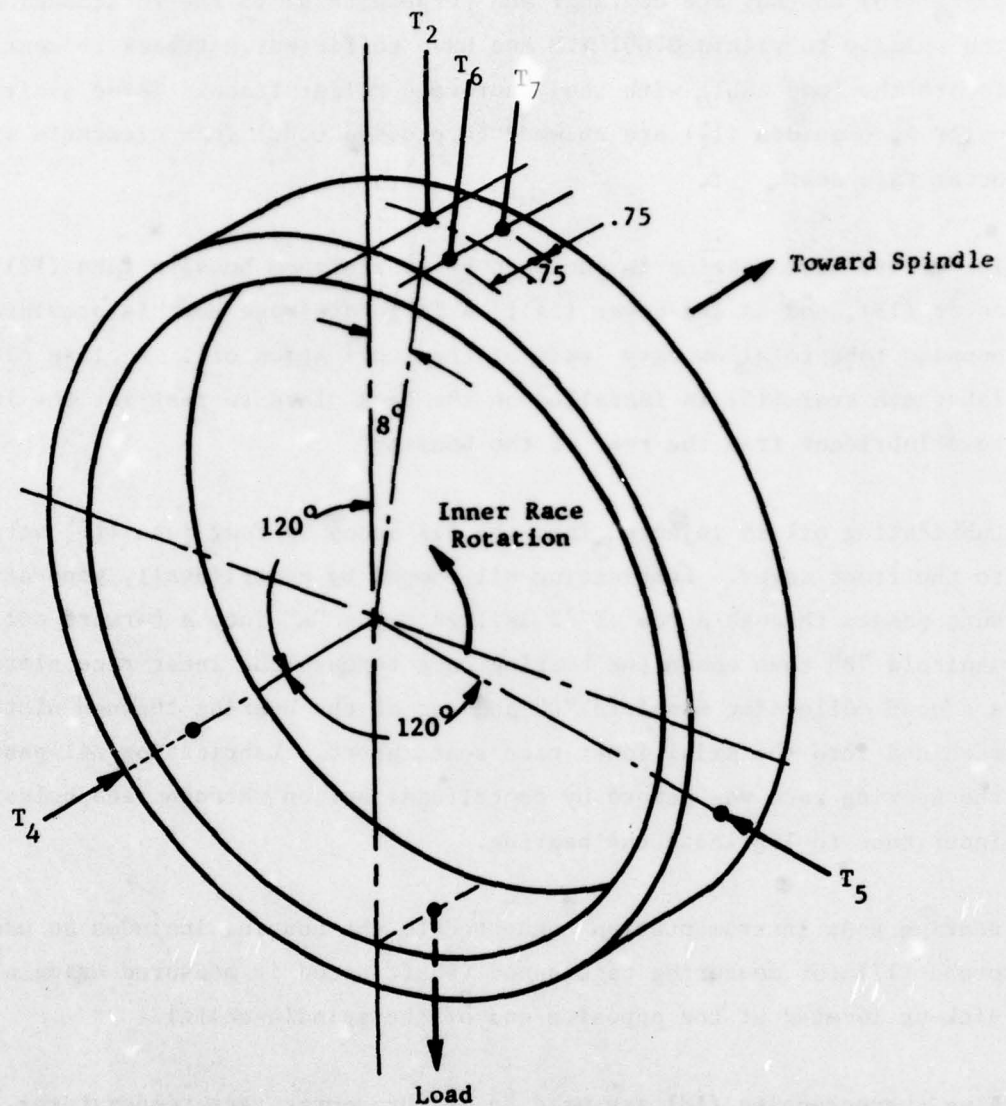
Figure 28. Outer Race Thermocouple Locations:
Baseline Bearing Test

MOUNTING PLATE

AXIAL RACE GUIDE

OUTER RACE SEAT

TEST BEARING

INNER RACE SEAT

OIL SCOOP

LOAD ATTACHMENT POINT
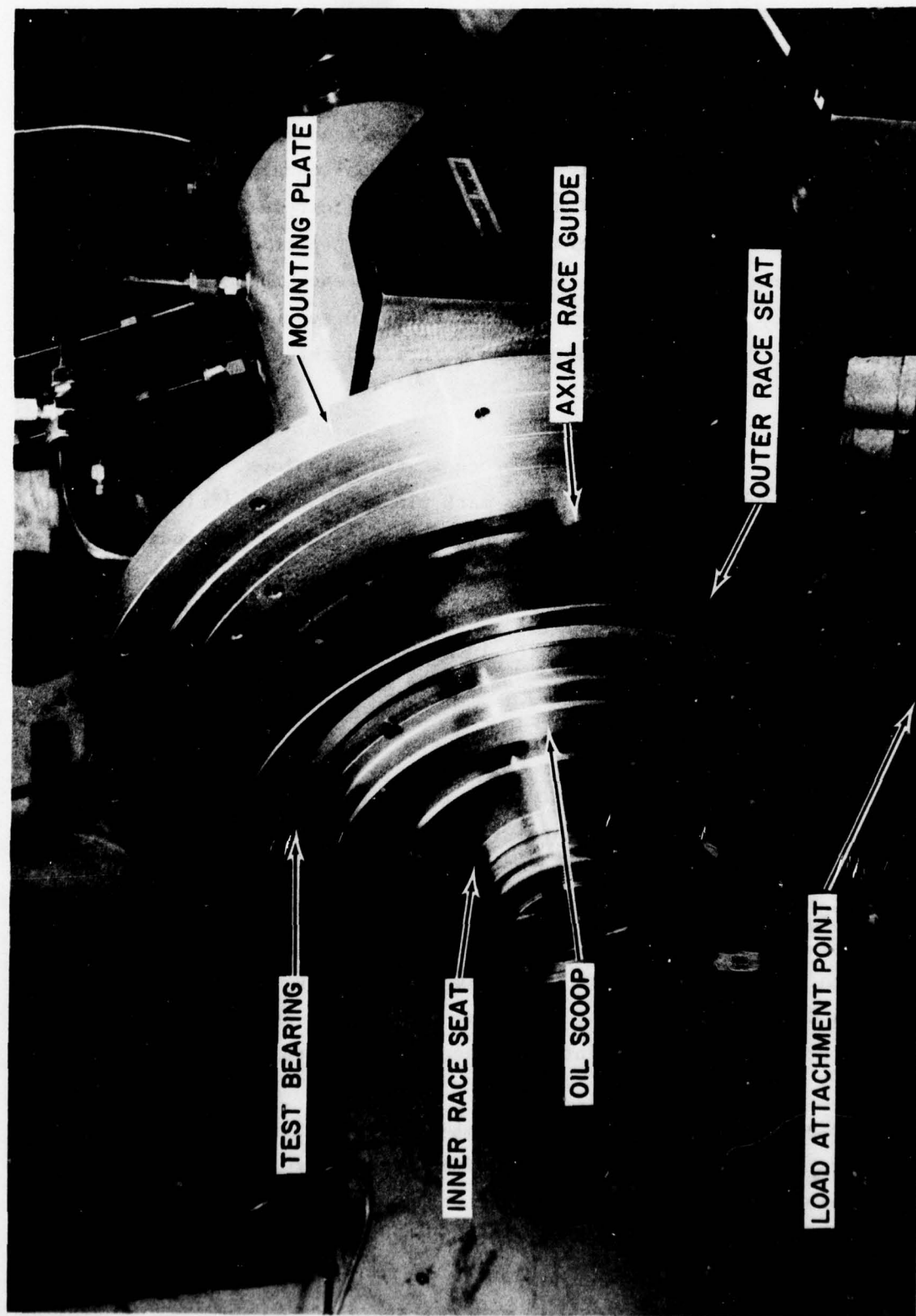
Figure 29. Test Bearing Installation

head components. The totally installed tester is shown in Figure 30 to
illustrate the assembly of the outer housing.

2. Roller Screening

Each of the 150 rollers supplied by the Air Force was spun-up in the air bearing
balancer rig to determine the relative level of residual unbalance. The rollers
supplied for unbalance screening and bearing tests were carefully selected for
uniformity of size, to assure uniform test results. Inspection results indica-
ting diameter and length variations were supplied with each roller to indicate
this uniformity. All the rollers were identified as to sequence and orientation
in the spin-up rig. This identification was maintained throughout the test
program.

The procedure followed for the screening process was as follows. Each roller
in turn was cleaned and had an identifying mark placed on the -SRA flat end.
The clean, identified roller was inserted into the spin-up rig and spun to
13,550 rpm at which time the balance data was recorded. When the recording
of the balance data was completed, the roller was removed from the spin-up
rig, covered with preservative, and stored in a numbered container; a plastic
sleeve identifying the +SRA roller end was slipped over the roller to complete
the identification.

The data from the roller screening evaluation is shown in Table 14. Included
in Table 14 is the listing of dimensional variations for each roller. The
deviations are based on increments of 0.0001 inch from the basic roller dimen-
sions of 0.6299 in. diameter and 0.6299 in. length. Therefore, a roller that
has a diameter variation of -3/4 - 1 and a length variation of +4 +6 is 0.6298
to 0.629825 inch diameter and is 0.6303 to 0.6305 inch long. Based on the
relative levels of the IRD readings, 32 rollers having the lowest amplitude
levels were selected for assembly into the baseline test bearing.

To complete the screening process, four additional rollers, selected from the
screened rollers having the largest IRD readings (identified as rollers A, B,
C, and D on Table 14) were set aside for the unbalance-skewing test sequence.
Each of the four rollers was checked further on the spin-up rig to determine
the circumferential location of the unbalance. Roller material was then removed

Figure 30. Roller Bearing Tester Installation

TABLE 14

ROLLER SCREENING DATA

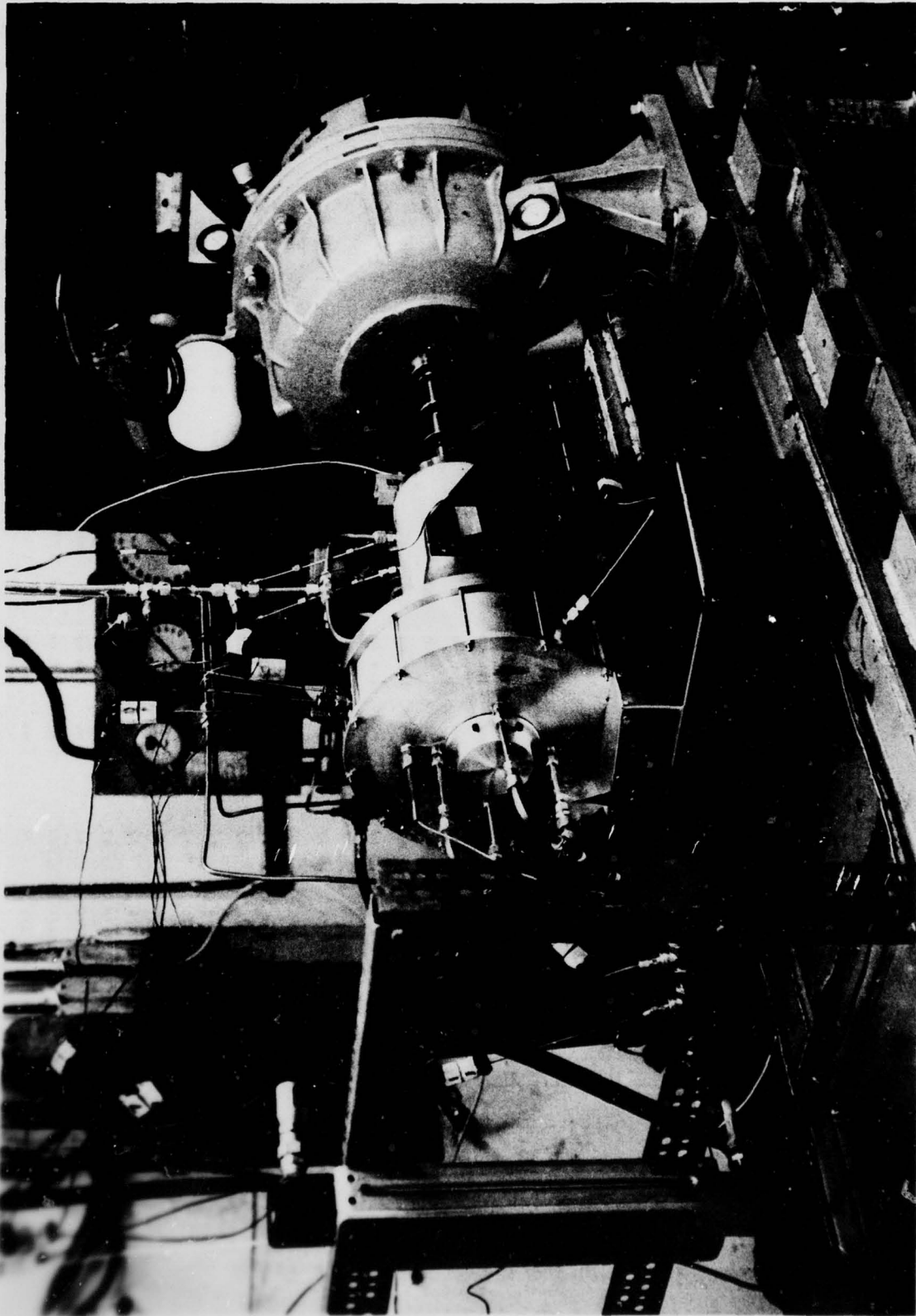| Roller Identification No.	Lot Serial No.	Dimension Variation Diameter	Length	+SRA Scope Reading Sensitivity mv/cm	AMP cm	IRD Reading AMP	Phase	+SRA Scope Reading Sensitivity mv/cm	AMP cm	IRD Reading AMP	Phase	Selected Roller	Gage Pocket Location
1	102	-1-1 1/4	+2	5 mv	3.4 cm	.15	310°	5 mv	2.2 cm	.115	115°		
2	102	-1-1 1/4	+2	5 mv	1.8 cm	.095	200°	5 mv	1.8 cm	.05	45°	*	1
3	102	-1-1 1/4	-2	5 mv	2.4 cm	.10	25°	5 mv	1.2 cm	.05	20°		
4	102	-1-1 1/4	-2	5 mv	1.7 cm	.07	330°	5 mv	1.6 cm	.075	230°	*	2
5	102	-1-1 1/4	-2	5 mv	1.1 cm	.04	180°	5 mv	1.4 cm	.06	95°	*	3
6	102	-1-1 1/4	-2	5 mv	3.2 cm	.14	45°	5 mv	2.0 cm	.07	170°		
7	102	-1-1 1/4	-2	5 mv	1.0 cm	.03	190°	5 mv	1.2 cm	.05	30°	*	4
8	102	-1-1 1/4	-2	5 mv	3.5 cm	.16	120°	5 mv	2.3 cm	.115	90°		
9	102	-1-1 1/4	-2	5 mv	2.3 cm	.10	5°	5 mv	1.0 cm	.035	210°	*	5
10	108	-3/4-1	-2-4	5 mv	3.1 cm	.14	165°	5 mv	2.5 cm	.125	355°		
11	102	-1-1 1/4	+2	5 mv	3.7 cm	.16	325°	5 mv	2.2 cm	.11	140°		
12	102	-1-1 1/4	+2	5 mv	1.3 cm	.04	165°	5 mv	1.5 cm	.065	195°	*	6
13	102	-1-1 1/4	+2	5 mv	3.1 cm	.14	270°	5 mv	2.0 cm	.095	80°		
14	102	-1-1 1/4	+2	5 mv	1.6 cm	.06	190°	5 mv	2.0 cm	.095	350°	*	7
15	102	-1-1 1/4	+2	5 mv	2.1 cm	.085	275°	5 mv	1.1 cm	.05	5°	*	8
16	102	-1-1 1/4	+2	5 mv	1.9 cm	.07	30°	5 mv	1.0 cm	.035	160°	*	9
17	102	-1-1 1/4	+2	5 mv	1.8 cm	.075	335°	5 mv	1.1 cm	.05	345°	*	10
18	102	-1-1 1/4	+2	5 mv	1.7 cm	.065	165°	5 mv	0.7 cm	.02	235°	*	11
19	102	-1-1 1/4	+2	5 mv	2.2 cm	.08	10°	5 mv	1.6 cm	.07	210°	*	12
20	102	-1-1 1/4	+2	5 mv	2.6 cm	.11	170°	5 mv	1.1 cm	.05	5°		
21	102	-1-1 1/4	+2	5 mv	3.3 cm	.145	110°	5 mv	1.7 cm	.085	10°		
22	102	-1-1 1/4	+2	5 mv	3.2 cm	.13	120°	5 mv	2.4 cm	.12	90°		
23	102	-1-1 1/4	+2	5 mv	4.1 cm	.175	315°	5 mv	2.4 cm	.12	115°	C	13
24	102	-1-1 1/4	+2	5 mv	1.9 cm	.085	340°	5 mv	1.1 cm	.045	225°	*	
25	102	-1-1 1/4	+2	5 mv	5.0 cm	.235	80°	5 mv	2.1 cm	.115	245°	A	14
26	102	-1-1 1/4	+2	5 mv	1.6 cm	.055	165°	5 mv	1.8 cm	.08	60°	*	
27	102	-1-1 1/4	+2	5 mv	2.4 cm	.105	265°	5 mv	1.2 cm	.06	140°		
28	102	-1-1 1/4	+2	5 mv	1.6 cm	.06	60°	5 mv	2.2 cm	.115	135°	*	15
29	102	-1-1 1/4	+2	5 mv	3.0 cm	.125	350°	5 mv	1.5 cm	.065	190°		
30	102	-1-1 1/4	+2	5 mv	4.5 cm	.19	170°	5 mv	2.6 cm	.135	35°	B	
31	102	-1-1 1/4	+2	5 mv	1.9 cm	.08	145°	5 mv	1.5 cm	.065	340°	*	16

TABLE 14 (Cont'd.)

ROLLER SCREENING DATA

Roller Identification No.	Lot Serial No.	Dimension Variation Diameter	Dimension Variation Length	+SRA Scope Reading Sensitivity mv/cm	Scope Reading AMP cm	IRD Reading AMP	IRD Reading Phase	+SRA Scope Reading Sensitivity mv/cm	Scope Reading AMP cm	IRD Reading AMP	IRD Reading Phase	Selected Roller	Gage Pocket Location
32	102	-1-1 1/4	+2	5 mv	2.3 cm	.095	265°	5 mv	2.1 cm	.10	150°	*	17
33	102	-1-1 1/4	+2	5 mv	1.5 cm	.06	170°	5 mv	1.2 cm	.05	350°	*	18
34	102	-1-1 1/4	+2	5 mv	1.4 cm	.055	125°	5 mv	1.9 cm	.095	230°	*	19
35	102	-1-1 1/4	+2	5 mv	2.7 cm	.115	260°	5 mv	1.2 cm	.05	45°		
36	102	-1-1 1/4	+2	5 mv	2.6 cm	.11	23°	5 mv	1.0 cm	.035	60°		
37	102	-1-1 1/4	+2	5 mv	1.2 cm	.045	165°	5 mv	1.3 cm	.06	270°	*	20
38	102	-1-1 1/4	+2	5 mv	1.6 cm	.06	35°	5 mv	1.4 cm	.055	80°	*	21
39	102	-1-1 1/4	+2	5 mv	1.9 cm	.075	235°	5 mv	1.3 cm	.06	195°	*	22
40	102	-1-1 1/4	-2-4	5 mv	.8 cm	.02	90°	5 mv	1.0 cm	.04	75°	*	23
41	102	-1-1 1/4	-2-4	5 mv	3.0 cm	.14	290°	5 mv	2.8 cm	.14	50°		
42	102	-1-1 1/4	-2-4	5 mv	2.5 cm	.11	355°	5 mv	1.8 cm	.085	125°		
43	102	-1-1 1/4	-2-4	5 mv	4.4 cm	.2	335°	5 mv	2.5 cm	.125	155°		
44	102	-1-1 1/4	-2-4	5 mv	1.9 cm	.075	300°	5 mv	1.3 cm	.055	180°	*	24
45	102	-1-1 1/4	-2-4	5 mv	2.7 cm	.13	50°	5 mv	2.6 cm	.125	180°		
46	102	-1-1 1/4	-2-4	5 mv	1.1 cm	.065	55°	5 mv	1.3 cm	.055	55°	*	25
47	102	-1-1 1/4	-2-4	5 mv	2.2 cm	.09	50°	5 mv	1.9 cm	.095	290°	*	26
48	102	-1-1 1/4	-2-4	5 mv	2.6 cm	.115	255°	5 mv	2.0 cm	.095	85°		
49	102	-1-2 1/4	-2-4	5 mv	1.4 cm	.05	55°	5 mv	1.6 cm	.07	40°	*	27
50	102	-1-1 1/4	-2-4	5 mv	2.7 cm	.115	180°	5 mv	2.1 cm	.11	300°		
51	102	-1-1 1/4	-2-4	5 mv	2.7 cm	.12	95°	5 mv	2.3 cm	.12	225°		
52	102	-1-2 1/4	-2-4	5 mv	3.4 cm	.145	280°	5 mv	1.8 cm	.095	120°		
53	102	-1-1 1/4	-2-4	5 mv	1.5 cm	.045	60°	5 mv	1.0 cm	.04	90°	*	28
54	102	-1-1 1/4	-2-4	5 mv	3.5 cm	.16	200°	5 mv	3.0 cm	.155	35°		
55	102	-1-1 1/4	-2-4	5 mv	3.5 cm	.155	75°	5 mv	2.4 cm	.12	245°		
56	102	-1-1 1/4	-2-4	5 mv	3.6 cm	.17	30°	5 mv	2.1 cm	.115	170°		
57	102	-1-1 1/4	-2-4	5 mv	2.2 cm	.09	45°	5 mv	1.4 cm	.06	165°	*	29
58	102	-1-1 1/4	-2-4	5 mv	3.0 cm	.14	225°	5 mv	2.6 cm	.135	110°		
59	102	-1-1 1/4	-2-4	5 mv	1.1 cm	.035	30°	5 mv	2.3 cm	.12	320°	*	30
60	102	-1-1 1/4	-2-4	5 mv	3.0 cm	.125	195°	5 mv	1.7 cm	.075	290°		
61	102	-1-1 1/4	-2-4	5 mv	4.0 cm	.225	90°	5 mv	2.6 cm	.135	260°		
62	102	-1-1 1/4	-2-4	5 mv	3.8 cm	.175	100°	5 mv	2.9 cm	.165	310°		
63	102	-1-1 1/4	-2-4	5 mv	2.8 cm	.125	75°	5 mv	2.1 cm	.105	290°		

TABLE 14 (Cont'd.)
ROLLER SCREENING DATA

Roller Identification No.	Lot Serial No.	Dimension Variation Diameter	Dimension Variation Length	+SRA Scope Reading Sensitivity mv/cm	+SRA AMP cm	+SRA IRD Reading AMP	+SRA IRD Reading Phase	+SRA Scope Reading Sensitivity mv/cm	+SRA AMP cm	+SRA IRD Reading AMP	+SRA IRD Reading Phase	Selected Roller	Gage Pocket Location
64	102	-1-1 1/4	-2-4	5 mv	1.6 cm	.065	345°	5 mv	1.1 cm	.045	0°	*	31
65	102	-1-1 1/4	-2-4	5 mv	2.9 cm	.13	50°	5 mv	2.2 cm	.115	95°		
66	102	-1-1 1/4	-2-4	5 mv	2.3 cm	.105	185°	5 mv	1.4 cm	.075	125°		
67	102	-1-1 1/4	-2-4	5 mv	2.3 cm	.095	295°	5 mv	1.5 cm	.075	165°		
68	102	-1-1 1/4	-2-4	5 mv	4.7 cm	.22	125°	5 mv	2.5 cm	.145	335°		
69	102	-1-1 1/4	-2-4	5 mv	2.6 cm	.115	55°	5 mv	1.6 cm	.08	305°	D	
70	102	-1-1 1/4	-2-4	5 mv	3.7 cm	.17	195°	5 mv	2.6 cm	.145	30°		
71	102	-1-1 1/4	-2-4	5 mv	3.4 cm	.155	35°	5 mv	2.6 cm	.145	240°		
72	102	-1-1 1/4	-2-4	5 mv	3.7 cm	.165	200°	5 mv	2.7 cm	.125	0°		
73	102	-1-1 1/4	-2-4	5 mv	2.5 cm	.11	290°	5 mv	1.3 cm	.055	175°		
74	102	-1-1 1/4	-2-4	5 mv	3.5 cm	.16	45°	5 mv	2.4 cm	.135	200°		
75	102	-1-1 1/4	-2-4	5 mv	1.3 cm	.05	75°	5 mv	1.6 cm	.085	355°	*	32
76	102	-1-1 1/4	-2-4	5 mv	2.8 cm	.135	265°	5 mv	2.5 cm	.14	155°		
77	102	-1-1 1/4	-2-4	5 mv	1.4 cm	.055	290°	5 mv	2.3 cm	.12	280°		
78	102	-1-1 1/4	-2-4	5 mv	2.7 cm	.12	315°	5 mv	1.6 cm	.085	200°		
79	108	-3/4-1	+4+6	5 mv	3.0 cm	.135	195°	5 mv	3.3 cm	.18	110°		
80	108	-3/4-1	+2	5 mv	2.3 cm	.1	45°	5 mv	1.4 cm	.075	230°		
81	108	-3/4-1	+2	5 mv	0.7 cm	.02	190°	5 mv	1.7 cm	.075	15°		
82	108	-3/4-1	-2	5 mv	3.3 cm	.155	15°	5 mv	1.7 cm	.08	180°		
83	108	-3/4-1	-2	5 mv	3.5 cm	.155	200°	5 mv	1.2 cm	.05	280°		
84	108	-3/4-1	-2	5 mv	2.7 cm	.125	165°	5 mv	0.7 cm	.02	265°		
85	108	-3/4-1	-2	5 mv	2.2 cm	.095	55°	5 mv	1.5 cm	.07	175°		
86	108	-3/4-1	-2	5 mv	2.9 cm	.13	135°	5 mv	1.8 cm	.095	5°		
87	108	-3/4-1	-2	5 mv	2.7 cm	.12	180°	5 mv	0.5 cm	.01	170°		
88	108	-3/4-1	-2	5 mv	3.4 cm	.155	190°	5 mv	2.4 cm	.125	35°		
89	108	-3/4-1	-2-4	5 mv	1.3 cm	.05	195°	5 mv	1.7 cm	.085	280°		
90	108	-3/4-1	-2-4	5 mv	3.4 cm	.155	355°	5 mv	2.8 cm	.15	195°		
91	108	-3/4-1	-2-4	5 mv	1.3 cm	.055	170°	5 mv	1.8 cm	.09	190°		
92	108	-3/4-1	-2-4	5 mv	3.0 cm	.135	235°	5 mv	2.7 cm	.15	110°		
93	108	-3/4-1	-2-4	5 mv	2.1 cm	.09	170°	5 mv	1.4 cm	.07	330°		
94	108	-3/4-1	-2-4	5 mv	2.8 cm	.13	315°	5 mv	2.3 cm	.12	200°		

TABLE 14 (Cont'd.)

ROLLER SCREENING DATA

Roller Identification No.	Lot Serial No.	Dimension Variation Diameter	Dimension Variation Length	+SRA Scope Reading Sensitivity mv/cm	+SRA AMP cm	IRD Reading AMP	IRD Reading Phase	Scope Reading Sensitivity mv/cm	+SRA AMP cm	IRD Reading AMP	IRD Reading Phase	Selected Roller	Gage Pocket Location
95	108	-3/4-1	-2-4	5 mv	2.1 cm	.085	265°	5 mv	2.6 cm	.14	190°	*	
96	108	-3/4-1	-2-4	5 mv	2.0 cm	.075	205°	5 mv	1.5 cm	.07	195°	*	
97	108	-3/4-1	-2-4	5 mv	2.8 cm	.125	320°	5 mv	1.1 cm	.045	65°	*	
98	108	-3/4-1	-2-4	5 mv	2.4 cm	.105	250°	5 mv	1.6 cm	.08	135°	*	
99	108	-3/4-1	-2-4	5 mv	1.9 cm	.08	25°	5 mv	1.4 cm	.07	0°	*	
100	108	-3/4-1	-2-4	5 mv	2.1 cm	.09	135°	5 mv	1.4 cm	.07	10°		
101	108	-3/4-1	-2-4	5 mv	2.6 cm	.115	355°	5 mv	1.3 cm	.07	115°		
102	108	-3/4-1	-2-4	5 mv	3.4 cm	.16	35°	5 mv	3.1 cm	.165	205°		
103	108	-3/4-1	-2-4	5 mv	2.1 cm	.095	95°	5 mv	1.3 cm	.06	225°		
104	108	-3/4-1	-2-4	5 mv	2.8 cm	.075	105°	5 mv	2.7 cm	.085	90°		
105	108	-3/4-1	-2-4	5 mv	2.1 cm	.09	275°	5 mv	1.2 cm	.055	345°		
106	108	-3/4-1	-2-4	5 mv	2.5 cm	.115	195°	5 mv	1.2 cm	.055	300°		
107	108	-3/4-1	-2-4	5 mv	2.4 cm	.11	115°	5 mv	2.1 cm	.11	20°		
108	108	-3/4-1	-2-4	5 mv	3.7 cm	.175	330°	5 mv	1.8 cm	.10	95°		
109	108	-3/4-1	-2-4	5 mv	2.2 cm	.10	325°	5 mv	0.9 cm	.035	25°		
110	108	-3/4-1	-2-4	5 mv	3.4 cm	.16	275°	5 mv	1.7 cm	.09	85°		
111	108	-3/4-1	-2-4	5 mv	1.7 cm	.07	300°	5 mv	2.3 cm	.12	270°		
112	108	-3/4-1	-2-4	5 mv	1.0 cm	.03	5°	5 mv	0.8 cm	.03	280°		
113	108	-3/4-1	-2-4	5 mv	5.6 cm	.265	230°	5 mv	2.3 cm	.13	20°		
114	108	-3/4-1	-2-4	5 mv	1.2 cm	.045	85°	5 mv	1.5 cm	.075	240°		
115	108	-3/4-1	-2-4	5 mv	4.0 cm	.185	345°	5 mv	3.1 cm	.165	240°		
116	108	-3/4-1	-2-4	5 mv	1.9 cm	.075	245°	5 mv	1.4 cm	.065	285°		
117	108	-3/4-1	-2-4	5 mv	2.0 cm	.08	5°	5 mv	2.2 cm	.115	145°		
118	108	-3/4-1	-2-4	5 mv	2.1 cm	.085	90°	5 mv	1.3 cm	.06	160°		
119	108	-3/4-1	-2-4	5 mv	4.0 cm	.18	310°	5 mv	2.4 cm	.125	105°		
120	108	-3/4-1	-2-4	5 mv	3.9 cm	.175	285°	5 mv	2.3 cm	.12	110°		
121	108	-3/4-1	-2-4	5 mv	2.4 cm	.115	340°	5 mv	2.0 cm	.11	190°		
122	108	-3/4-1	-2-4	5 mv	2.3 cm	.11	300°	5 mv	2.7 cm	.155	170°		
123	108	-3/4-1	-2-4	5 mv	3.0 cm	.135	100°	5 mv	2.1 cm	.115	330°		
124	108	-3/4-1	-2-4	5 mv	2.3 cm	.10	180°	5 mv	0.8 cm	.02	95°		

TABLE 14 (Cont'd.)

ROLLER SCREENING DATA

Roller Identification No.	Lot Serial No.	Dimension Diameter	Variation Length	Scope Reading Sensitivity mv/cm	+SRA IRD Reading AMP cm	AMP	Phase	Scope Reading Sensitivity mv/cm	+SRA IRD Reading AMP cm	AMP	Phase	Selected Roller	Gage Pocket Location
125	108	-3/4-1	-2-4	5 mv	1.8 cm	.075	270°	5 mv	1.5 cm	.075	55°		
126	108	-3/4-1	-2-4	5 mv	3.5 cm	.16	20°	5 mv	2.3 cm	.135	230°		
127	108	-3/4-1	-2-4	5 mv	2.2 cm	.095	170°	5 mv	2.0 cm	.105	265°		
128	108	-3/4-1	-2-4	5 mv	2.0 cm	.085	315°	5 mv	2.1 cm	.110	195°		
129	108	-3/4-1	-2-4	5 mv	3.4 cm	.155	270°	5 mv	2.2 cm	.115	145°		
130	108	-3/4-1	-2-4	5 mv	3.0 cm	.135	340°	5 mv	2.0 cm	.105	220°		
131	108	-3/4-1	-2-4	5 mv	3.0 cm	.135	130°	5 mv	3.3 cm	.175	300°		
132	108	-3/4-1	-2-4	5 mv	1.5 cm	.06	55°	5 mv	1.1 cm	.045	70°		
133	108	-3/4-1	-2-4	5 mv	3.8 cm	.17	215°	5 mv	2.7 cm	.145	55°		
134	108	-3/4-1	-2-4	5 mv	3.2 cm	.135	255°	5 av	2.1 cm	.105	110°		
135	108	-3/4-1	-2-4	5 mv	1.1 cm	.035	125°	5 mv	1.4 cm	.07	165°		
136	108	-3/4-1	-2-4	5 mv	1.8 cm	.075	345°	5 mv	1.5 cm	.065	300°		
137	108	-3/4-1	-2-4	5 mv	2.3 cm	.10	130°	5 mv	1.3 cm	.055	290°		
138	108	-3/4-1	-2-4	5 mv	1.8 cm	.075	190°	5 mv	1.4 cm	.07	70°		
139	108	-3/4-1	-2-4	5 mv	2.1 cm	.09	110°	5 mv	1.4 cm	.07	205°		
140	108	-3/4-1	-2-4	5 mv	1.8 cm	.075	220°	5 mv	2.1 cm	.11	115°		
141	108	-3/4-1	-2-4	5 mv	4.0 cm	.175	115°	5 mv	2.5 cm	.135	245°		
142	108	-3/4-1	-2-5	5 mv	2.2 cm	.10	85°	5 mv	1.8 cm	.095	240°		
143	108	-3/4-3	-2-4	5 mv	1.7 cm	.07	160°	5 mv	1.8 cm	.095	215°		
144	108	-3/4-1	-2-4	5 mv	2.3 cm	.10	50°	5 mv	2.4 cm	.125	305°		
145	108	-3/4-1	-2-4	5 mv	2.1 cm	.085	275°	5 mv	1.9 cm	.10	190°		
146	108	-3/4-1	-2-4	5 mv	3.5 cm	.15	160°	5 mv	3.0 cm	.16	20°		
147	108	-3/4-1	-2-4	5 mv	1.6 cm	.055	110°	5 mv	1.7 cm	.08	45°		
148	108	-3/4-1	-2-4	5 mv	3.0 cm	.125	305°	5 mv	2.5 cm	.14	185°		
149	108	-3/4-1	-2-4	5 mv	2.3 cm	.100	315°	5 mv	1.0 cm	.04	90°		
150	108	-3/4-1	-2-4	5 mv	2.8 cm	.115	130°	5 mv	2.4 cm	.13	325°		

from the +SRA side of each roller at the corner radius in line with measured unbalance so that the roller unbalance and weight removed would be additive.

Table 15 lists the roller by number and indicates the amount of material removed and the increase in unbalance the metal removed represented.

When compared to the unbalance mean value of 5.4×10^{-6} in.-oz. found during the roller evaluation described in report Section II, the unbalance changes built into the four test rollers are substantial.

TABLE 15
UNBALANCE ROLLERS FOR SKEW TEST

Roller Identification No.	Metal Removed (10^{-3} g)	Unbalance Change (10^{-6} in.-oz.)
23	6	127.0
25	2	42.3
30	4	84.6
68	8	169.0

3. Roller Bearing Tests

The baseline bearing assembled with 32 rollers* showing minimum levels of unbalance was assembled and run for 40 hours at the specified test conditions. The resulting test data is shown on Table 16. To compare the cage speed test data with the cage speed expected at ideal non-skid conditions, a calculation for cage speed was made using the equation:

$$\overline{N} = 1/2 \left[1 - \frac{D}{P_d} \right]$$

where: $\overline{N}$ = Cage Speed Ratio = $\dfrac{\text{Cage Speed}}{\text{Inner Race Speed}}$

D = Roller Diameter = 16 mm

P_d = Bearing Pitch Diameter = 7.6795 inch

---

*The +SRA roller ends faced the high-speed spindle.

TABLE 16

BASELINE BEARING TEST

Time	Date	Shaft rpm	Cage Hz	Oil Inlet °F T1	Test Bearing °F T2	T4	T5	T6	T7	Oil Discharge °F T10	Flow Rate gpm	Power KW	Load Pressure psig
1305	2/11	3360	22	200	200	20	200	200	200	-			
1336	2/11	3270	10	233	242	242	244	241	238	230			
1401	2/11	5070	27	262	276	278	281	276	272	255			
1516	2/11	7530	21	250	279	284	287	276	273	250	2.1	2	20
1329	3/11	10120	78	258	297	308	310	286	297	268	2.25	3	40
1344	3/11	12630	98	256	325	336	337	301	321	228	2.2	4 1/2	40
1327	4/11	10040	77	257	298	305	310	286	297	266	2.0	7.0	60
1336	4/11	12720	98	258	315	334	331	303	317	277	2.0	9.5	69 1/2
1349	4/11	14900	114	259	341	358	358	323	342	292	2.0	6.5	40
1400	4/11	14920	119	260	342	358	358	324	343	293	2.0	9.5	60
1500	4/11	14910	115	257	341	355	356	322	341	291	2.0	13.0	50
1600	4/11	15060	116	261	345	360	361	327	346	294	2.0	13.0	50
1700	4/11	14900	115	260	343	359	358	324	344	293	2.0	12.5	50
1800	4/11	14990	116	259	343	359	358	325	344	292	2.0	13.0	50
0952	5/11	10110	76	257	297	305	308	285	296	265	2.0	12.5	50
1003	5/11	15030	116	257	339	357	355	321	340	290	2.0	12.5	50
1100	5/11	14910	114	261	343	360	358	325	344	294	2.0	7.5	50
1200	5/11	14880	117	259	342	359	357	323	343	293	2.0	13.0	50
1300	5/11	14890	114	258	341	359	355	322	341	291	2.0	12.5	50
1400	5/11	14920	114	258	341	358	356	323	341	292	2.0	12.5	50
1500	5/11	14960	115	258	342	358	357	323	341	292	2.0	12.5	50
1600	5/11	14900	114	259	341	359	357	323	341	292	2.0	12.5	50
1030	7/11	15050	117	257	342	359	358	324	343	296	2.0	12.5	50
1100	7/11	15030	115	257	343	359	357	324	343	296	2.0	12.5	50
1210	7/11	15030	116	254	338	355	354	319	339	291	2.0	12 1/2	50
1315	7/11	14990	115	236	328	342	342	307	328	280	2.0	12 1/2	50
1400	7/11	15020	119	255	342	358	357	322	342	297	2.0	12 1/2	55
1500	7/11	15050	116	258	343	360	359	324	344	298	2.0	12 1/2	50
1600	7/11	15020	115	258	343	360	358	323	343	299	2.0	12.5	50
1700	7/11	15060	115	257	343	360	359	323	343	299	2.0	12.5	50
1800	7/11	15020	115	258	343	360	360	323	344	299	2.0	12.5	50
1900	7/11	15000	115	260	345	360	361	325	344	299	2.0	12.5	50

TABLE 16 (Cont'd.)

BASELINE BEARING TEST

Time	Date	Shaft	Cage	Oil Inlet °F T_1	Test Bearing °F T_2	T_4	T_5	T_6	T_7	Oil Discharge °F T_{10}	Flow Rate gpm	Power KW	Load Pressure psig
2000	7/11	15020	117	260	345	360	361	326	345	299	2.0	12.5	50
2100	7/11	15020	118	260	346	360	361	326	345	300	2.0	12.5	50
2200	7/11	15020	117	260	345	361	362	326	345	299	2.0	12.5	50
2300	7/11	15000	118	260	345	360	361	326	345	299	2.0	12.5	50
2400	7/11	15010	117	261	345	360	361	325	344	299	2.0	12.5	50
1008	8/11	10170	73	256	295	307	304	284	298	269	2.0	6.5	50
1108	8/11	10280	75	259	297	310	306	287	301	273	2.0	6.5	50
1134	8/11	10220	74	260	299	311	307	287	301	272	2.0	6.5	50
1200	8/11	15060	117	260	344	360	361	326	345	299	2.0	12.5	50
1300	8/11	15040	115	259	345	360	360	325	344	299	2.0	12.5	50
1400	8/11	15040	116	261	345	361	361	327	346	300	2.0	12.5	50
1500	8/11	15010	116	261	344	360	362	327	346	300	2.0	12.5	50
1600	8/11	14980	114	260	340	360	361	325	346	299	2.0	12.5	50
1700	8/11	15000	115	261	343	361	363	328	347	300	2.0	12.5	50
1800	8/11	15010	115	263	345	364	364	328	350	302	2.0	12.5	50
1900	8/11	15010	114	263	345	362	364	328	349	301	2.0	12.5	50
2000	8/11	15040	116	260	344	361	363	327	347	300	2.0	12.5	50
0930	9/11	10300	76	255	295	307	304	282	296	266	2.0	7.0	50
1000	9/11	15070	115	259	341	360	362	325	345	297	2.0	12	50
1100	9/11	15010	115	261	344	362	364	327	347	300	2.0	12	50
1200	9/11	15030	115	261	345	363	366	329	349	301	2.0	12.5	50
1300	9/11	15000	114	259	340	359	361	325	345	297	2.0	12.5	50
1400	9/11	14880	114	259	340	359	361	324	345	297	2.0	12.5	50
1500	9/11	15030	115	260	343	360	362	327	346	299	2.0	12.5	50
1530	9/11	15030	115	261	344	361	364	327	347	300	2.0	12.5	50

-81-

For the values shown, the cage speed ratio was found to be 0.459, which at an inner race speed of 15,000 rpm shows a cage speed of 114.8 Hz. This compares well with the measured speed of 115/116 Hz.

The actual radial load to prevent roller skidding was obtained by gradually increasing the load pressure until no further change in cage speed was noted; this occurred at a cylinder pressure of 50 psig corresponding to a 560 lb load. The power loss measured at full bearing speed was 12.5 kw. The test system's tare loss at 15,000 rpm was measured without the test bearing installed and was found to be 6.5 kw resulting in a net bearing loss of 6 kw (8 HP). Figure 31 shows the load piston calibration curve.

The outer race temperatures, taken at the positions indicated on Figure 28, show that T_2, located at top dead center at the bearing center plane in the loaded zone is lower than both T_4 and T_5 which are located at plus and minus 120° from top dead center and are in the unloaded zone. In addition, T_6 and T_7 which are separated by 0.75 inch show large differences and indicate axial temperature gradients as high as 28 degrees per inch exist across the outer race.

At the conclusion of the 40-hour baseline test, the bearing was disassembled and inspected for abnormal wear patterns. Except for some eccentric wear on the cage guiding lands determined to be the result of an off-center radial load (the load cylinder was found to be mispositioned by 0.808 inch), the cage showed no unusual wear patterns. None of the rollers indicated any non-uniform edge wear or other signs of distress. Figure 32 shows photographs taken at some typical rollers after the baseline test. The concentric ring patterns visible on the roller end are discolorations and not wear patterns.

The bearing was reassembled with all the rollers installed into the pockets they originally were in with the exception that the purposely unbalanced rollers were installed as follows: roller 25 was installed in pocket 28, roller 30 into pocket 22, roller 23 into pocket 16, and roller 68 into pocket 10. The cage pockets were numbered consecutively clockwise from an arbitrarily selected pocket, which was appropriately marked.

The reassembled bearing was tested at the same conditions previously employed with the resulting data shown in Table 17. Visual inspection of the bearing after 40 test hours disclosed no effects from the unbalanced rollers. Two
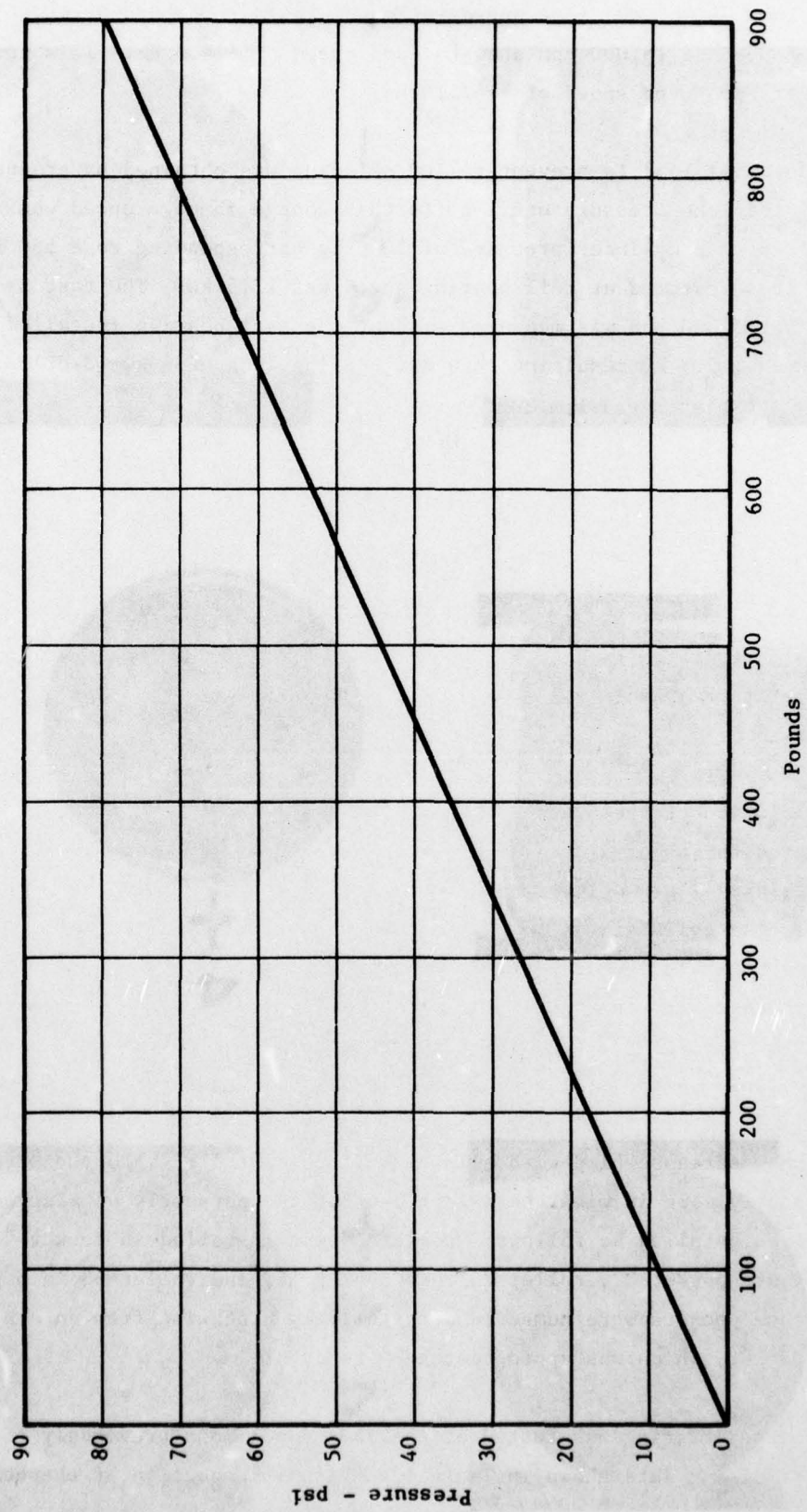
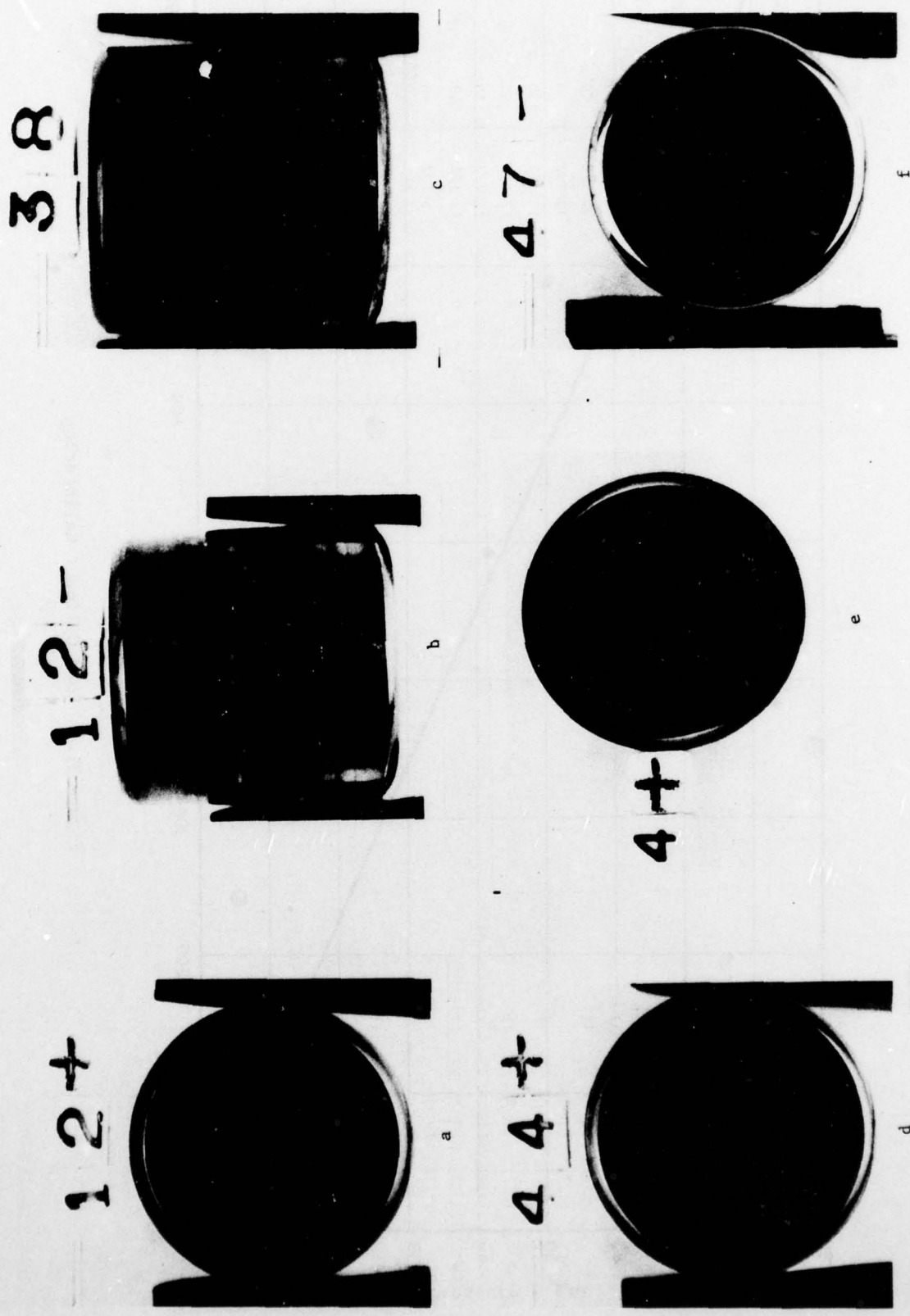-82-

Figure 31. Load Cylinder Calibration

Figure 32. Baseline Bearing Test - Roller Photographs

TABLE 17

UNBALANCED ROLLER BEARING TEST

Time	Date	Shaft rpm	Cage Hz	Oil Inlet °F T_1	T_2	Test Bearing °F T_4	T_5	T_6	T_7	Oil Discharge °F T_{10}	Flow Rate gpm	Power KW	Load Pressure psig
1400	14/11	5260	40	257	272	276	277	270	265	251	2.0	2 1/2	30
1406	14/11	9900	71	256	293	297	300	281	291	267	2.0	6 1/2	40
1420	14/11	15110	116	257	349	354	359	325	340	291	2.0	13-	50
1500	14/11	15060	115	257	349	354	359	326	341	292	2.0	12 1/2	50
1600	14/11	15030	115	258	348	355	357	325	341	293	2.0	12 1/2	50
1700	14/11	14950	114	255	346	353	354	323	339	290	2.0	12 1/2	50
1800	14/11	15000	115	260	350	356	359	327	343	294	2.0	12 1/4	50
1900	14/11	15020	115	256	348	354	357	325	341	291	2.0	12 1/2	50
2000	14/11	14990	114	260	350	356	360	327	343	293	2.0	12 1/2	50
2100	14/11	15020	115	258	350	355	359	327	342	293	2.0	12 1/2	50
2200	14/11	15000	115	258	349	355	359	327	342	292	2.0	12 1/2	50
2300	14/11	15020	114	257	348	355	357	325	341	293	2.0	12 1/2	50
2400	14/11	15000	115	257	348	355	357	325	341	292	2.0	12 1/2	50
0915	15/11	10460	75	254	295	302	302	282	294	267	2.0	6 1/2	40
0930	15/11	15060	115	257	349	355	357	325	342	293	2.0	12	50
1000	15/11	15020	115	260	350	359	360	328	344	296	2.0	12	50
1100	15/11	15010	115	260	351	360	360	328	345	297	2.0	12	50
1200	15/11	15000	114	259	351	356	360	328	346	298	2.0	12	50
1300	15/11	14980	114	262	352	360	361	330	345	298	2.0	12	50
1400	15/11	15030	115	261	253	359	362	330	345	296	2.0	12	50
1500	15/11	14960	114	261	351	360	361	329	344	296	2.0	12	50
1600	15/11	14990	114	262	353	361	362	330	346	298	2.0	12	50
1700	15/11	15060	115	263	355	361	364	332	347	299	2.0	12	50
1800	15/11	15000	115	263	353	360	362	331	346	298	2.0	12	50
1900	15/11	15000	115	263	354	361	363	331	347	299	2.0	12	50
2000	15/11	1502	115	262	353	361	362	330	346	298	2.0	12	50
2100	15/11	15000	115	261	353	360	361	329	346	297	2.0	12	50
2200	15/11	15000	115	261	253	360	361	330	345	297	2.0	12 1/4	50
2300	15/11	15000	115	261	353	360	361	330	346	297	2.0	12 1/4	50
2400	15/11	15010	115	261	352	360	361	330	345	297	2.0	12 1/4	50
945	16/11	10240	79	258	301	313	310	288	301	271	2.0	7.0	50

TABLE 17 (Cont'd.)

UNBALANCED ROLLER BEARING TEST

Time	Date	Shaft rpm	Cage Hz	Oil Inlet °F T$_1$	Test Bearing °F T$_2$	T$_4$	T$_5$	T$_6$	T$_7$	Oil Discharge °F T$_{10}$	Flow Rate gpm	Power KW	Load Pressure psig
1000	16/11	15010	115	260	352	360	361	328	344	296	2.0	12	50
1100	16/11	14940	115	260	352	360	361	329	345	296	2.0	12	50
1200	16/11	14920	114	254	354	362	364	331	347	299	2.0	12	50
1300	16/11	15010	114	262	354	362	364	331	347	299	2.0	12	50
1400	16/11	14940	115	264	355	362	364	332	348	300	2.0	12	50
1500	16/11	15000	115	264	354	363	365	331	348	300	2.0	12	50
1600	16/11	15000	114	264	355	363	366	332	348	300	2.0	12	50
1700	16/11	15010	115	265	357	364	367	333	349	300	2.0	12	50
1800	16/11	15000	115	266	357	364	367	334	350	301	2.0	12 1/4	50
1900	16/11	15000	115	265	357	364	367	333	349	301	2.0	12 1/4	50
2000	16/11	15000	115	262	355	362	365	331	347	297	2.0	12 1/4	50
2100	16/11	14990	114	264	356	363	369	333	349	299	3.0	12 1/4	50
2200	16/11	15000	115	266	357	364	369	335	351	301	2.0	12 1/4	50
2300	16/11	15020	115	265	357	364	368	334	351	301	2.0	12 1/4	50
2400	16/11	15010	115	266	358	365	369	335	351	301	2.0	12 1/4	50
9:15	17/11	10110	76	254	295	304	304	282	292	266	2.0	7 1/2	40
9:45	17/11	15030	115	262	354	363	366	331	348	296	2.0	12 1/2	50
1000	17/11	15040	115	263	356	363	368	333	348	298	2.0	12.1/2	50
1100	17/11	15000	115	265	357	365	369	334	351	300	2.0	12 1/4	50
1200	17/11	15020	115	264	357	366	369	334	350	300	2.0	12 1/4	50
1300	17/11	15020	115	263	357	364	369	333	350	299	2.0	12 1/4	50
1425	17/11	10160	76	259	302	312	311	289	301	272	2.0	6.1/2	40
1500	17/11	14980	117	264	355	364	367	333	350	300	2.0	12 1/4	50
1600	17/11	14980	114	264	356	365	368	335	351	301	2.0	12 1/4	50
1700	17/11	15010	116	268	359	369	372	337	355	304	2.0	12 1/4	50
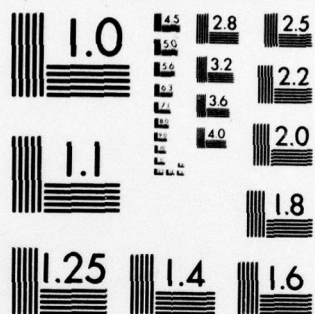
MICROCOPY RESOLUTION TEST CHART
NATIONAL BUREAU OF STANDARDS-1963-A

pockets show some edge wear, but these pockets were not the pockets in which the unbalanced rollers were located. The rollers from the two questionable pockets did not show any evidence of skewing. Figure 33 shows photographs of the unbalanced rollers after the 40-hour test. Photos 33 (a) and 33 (b) show one of the cage pockets where roller edge wear is evident; the remaining photographs are self-explanatory.
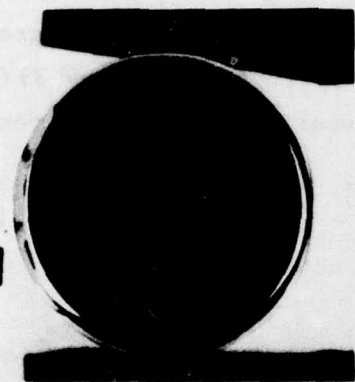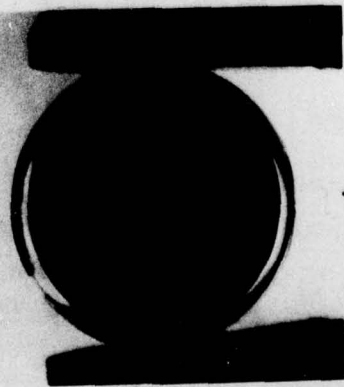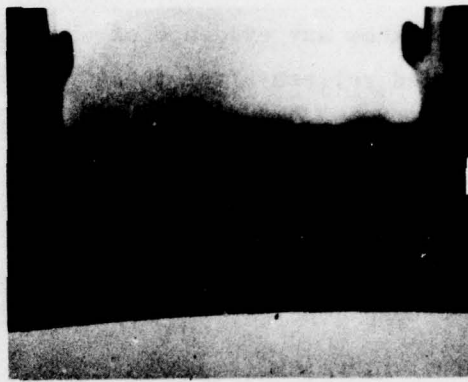
Figure 33. Unbalance Roller Test - Roller Photographs

V.I. CONCLUSIONS

The study of the residual unbalance found in the rollers investigated in this program has led to the following conclusions:

1. Analytically, it has been demonstrated that roller unbalance contributes to skew.

2. It is feasible to evaluate the roller unbalance in rollers using a simple spin-up balancing device.

3. Laser techniques, in the ranges tested, to be used for the removal of roller material for balance improvement were shown to produce undesired cratering and metal spattering effects making the technique suspect without further parametric evaluations.

4. The number of rollers exhibiting levels of unbalance significantly different than the mean values determined from a group of 21 rollers is very small.

5. Unbalance by itself may not be the sole factor producing roller skew as indicated by the lack of skewing exhibited by highly unbalanced rollers in the full bearing tests made at 2.5×10^6 DN.

Discussions with bearing users have indicated that roller skew failures are common to only a small number of the bearings in use and usually occur at a single roller in the failed bearing.

Although the roller bearing tests conducted under this program did not indicate roller skewing, roller unbalance cannot be eliminated as a potential source of roller skew failure. The interaction (not found in these tests) of roller unbalance with varying degrees of other bearing variables such as pocket spacing and squareness, axial and radial play, and misalignment may be required to produce failure.

The experimental results indicated a cominbed mean and standard deviation of unbalance equal to 10×10^{-6} in.-oz. for the group of rollers examined. These results, when weighted against the small number of bearings which have experienced roller skew type failures in the field, would suggest that, technically, the measured level of roller unbalance requires no corrective action. It does not,

however, eliminate the determination of roller unbalance as a viable inspection requirement.

Since it also has been analytically demonstrated that roller unbalance contributes to roller skew failures, unbalance as a potential cause of these failures cannot be disregarded.

Based on the results obtained from this program, it is recommended that the following steps be taken:

1. A parametric test to evaluate the effects of roller-unbalance on the problem of roller skew failures be initiated. This study should be guided by the analytical tools already available to eliminate the less promising variable combinations to reduce the test matrix.

2. Further work with laser techniques, extending the program to include roller rotation, would settle the question of laser burst requirements related to metal removal and both cratering and loose debris difficulties experienced during the laser test of this program.

3. The identification of roller unbalance for screening purposes requires the design of balancing spin-up device suitable for automated roller processing.

VII. ROLLER SPIN-UP INSPECTION MACHINE PROTOTYPE SPECIFICATIONS

In the anticipated spin-up screening of rollers, a roller meeting dimensional tolerances but not meeting a pre-selected unbalance level would be rejected during the inspection process for possible use in low DN bearings.

A reasonable set of specifications for a possible automated screening type spin-up inspection system would be:

1. The support bearing shall be an externally pressurized gas bearing having a calculated radial stiffness in the range of 100-150 lb/in. and an angular stiffness in the range of 1.7-2.0 in.-lb/RAD.

2. Two opposed axial air jets shall be used to position the roller in the spin-up bearing to within 0.0005 of true position. One jet shall be fixed, the second jet moveable to permit insertion and removal of rollers. Accurate return of the moveable jet into its proper operating position should not require operator intervention. The device for moving the jet shall be suitable for inclusion in an automated system, but should be manually operated.

3. Four spin-up air jets shall be tangentially oriented in diametrically opposed pairs on either side of the roller. The jet holder shall be capable of operation with one pair of jets removed.

4. Two position sensors shall be provided to measure roller position relative to the support bearing. The sensors should not be larger in diameter than 0.065 with a sensitivity not less than 800 volts/inch. The probes should be positioned normal to the roller surface at the greatest center distance possible without extending beyond the corner breakout location.

5. A speed control feedback loop for the drive nozzle pressure control is desirable to minimize operator adjustment requirements.

6. Cam operated roller positioning, inserting, and withdrawal devices should be provided to eliminate operator roller handling and to assure minimum retrofit in the event the spin-up rig is to be added to an automated roller inspection system.

7. Commercially available sensor transducers and balancer electronics should
    be given prime consideration.

The spin-up balancer built to the above specifications should result in a compact,
easily handled system for evaluating roller unbalance. The system would be versa-
tile enough so that it could easily be designed for any level of automation
desired and require minimal retrofit to make it totally automated.

At some future time should balance correction be required and a suitable technique
developed for metal removal, the spin-up rig could readily be modified to become
a totally automated roller balancer.

REFERENCES

1. Gupta, P. K., "Dynamics of Rolling Element Bearings - Part I: Cylindrical Roller Bearing Analysis", to be published.

2. Gupta, P. K., "Dynamics of Rolling Element Bearings - Part II: Cylindrical Roller Bearing Results", to be published.

3. Synge, J. L. and Griffith, B. A., PRINCIPLES OF MECHANICS, McGraw Hill, 1959.

4. Harris, T. A., ROLLING BEARING ANALYSIS, Wiley 1966.

5. Walowit, J. A. and Smith, R. L., "Traction Characteristics of MIL-L-7808 Oil", J. Lub. Tech., ASME Trans., Vol. 98F, (1976) pp. 607-612.

6. Gupta, P. K., Winn, L. W., and Wilcock, D. F., "Vibrational Characteristics of Ball Bearings", J. Lub. Tech., ASME Trans., Vol. 99F, (1977) pp. 284-289.